University of Alberta

Inhalable nanoparticles in lung cancer treatment; efficacy, safety, distribution and nanoparticle-macrophage interactions

by

MHD Kamal Al-Hallak

A thesis submitted to the Faculty of Graduate Studies and Research

in partial fulfillment of the requirements for the degree of

Doctor of Philosophy

in

Pharmaceutical Sciences

Faculty of Pharmacy and Pharmaceutical sciences

Fall 2012

Edmonton, Alberta

Dedication

I would like to dedicate this work to four people who made me the man I am right now; my parents MHD Nizar Al-Hallak (RIP) and my mother Daad Shiekho, my precious wife Dima Omran and my son Nizar.

ABSTRACT

In 2002, lung cancer was responsible for 17.6% of the total worldwide deaths from cancer. Beyond the three traditional forms of cancer treatment, surgery, radiation therapy, and chemotherapy, targeted drug delivery therapy has shown to be a potential treatment option. The design of a successful delivery system requires consideration of many factors, some of which include *(i)* the location and main organ(s) affected; *(ii)* the complexity of the associated physiological changes; *(iii)* the changes in receptor expression in cancerous cells; *(iv)* the physiochemical properties of the delivery system; *(v)* the interactions between the cancerous cells and other adjuvant cells, such as macrophages, with the delivery system; and *(vi)* the safety and tolerability of the delivery system. Considering the above factors of a successful delivery system, the aim of the present work was to design an innovative delivery system for lung cancer treatment incorporating inhalable nanoparticles (NP). To achieve this goal, several objectives were developed: *(i)* to investigate the interactions of different NP formulations with macrophages and the resulting effects on the behavior of macrophages; *(ii)* to assess and correlate the pulmonary toxicity of inhalable NPs using *in vivo* and *in vitro* methods; *(iii)* to develop a method to assess in real-time the effect of the formulation modifications on the uptake by macrophages of NPs; *(iv)* to assess the *in vivo* efficacy of an innovative formulation of effervescent inhalable NPs, thus actively releasing NPs; and finally, *(v)* to investigate the distribution of effervescent inhalable NPs after pulmonary delivery.

Our results demonstrate that after exposure to NPs, macrophages undergo cellular changes to gain the ability to produce Th1 cytokines that are able to affect the viability of cancerous cells. The tolerability of inhalable NPs was related mainly to the additives used in the NP formulation. There was a good correlation between the *in vivo* and *in vitro* results. Effervescent inhalable NPs proved to be an effective and tolerable treatment for lung cancer treatment. Whole body autoradiography showed that inhalable NPs were able to achieve deep lung deposition and become distributed in time over the whole lung with some extra-pulmonary distribution.

ACKNOWLEDGMENTS

I would like to express my sincere gratitude and appreciation to my supervisor, Dr. Raimar Löbenberg, for his continuous guidance, unlimited support and invaluable supervision throughout my work on these research projects.

I wish also to thank my supervisory committee members, Dr. Wilson Roa and Dr. Warren Finlay, for their unlimited guidance and endless advice.

I would also like to thank Dr. Shirzad Azarmi, who tought me several techniques and offered me valuable advice and ideas, and my colleague Mohammad Khan Sarfraz for his assistance with some experiments. I am grateful to have been generously offered the technical support when using the Cross Cancer Vivarium and the 9.4T imaging unit within the imaging facility at the Cross Cancer Institute.

I am grateful to the reviewers who had the time to review the publications which resulted from this work. Their invaluable comments and scientific critique helped me to greatly improve the quality of the manuscripts.

I am grateful to Dr. Ayamn El-Kadi, the Associate Dean for Research and Graduate Studies for his generous support of all graduate students.

I am grateful to have received the financial support from the Syrian Ministry of High Education, a Pharmacy PhD Alumni Graduate Student Scholarship, a Shoppers Drug Mart Graduate Scholarship, and a BioChem Pharma Graduate Scholarship.

Last but not least, I wish to thank all the administrative and support staff in the Faulty of Pharmacy and Pharmaceutical Sciences for their kindness. Special

thanks go to Mrs. Joyce Johnson and Mr. Jeff Turchinsky.

TABLE OF CONTENTS

CHAPTER 1 – INTRODUCTION ……. 1

1.1. Lung cancer ……..……... 2

1.1.1. Staging and conventional treatment of lung cancer ……... 2

1.1.2. Animal model of lung cancer ……. 3

1.1.2.1. Chemically induced lung tumor …… 4

1.1.2.2. Human lung tumor xenografts …….……. 4

1.1.2.3. Orthotopic lung cancer models ……. 5

1.2. Cancer drug-targeting and nanoparticles (NPs) ……..….. 5

1.2.1. Passive targeting ……. 6

1.2.2. Active targeting …….. 8

1.2.3 Preparation methods of polymeric NPs …….. 9

1.2.3.1. Preparation of NPs from performed polymer …… 9

1.2.3.2. Preparation of NPs from monomers …….. 10

1.3. Macrophage-NP paradigm and assessment ……..... 10

1.3.1. Effect of NPs on macrophages (Secondary cytotoxicity) …….. 12

1.3.2. Evaluation of the phagocytosis process ……..……..……. 12

1.4. Inhalable NP formulation and pulmonary delivery …….. 13

1.4.1 Porous NP aggregates (LPNP) …… 15

1.4.1.1. Hollow nanoaggregates ……. 16

1.4.1.2. Nanocomposites …… 19

1.4.2. Microparticle carriers ……..... 23

1.5. Toxicity of inhalable NPs …….…. 25

1.6. Distribution of inhalable NPs ……... 28

1.7. Rationale, hypothesis and objectives …….….. 29

1.7.1. Rationale ……. 29

1.7.2. Hypothesis …… 32

1.7.3. Objectives ……... 33

CHAPTER 2 – MATERIALS AND METHODS ……..... 34

2.1. Secondary cytotoxicity of NPs mediated by alveolar macrophages …….. 35

2.1.1. NP preparation and characterization …….……. 35

2.1.2. Cell culture ……. 36

2.1.3. Primary cytotoxicity and EC50 values of treatments …… 36

2.1.4. Secondary cytotoxicity mediated by macrophages …… 37

2.1.5. Sample collection ……... 38

2.1.6. HPLC analysis …… 38

2.1.7. Cytokine analysis …….…….. 39

2.1.8. Statistical analysis …….. 39

2.2. Pulmonary toxicity of polysorbate-80-coated inhalable NPs ……. 40

2.2.1. Surface pressure-area isotherm …….……. 40

2.2.2. Animal study ……. 41

2.2.3. Histopathological study ……. 42

2.2.4. Statistical analysis ……. 42

2.3. Microcalorimetric method to assess phagocytosis: macrophage-NP interactions …… 43

2.3.1. Cell culture ……..…… 43

2.3.2. Preparation and characterization of NPs ……..….. 43

2.3.3. Isothermal microcalorimetry (ITMC) and thermal activity …….. 45

2.3.4. Flow cytometry analysis …….. 48

2.3.5. Statistical analysis ……. 49

2.4. Inhalable NPs as lung cancer treatment in mouse model …….. 49

2.4.1. Preparation of characterization of NPs ……... 49

2.4.2. Determination of drug loading efficiency and capacity ……. 49

2.4.3. Preparation of effervescent carrier particles ……... 50

2.4.4. Preparation of non-effervescent carrier particles ……... 51

2.4.5. Measurement of mass median aerodynamic diameter …… 51

2.4.6. Animal studies …… 51

2.4.6.1. Implantation of lung cancer cells …….. 51

2.4.6.2. Treatment protocol …… 52

2.4.6.3. Animal monitoring …… 53

2.4.6.4. Histological study ……. 53

2.4.6.5. MRI imaging ……. 54

2.4.6.6. Cardiac toxicity of inhaled doxorubicin …… 54

2.4.7. Statistical calculation and analysis …….. 55

2.5. Distribution of inhalable effervescent NPs …….. 55

2.5.1. NPs and inhalable NPs ……. 55

2.5.2. NPs and inhalable NPs characterization …….. 56

2.5.3. Animal study …… 57

2.5.4. Inhalable NP administration ……. 57

2.5.5. Whole body autoradiography…… 58

2.5.6. Confocal laser scanning microscopy …… 59

CHAPTER 3 – RESULTS …….. 60

3.1. Secondary cytotoxicity of NPs mediated by alveolar macrophages ……. 61

3.1.1 NP properties ……..…… 61

3.1.2. Primary toxicity and EC50 ……...…….. 61

3.1.3. Secondary cytotoxicity of NPs mediated by macrophages …….. 64

3.1.4. DOX released from macrophages ……..…… 64

3.1.5. Cytokine secreting profile ……..…… 67

3.2. Pulmonary toxicity of polysorbate-80-coated inhalable NPs ……. 72

3.2.1. NP characteristics …….……. 72

3.2.2. Surface pressure-area isotherm of DPPC film over different subphases 72

3.2.3. *In vivo* pulmonary toxicity ……. 75

3.3. Microcalorimetric method to assess phagocytosis: macrophage-NP interactions 77

3.3.1. NP characteristics ……...…… 77

3.3.2. Thermal activity of macrophages ……... 80

3.3.3. Flow cytometry analysis …… 89

3.4. Inhalable NPs as lung cancer treatment in a mouse model …… 92

3.4.1. NPs and inhalable NP characteristics ……. 92

3.4.2. Treatment efficacy and animal survival data ….……... 92

3.4.3. Histology results ……..…….. 95

3.4.4. MRI results ……..…….. 101

3.4.5. Cardiac toxicity of inhaled doxorubicin ……...…….. 101

3.5. Distribution of inhalable effervescent NPs …… 105

3.5.1. NPs and inhalable NPs characterization …….. 105

3.5.2. Results of whole-body autoradiography …….. 105

3.5.3. Results of confocal laser scanning microscopy ……... 111

CHAPTER 4 – DISCUSSION …… 113

4.1. Secondary cytotoxicity of NPs mediated by alveolar macrophages …. 114

4.2. Pulmonary toxicity of polysorbate-80-coated inhalable NPs ..……. 119

4.3. Microcalorimetric method to assess phagocytosis: macrophage-NP interactions 121

4.4. Inhalable NPs as lung cancer treatment in mouse model ……. 125

4.5. Distribution of inhalable NPs after pulmonary delivery …… 128

4.6. General conclusion ……... 132

4.7. Future prospective ……..……... **135**

CHAPTER 5 – REFERENCES …… **137**

List of Tables

Table 1	The EC_{50} values of different treatment on MH-S cells (macrophages) and H460 cells (lung carcinoma).....	63
Table 2	A complete list for cytokines included in the antibody array test.....	70
Table 3	Characteristics of poly (isobutyl cyanoacrate) and gelatine nanoparticles	49
Table 4	Values of total heat exchange and the affinity constant of different NP formulations	88
Table 5	Blood concentration of AST, ALT and CPK in control mice and mice treated with either 1 mg nanoparticle powder containing 30 µg doxorubicin or 1 mg doxorubicin powder containing 30 µg doxorubicin	104

List of Figures

Figure 1	Primary cytotoxicity of four different treatments .....……..	62
Figure 2	The secondary cytotoxicity mediated by murine alveolar macrophages (MH-S) on human non-small cell lung carcinoma cells (H460) ….....…….	66
Figure 3	The amount of free and total DOX detected in samples collected from macrophages treated with DOX-loaded NPs at different time points ….....…….	68
Figure 4	Blots of the cytokines antibody-array membranes of naïve macrophages (no treatment) and macrophages treated with three different treatments ….....……..	69
Figure 5	The increase in cytokine secretion induced by blank NPs and DOX-loaded NPs at different time points ..……	71
Figure 6	Surface pressure-area isotherms of DPPC on the top of different subphases	73
Figure 7	Lung tissue section taken from mice treated with different treatments	76
Figure 8	The IR spectrum of mannosylated gelatin nanoparticles ……	78

Figure 9	The thermal activity profiles of macrophages alone, macrophages after titration of uncoated poly(isobutyl cyanoacrylate) nanoparticles, and macrophages after titration of polysorbate-80-coated poly(isobutyl cyanoacrylate) nanoparticles……..	83
Figure 10	The thermal activity profiles of macrophages alone, macrophages after titration of non-coated poly(isobutyl cyanoacrylate) nanoparticles, and macrophages after titration polysorbate-80-coated poly(isobutyl cyanoacrylate) nanoparticles after the cytochalasin B was added concentration to the medium used in all experiment ……..……..	84
Figure 11	The thermal activity profiles of macrophages alone, macrophages after titration gelatin nanoparticles, and C macrophages after titration of mannosylated gelatin nanoparticles ….…….	86
Figure 12	The thermal activity profiles of macrophages after titration mixture of gelatin nanoparticles and mannose, macrophages after titrating mannosylated solution and macrophages after titration of mannosylated gelatin nanoparticles with cytochalasin B ……..……..	87

Figure 13	Flow cytometric dot plots of macrophages treated with different treatment	90
Figure 14	Flow cytometric analysis of the macrophage uptake of nanoparticles ….....…....	91
Figure 15	Percent animal survival versus time	94
Figure 16	Lung section of mouse from the non-treatment group	96
Figure 17	Heart section showing growth of tumor in the ventricular lumen ……..	97
Figure 18	Lung section of a mouse treated with doxorubicin solution intravenously ….....	98
Figure 19	Lung section of a mouse treated with non-effervescent doxorubicin nanoparticle powder .....……	99
Figure 20	Lung section of mouse treated with effervescent doxorubicin nanoparticle powder .....……	100
Figure 21	Weighted, transverse spin echo scans (TE/TR = 13/1500 ms, BW = 50 KHz, the FOV = 26 X 26 mm with 128 × 128 matrix, thickness = 0.5 mm) for mice treated with different treatment	103

Figure 22	Whole body autoradiogram of the distribution of 14C from a mouse that received a single dose of effervescent inhalable NPs and euthanized 1 hour post-inhalation	107
Figure 23	Whole body autoradiogram of the distribution of 14C from a mouse that received a single dose of effervescent inhalable NPs and euthanized 8 hour post-inhalation …….	108
Figure 24	Whole body autoradiogram of the distribution of 14C from a mouse that received a single dose of effervescent inhalable NPs and euthanized 24 hour post-inhalation	109
Figure 25	Whole body autoradiogram of the distribution of 14C from a mouse that received a single dose of DOX solution intravenously and euthanized 8 hours post-administration	110
Figure 26	Confocal laser scanning microscopy images taken for cryosections of isolated lungs from mice received a single dose of effervescent inhalable NPs and euthanized after 1, 8 and 24 hours	112

List of abbreviations

ALT	Alanine transaminase
AST	Aspartate transaminase
CPK	Creatine phosphokinase
CT	Computed tomography
DOX	Doxorubicin
DPI	Dry powder inhalers
DPPC	1,2-Dipalmitoyl-sn-Glycero-3-Phosphocholine
EPR	Enhanced Permeability and Retention
FPF	Fine particle fraction
GSD	Geometric standard deviation
i.v.	Intravenous
IFN-γ	Interferon gamma
ITMC	Isothermal microcalorimetry
LLPs	Large porous particles
LPNP	Large porous NP aggregates
MCP-1	Monocyte chemoattractant protein-1
MFI	Fluorescence intensity
MIP-1	Macrophage inflammatory protein-1
MMAD	Mass median aerodynamic diameter
MPS	Mononuclear phagocytotic system
MW	Molecular weight
NPs	Nanoparticles
NSCLC	Non-small cell lung cancer
PBS	Phosphate-buffered saline
PCL	Polycaprolactone
Pe	Péclet number
PEG	Polyethylene glycol
PIBCA	Poly (isobutyl cyanoacrylate)
PLA	Poly lactic acid
pMDI	Pressurised metered -dose inhaler
PVA	Polyvinyl alcohol
siRNA	Short interfering RNA
SLNs	Solid lipid nanoparticles
TAM	Tumor-associated macrophages
TB	Tuberculosis
Tg	Glass transition temperature
TNF-α	Tumor necrosis factor α
VEGF	Vascular endothelium growth factor

CHAPTER 1 – INTRODUCTION

1.1. Lung cancer

Despite advances in early diagnosis techniques and treatment approaches, lung cancer remains a disease with a dismal prognosis and remains the main cause of cancer death worldwide [1-3]. Although one-year all-stage survival is reported to have increased from 32% in 1973 to 41% in 1994, five-year survival has remained unchanged at about 15% [4, 5]. New chemotherapy agents such as pemetrexed (antifolate agent) [6], gefitinib [7] and erlotinib (epidermal growth factor receptor inhibitor) [8] have been approved by the FDA for the treatment of lung cancer; however, chemotherapy of advanced cases of lung cancer has been of limited benefit and seems to have reached a plateau [9]. Therefore, the focus of cancer treatment research has shifted to the development of delivery strategies to selectively target cancerous cells and minimize side effects when using existing anticancer agents.

1.1.1. Staging and conventional treatment of lung cancer

Non-small cell lung cancer (NSCLC) accounts for 85% of all lung cancer incidents. NSCLC can be divided into three major histologic subtypes: squamous-cell carcinoma, adenocarcinoma, and large-cell lung cancer [10]. The currently adopted staging system within each subtype of lung cancer depends on the TNM subsets (T=primary tumor, N=regional lymph nodes, M=distant metastasis). The present classifications of lung cancer stage include: T1N0M0 (stage IA); T2N0M0 (stage IB); T1N1M0 (stage IIA); T2N1M0 and T3N0M0 (stage IIB); T3N1M0, T1N2M0, T2N2M0, and T3N2M0 (stage IIIA); T4N(any)M0 (stage IIIB); and T(any)N(any)M1 (stage IV). [11]

The recommended treatment of lung cancer is usually chosen according to the cancer stage. For stage I and stage II NSCLC, if no contraindications exist such as impaired pulmonary function and other medical disorders, a lobectomy (removal of an entire lobe of the lung) has

been shown to be the most effective type of surgery, even when the lung tumor is very small. If lobectomy is not suitable for any reason, the surgeon can remove the tumor and a surrounding margin of normal lung tissue in a procedure called a wedge. Surgery is usually followed by adjuvant therapy consisting of radiation or chemotherapy [12]. For patients with stage I and stage II NSCLS for whom operation is not feasible, radical radiation followed by chemotherapy is recommended [13]. For other stages, cycles of chemotherapy and radiation are recommended however the duration and number of the cycles is still debatable [14]. Platinum-based combination chemotherapy (cisplatin + vinblastine) is the standard first-line chemotherapy regimen for NSCLC. Second-line chemotherapy, using for example docetaxel, pemetrexed, gefitinib, or erlotinib, has been considered when disease progression is confirmed [15]. The immunologic, vascular and stromal interactions between cancer cells and the host biological entity are poorly modeled *in vitro*. Therefore, an *in vitro* model system that faithfully reflects the process of lung cancer development and progression, and the efficacy of different treatments, is unlikely to be developed. Consequently, it is important that the efficacy of any new treatment is tested in a reflective animal model.

1.1.2. Animal model of lung cancer

The pathogenesis of lung cancer has been extensively studied, however a full understanding is limited due to its aggressive biologic nature and considerable heterogeneity as compared to other cancers. It is thus necessary to study and evaluate lung cancer in an experimental animal model that can be examined under the uniform, controlled conditions that are not achievable in the clinical setting [16]. Unfortunately, humans are susceptible to develop lung cancer spontaneously and lung tumors in other species are observed by veterinarians only periodically. The first conceptualization of the use of an animal model for cancer was more than

100 years ago, when Livingood [17] described a papillary tumor in a mouse. Currently, several types of animal models are widely used in lung cancer research when investigating early diagnosis and treatment. These may incorporate chemically induced lung tumors, transgenetics, and human tumor xenografts.

1.1.2.1. Chemically induced lung tumor

Humans and other living species are constantly exposed to potentially harmful mixtures of chemical and physical pollutants. Between different species, mice are prone to develop spontaneous lung cancer and have been used to investigate the effects of different agents on inducing lung cancer [18]. Chemically induced tumors in animal models are generally similar to those found in the clinical situation in humans [19, 20]. It has been shown that lung tumors developed in mice or rats after exposure to carcinogenic agents such as N-nitroso-tris-chloroethylurea [21, 22] are comparable in histology and their molecular characteristics to those in humans [23]. Unfortunately, experimental models using these tumors for new treatments suffer from some limitations including the long time requirement for the animal model to develop the tumor (with it being measurable only late in their course), the sporadic metastatic pattern, and their generally poor response to therapy [24]. Because of these limitations, chemically induced model systems are usually reserved for studies of carcinogenesis and cancer prevention rather than new treatment efficacy.

1.1.2.2. Human lung tumor xenografts

Human lung tumor xenografts are created by transplanting the human tumor directly on the site or organ of interest, this maintaining the histologic and biologic identity of the implanted tumor. Normally, human neoplasms are rejected when implanted into another species, unless the host animal is immunosuppressed [25]. Historically, knocking down the host animal's immunity

has been completed using irradiation, thymectomy, splenectomy or corticosteroids. With the breeding of hairless nude mouse mutants (nu/nu homozygotes), severe combined immunodeficient mice, and Rowett nude rats, laboratory animals are now readily available for the transplantation of human tumors [16]. This method is mainly used for skin tumors where the melanoma is implanted subcutaneously in the immune-suppressed host animal. The main disadvantage of this method is that it requires a fresh clinical specimen. Moreover, the response of a tumor to a specific treatment might be altered by the location of implantation, creating some kind of site-specific chemosensitivity rather than the desired tumor-specific sensitivity [26].

1.1.2.3. Orthotopic lung cancer models

In orthotopic models, the tumor is introduced to the host animal as a cell suspension through endobronchial, intrathoracic or intravenous (*i.v.*) injection [27-30]. One the most common methods to produce a lung cancer animal model uses a traditional *i.v.* injection of the human NSCLC cell line NCl-H460 [26, 31]. Even though cancerous cells will be widely distributed in the body of the host animal after tail vain injection, the cancerous cells preferentially colonize the lungs. An organ-specific site presumably provides tumor cells with the most appropriate milieu for local growth and metastasis. In other words, lungs will be the most appropriate site for the H460 to colonize and multiply, and any active tumor growth in other organs, such as the liver and heart, will be to a lesser extent. This model is considered the most trusted animal model for studying lung cancer and for testing the efficacy of new agents and approaches for lung cancer treatment [32-34].

1.2. Cancer drug-targeting and nanoparticles (NPs)

Since Paul Ehrlich invented the concept of the “magic bullet”, the drug-targeting field has come along way from theory into practice. The focus of the concept as it can be easily described

is to direct treatment to where it is needed to maximize the effect and minimize the side effects. Most of the available anticancer agents are highly active *in vitro,* yet their use is limited by their lack of selectivity and dose-limiting side effects. Respectively, it was logical to envision a way to target the anticancer agents to cancerous cells while sparing the healthy ones [35].

Colloidal delivery systems and nanotechnology have evolved as an exciting platform in the field of anticancer research with promises to improve the pharmacology of current cancer therapeutics [36]. Within different colloidal delivery systems, NPs have important technological advantages such as higher stability, higher drug-loading capacity and easier formulation methods [37]. The potential use of NPs as a colloidal delivery system for pharmaceutical applications has received considerable interest in the past three decades [38]. In part, this interest emerged due to the ability of NPs to circumvent undesirable physiochemical properties of the active ingredient (such as poor water solubility) [39], to protect it from early degradation (such as enzymatic proteolysis) [40] and to enhance its cellular uptake [41].

The potential of using NPs in cancer treatment is supported by the ability of NPs to accumulate in cancerous tissues passively by a phenomenon entitled Enhanced Permeability and Retention (EPR) [42, 43] and/or actively by using different targeting probes [44].

1.2.1. Passive targeting

Due to an abnormal rate of cellular division and growth, cancer is associated with enhanced vascularization via a process called angiogenesis [45, 46]. A solid tumor consists of two major cellular sets, the tumor parenchyma and the stroma; the latter incorporates the vasculature and other supporting cells. Due to the increasing metabolic requirements of the growing tumor, the pre-existing blood vessels become incapable of providing enough blood and they undergo intense angiogenic pressure [47]. The angiogenesis is promoted by different factors

such as vascular endothelium growth factor (VEGF), bradykinin, some cytokines, and prostaglandins. The process is not without defects; it results in heterogeneous vascularization with regions of hemorrhage and necrosis [48]. Additionally, the blood vessels themselves suffer several abnormalities such as having proliferating endothelial cells, higher tortuosity, a deficiency of pericytes lining their endothelial cells, and aberrant basal membrane formation [49, 50]. The abnormal tumor vasculature results in leaky vessels with gaps ranging in size between 100 nm to 2 μm depending on the type and the size of the tumor [51]. Moreover, tumors in general suffer from poor lymph draining due to lack of a well-defined lymphatic system [52]. The leaky vasculature combined with the poor lymphatic drainage results in EPR [43].

As a result of the EPR, colloidal delivery systems with appropriate size and surface characteristics will, theoretically, pass through the fenestrations of the leaky vessel to enter the tumor's interstitium and also have long retention time. EPR is considered the cornerstone theorem of passive targeting through colloidal delivery systems using micelles, liposomes and NPs [44]. Therefore, it is essential for NPs to remain in the circulation for periods long enough to reach the leaky vasculature at the site of action. In fact, the failure of early attempts of using NPs for cancer targeting was mainly attributed to the interference from macrophages of the mononuclear phagocytotic system (MPS). Macrophages are widely distributed in many of the bodily tissues and organs. They are strategically placed within the body to recognize and clear altered and senescent cells, foreign particulates, as well as macromolecular ligands [53]. The rapid capture of intravenously injected NPs from the blood by hepatic Kupffer cells is problematic for efficient targeting of drug carriers or diagnostic agents to other macrophage populations (e.g., splenic) as well as to non-macrophage sites [54]. Thus, in order to evade early sequestration and prolong NP circulation time, a new strategy was implemented by changing the

NP's surface properties to allow them to be considered "long-circulating NPs" [44]. The first step to ensure that NPs will have long circulating times is to stop, or at least delay, the opsonization process. Opsonization is an essential step that precedes clearance of unwanted particulates by phagocytotic cells. It involves the adsorption of opsonins on the surface of the foreign bodies or pathogens to mark them as unwanted and to promote their recognition by the phagocytotic cells [55, 56]. Some well known examples of opsonic molecules include various subclasses of immunoglobulins, complement proteins like C1q and generated C3 fragments (C3b, iC3b), apolipoproteins, thrombospondin, fibronectin, and mannose-binding protein [57, 58]. It has been proven that the physiochemical properties of NPs, mainly the size and surface characteristics, enable extreme control of the opsonization process [59-61]. It has been shown that small particulates, size range of 200 nm, with hydrophilic surface properties and neutral surface charges have a higher chance of evading phagocytotic cells. NPs are within the optimal size range for the long-circulating colloidal systems. The hydrophilicity of the NP surface can be altered by various strategies including coating them with polysaccharides, hydrophilic surfactants or grafting the surface with low-molecular hydrophilic copolymers [62]. Moreover, using the hydrophilic coating strategy not only helps NPs evade phagocytotic cellular uptake, but it might also alter the bodily distribution after *i.v.* injection [63].

1.2.2. Active targeting

One way to enhance tumor targeting is to program the NPs to actively bind to specific cells after extravasation. This selective interaction of NPs with target cancerous cells may be achieved by attaching targeting agents that bind to specific receptors. NPs will recognize and bind to target cells through ligand–receptor interactions, and bound particles can then be internalized. Various endogenously occurring homing devices and targeting ligands have been

attached to long-circulating colloidal delivery systems; examples include oligosaccharides that mimic ligands for selectins, folic acid, oligopeptides, plasminogen and, interestingly, antibodies and their fragments [64-67].

Active targeting is not without problems; coupling the homing device or the targeting ligand to the NP surface requires chemical modifications of the polymeric NPs or use of an anchor such as a low molecular polyethylene glycol (PEG), where longevity becomes an issue. Moreover, the active targeting may prevent the NPs from penetrating deeply into the solid tumor, since the majority of the NPs will bind to the peripheral cells at the sites of action. Due to their intrinsic immunogenicity properties, using antibodies as the targeting ligand might also shorten the NPs circulation time [68].

1.2.3. Preparation methods of polymeric NPs

Nonpolymeric NPs are mainly used to enhance photodynamic cancer therapy, therefore the application and the preparation of the nonpolymeric NPs will not be covered in this thesis.

Polymeric NPs are usually made of biodegradable polymer in the forms of nanospheres and nanocapsules where the drug is dissolved, entrapped, encapsulated or attached to a NP matrix, depending upon the method of preparation. Nanocapsules are nanovesicles in which the drug is trapped into a cavity made by a unique polymer membrane; nanospheres are matrix systems within which the drug is physically and uniformly dispersed [69]. In general, polymeric NPs can be prepared by two methods: dispersion of preformed polymers, and controlled polymerization of monomers.

1.2.3.1. Preparation of NPs from preformed polymer

Various strategies can be used for the pre-formed polymer method, *(i)* solvent evaporation, *(ii)* salting out, and *(iii)* supercritical fluid technology. All three methods share the

same basic procedure, with dissolving the performed polymer of a suitable molecular weight in an appropriate solvent (organic solvent or liquid CO_2) prior to forming an emulsion with water and then removing the solvent. The results typically create poly lactic acid (PLA), poly (lactic-co-glycolic acid) PLGA and poly (ϵ-caprolactone) [70-72].

1.2.3.2. Preparation of NPs from monomers

Nanoparticles can also be prepared by controlled polymerization of monomers such as poly (isobutyl cyanoacrylate) (PIBCA). Historically, poly (alkylcyanoacrylate) derivatives have been used as tissue adhesives in surgery due to their safety and tolerability [73].

The synthesis of PIBCA starting from an isobutyl cyanoacrylate monomer using emulsion-polymerization methods is well documented [54, 74]. The polymerization process is controlled by the pH, and the formulated NPs are usually stabilized by using a polysaccharide such as dextran without a reaction initiator. This method of preparation produces PIBCA NPs with a full polymer core and allows for an excellent loading efficiency and capacity of water soluble materials such as doxorubicin (DOX) [75]. The resultant polymer is biodegradable, undergoing different enzymatic degradation processes with the predominant one being ester hydrolysis [76]. In fact, the drug release rate from PIBCA NPs was found to be related to the rate of ester hydrolysis [76, 77].

1.3. Macrophage-NP paradigm and assessment

The main problem encountered when NPs are used as drug carriers for cancer treatment is the interference from macrophages of the MPS, mainly in the liver and spleen [78]. The clearance of NPs by MPS organs is mediated by phagocytic cells such as macrophages and Kupffer cells. This will alter the biodistribution of NPs after *i.v.* injection and the side effect profile of the anticancer agent loaded in the NPs [79].

Phagocytosis mediated by macrophages is an innate immune defense mechanism that has a substantial impact on the success or failure of any treatment that involves colloidal delivery systems, including NPs [80, 81]. Macrophages are considered targets and/or sites of action in specific diseases, such as AIDS, Leishmania infections and tuberculosis (TB), in which phagocytotic cells are hosts for the virulent agent [82-84]. In other diseases such as cancer, macrophages are normally considered obstacles to be avoided in order to enable NPs to have longer circulation times, thus increasing their chance of reaching cancerous cells [44, 85]. To control the cellular response of macrophages to enhance or inhibit phagocytosis, different techniques have been undertaken to produce long-circulating NPs, mainly by changing the physiochemical properties of the NP surface [86, 87]. Coating the surface of NPs with a hydrophilic surfactant such as polysorbate-80 was has been one such strategy [88]. NP surfaces have also been decorated with hydrophilic polymers, such as low molecular weight PEG [89, 90]. On the other hand, phagocytosis can be enhanced by targeting special receptors, especially the mannose receptor, on the surface of macrophages,. This targeting was achieved by tagging NP surfaces with mannose moieties using surface association and/or chemical linkage [91, 92]. Changing the NP's surface to be more hydrophilic aims to inhibit opsonization, thus the precipitation of antibodies and other proteins on the surface of the NPs [93]. This strategy was shown to successfully prolong the circulation time of NPs and also to enhance the distribution of NPs to some organs such as the brain [63]. Monitoring changes in phagocytosis is essential to assess the macrophage cellular response to NPs of different structures.

1.3.1. Effect of NPs on macrophages (secondary cytotoxicity)

As discussed earlier, macrophages are responsible of clearing NPs and other foreign objects through phagocytosis processes, whereby phagocytotic cells, including macrophages,

will go through different activation pathways upon exposure to NPs [94]. This will be accompanied sequentially by upregulated production (by the phagocyte oxidase and nitric oxide synthetase enzyme systems) of reactive oxygen species and nitrogen intermediates, induction of proinflammatory macrophage cytokines, and finally, induction of apoptosis [95, 96]. Most of these events have been linked to pulmonary side effects after the administration of inhalable NPs in healthy humans and animal models, especially when using smaller NPs (less than 100 nm) and under long exposure [97, 98]. However, the activation of alveolar macrophages in lung disease (such as lung cancer and TB) can lead to a special immune response that might contribute to the total efficacy of inhalable NPs, depending of the type of the inflammation process and the cytokines released [99]. If macrophage activation was in favor of the treatment (cancer rejection in the case of lung cancer) this would be considered an additive effect to the efficacy of inhalable NPs. This effect of NPs will be referred to here as NP secondary cytotoxicity because it should be differentiated from the direct effect of the NPs on cancer cells (primary cytotoxicity). The activation of macrophages upon exposure to NPs and the effect of activated macrophages on cancerous cells were investigated in the current work using two-compartment cell culture methods.

1.3.2. Evaluation of the phagocytosis process

Fluorescence microscopy and flow cytometry are normally used to assess phagocytosis. Because these techniques estimate the percentage of cell populations through their expression of the fluorescent properties of the probe, NPs need to possess fluorescence in order to be detected intracellularly after being phagocytosed by macrophages [100, 101]. Fortunately, NPs or any other colloidal delivery system can be tagged with fluorescent probes [102]. Moreover, while these techniques can assess the extent of phagocytosis that has been undergone, they cannot

monitor phagocytosis in real time. Isothermal microcalorimetry (ITMC) is a universal analytical technique that measures heat exchange to monitor physical, chemical, and biological reactions [103]. Samples tested by ITMC are surrounded by an isothermal heat sink that compensates for any thermal activity taking place in the sample, thus maintaining an isothermal environment [104]. During a reaction, heat exchange between the sample and the heat sink is monitored and recorded continuously in real time [105]. Results are expressed in thermal activity profiles where power (usually in microwatts) is plotted against time. Most biological functions are associated with changes in cellular metabolism and, consequently, heat exchange with the surrounding environment [106]. Similar to other biological functions, metabolism is the only source of energy required to perform phagocytosis [107]. Therefore, ITMC has two advantages over other techniques that monitor NP phagocytosis: *(i)* there is no need to tag NPs with a fluorescent probe for intracellular detection; and *(ii)* ITMC provides a continuous thermal record of the phagocytosis process [108]. Using other analytical and monitoring techniques to evaluate NP-macrophage relationships might be helpful to better design delivery systems that have the ability to evade or target macrophages.

1.4. Inhalable NP formulation and pulmonary delivery

Multiple routes of administration can be used for delivery of NPs, including *i.v.*, transdermal, ocular, nasal, and pulmonary [109-112]. The route of administration chosen should be appropriate to the disease or disorder being targeted and the intended results. Pulmonary delivery is becoming an important route of drug administration for the treatment of intra- and extra pulmonary diseases. This is supported by the lungs' unique characteristics such as their large surface area, thin epithelial layer, high vascularization, and avoidance of first-pass metabolism [111].

Three approaches to inhaled drug delivery use nebulizers (solutions inhalers), pressurized metered-dose inhalers (pMDIs), and dry powder inhalers (DPIs), with each having their unique strengths and weaknesses [113]. Nebulizers have been used to deliver inhalable NPs of different types, but their requirement of bulky compressors or a source of compressed air limits their use to hospital and ambulatory care settings. Children, the elderly, and people with inadequate physical or mental ability to use pMDIs and DPIs may use nebulizers [114-116].

pMDIs are the most popular inhaled drug delivery system; however, it is challenging to formulate NPs for pMDIs because they are typically unstable due to their potential for sedimentation, crystal growth, and polymorphism. In addition, pMDIs emit the dose at high velocity, which makes deposition in the oropharynx more likely. The aforementioned characteristics make pMDIs less suitable for delivery of inhalable NPs [117].

DPIs were introduced to overcome some of the drawbacks associated with pMDIs [118]. DPIs offer higher formulation stability and can provide deep lung deposition [119, 120]. An advancement in the pulmonary delivery of DPIs was the introduction by Edwards and colleagues of large porous particles (LPPs) having small mass densities and large geometric diameters. Due to their physical characteristics, LPPs were able to escape the lung's natural clearance mechanisms and achieve deep lung activity [121].

The delivery of NPs from DPIs combines the advantages of nano scale formulation and the localized effect of NPs in the lungs, especially in the treatment of TB [122], cystic fibrosis [123, 124], and lung cancer [111, 125]. The pulmonary delivery of NPs showed clear advantages over the use of microparticles and other inhalable formulations, including enhanced activity [126], increased cellular uptake [127], elevated immunological response [128, 129], longer lung

retention [122, 130], and modified pharmacokinetics with an extended release profile, improved tolerability, and reduced toxicity [125].

However, the direct inhalation of NPs from DPIs is not feasible. Due to their submicron diameter, NPs are mostly exhaled after inhalation resulting in minimal deep-lung deposition [131]. Other studies report that NPs tend to strongly agglomerate when formed as dry powder; moreover, the dry powder is difficult to handle and has low ability to release NPs having similar characteristics to the original NPs (low redispersibility) [132-135]. The phagocytotic clearance of inhaled NPs may also hinder the maximum efficacy of NP treatment. On the other hand, targeting macrophages might be preferable in lung diseases such as TB [136].

Different pharmaceutical approaches have been used to overcome the difficulties of formulating NPs in DPIs for pulmonary delivery. These interventions have mainly sought to increase the mass median aerodynamic diameter (MMAD) of the inhalable powder to 1–5 μm, optimize the fine particle fraction (FPF), and enhance the redispersibility of NPs after pulmonary delivery. Increasing the MMAD of inhalable NPs can be achieved by forming large porous NP aggregates (LPNP) or loading NPs in a form of microcarrier particles that have optimal inhalable properties.

1.4.1. Porous NP aggregates (LPNP)

NPs in the form of LPNPs are held together by physical means, such as van der Waals forces (as in hollow nanoaggregates) [132, 137], or by using binders such as polymers, phospholipids, or sugars (as in nanocomposites) [138, 139].

1.4.1.1. Hollow nanoaggregates

Hollow nanoaggregates are prepared by spray drying an NP dispersion to form hollow microparticles in which the crust or shell is made of layers of NP aggregations. In general, the

spray drying technique atomizes the NP dispersion mixture, and other excipients, to a spray form that is placed immediately into thermal contact with a hot gas resulting in the rapid evaporation of the droplets to form dried solid particles. The dried particles are then separated from the gas by means of a cyclone.

To obtain hollow nanoaggregates, the drying time of the sprayed droplets should be sufficiently shorter than that typical for redistribution of NPs by diffusion within the drying droplet [140, 141]. Tsapis et al. [132] proposed two critical times in the drying process to produce such particles. The first is the time required for a droplet to dry and the second is the time required for the NPs to diffuse from the edge to the center of the droplet. The ratio of these two characteristic times (the first over the second) defines a Péclet number (Pe). NP aggregations in the form of hollow microparticles will be produced when the spray drying settings result in a large enough Péclet number (Pe >> 1). Three main variables can be controlled in order to maximize the Péclet number and to form hollow particles: inlet temperature, droplet atomization efficiency, and feed rate. High inlet temperature (110 °C) can be accompanied by lower droplet atomization efficiency and a higher feed rate (70 ml/min), whereas lower inlet temperature (95 °C) requires higher atomization efficiency and a lower feed rate (40 ml/min). Kawakami et al. [137] proposed a more efficient drying process and, consequently a shorter droplet drying time, by adding the surfactant sodium dodecyl sulfate to the sprayed mixture.

Trojan particles produced by Tsapis el al. [132] were spherical in shape and had a mass density around unity and a MMAD of approximately 3 μm, which is suitable for deep pulmonary delivery. The shell-wall of the Trojan particle was made of several layers of NP aggregations. In spite of the appealing characteristics of Trojan particles produced by Tsapis et al., their ability to release and redisperse NPs *in vivo* remains uncertain. The *in vitro* redispersibility test was

performed by vortexing the dry powder of Trojan particles in a mixture of ethanol/water (70:30 by volume). This may be inappropriate as it does not represent the actual redispersion mechanism in lung fluid, where dispersion is caused by spontaneous particle wetting. The presence of a water-soluble excipient (mannitol) that forms "excipient bridges" interconnecting the NPs was found by Kho et al. [140] to be required to enable spontaneous redispersion.

Hadinoto el al. [142] showed that the morphology and degree of hollowness of nanoaggregates prepared by spray drying depend on the chemical nature of the NPs, but not on their size. Polyacrylate, silica, and polystyrene NPs of similar size and concentration produced different hollow particles under the same spray drying condition. This can be explained by the differing types of stabilizing forces imposed by the differing chemical natures of the NPs.

In addition to the inlet temperature and feed rate, Cheow et al. [143] studied the effect of feed concentration, feed pH, and the ratio of the gas atomizing flow rate to the feed rate on the morphology of silica hollow nanoaggregates. This study showed that there is a minimum feed concentration below which Trojan particles cannot be formed (0.18%, w/w for silica NPs). The optimal spray drying formulation parameters, from which hollow spherical nanoaggregates with a narrow bimodal distribution were produced, were identified by these authors as: inlet temperature 120 °C, pH 9, feed concentration 0.8% (w/w), feed rate $0.18 \times 10^{-3} m^3/h$, and gas atomizing flow rate $0.332\ m^3/h$.

It has been shown that the degree of hollowness (ψ), defined as the ratio of the effective density (ρe) to the true density ($\rho true$) of the nanoaggregates, can be increased by using phospholipids during the spray drying process [144]. The degree of hollowness of hollow nanoaggregates made of polyacrylate NPs with a size close to 160 nm was increased from 0.1 to 0.4 as the phospholipid concentration increased from 0 to 60% w/w. In another study, Kho et al.

[140] showed that the redispersibility of the hollow nanoaggregates was related to the degree of hollowness. In this study, the degree of hollowness was controlled by the NP:mannitol ratio.

Two parameters were proposed by Kho et al. [140] to evaluate redispersibility: *(i)* the ratio of NP diameter retrieved from the nanoaggregates (Sf) to original NP diameter (Si), where a Sf-to-Si ratio ≈ 1 suggests that the nanoaggregates are fully redispersible into the primary NPS; and *(ii)* the turbidity level of an NP dispersion produced by hollow nanoaggregates upon exposure to moisture, with higher turbidity levels indicating bigger NPs and poor dispersibility. Nanoaggregates with a higher shell-thickness-to-particle-radius ratio exhibited weaker redispersibility due to poor particle wetting. Hollow nanoaggregates with the highest redispersibility were obtained from spray drying using a 0.72% (w/w) nanoparticle concentration and a silica-to-mannitol ratio of 1:4. The thickness of the hollow nanoaggregate shell was found to be influenced more by process parameters acting at the colloidal level (such as pH) than by the spray drying operation settings.

The effect of different excipients on the morphology and redispersibility of hollow nanoaggregates of silica NPs was assessed by the same group in a different study [145]. Comparing leucine, mannitol, lactose, and a mixture of these materials, the laboratory determined the nanoparticle-to-excipient concentration ratio required to produce hollow nanoaggregates with the best morphology and redispersibility characteristics. Mannitol alone produced particles with large, hollow, and spherical morphologies, but with poor redispersibility. Lactose alone showed highly redispersible particles at the expense of morphology. The best results were achieved with a multiple-excipient formulation of leucine and lactose at a 1:6 concentration ratio. The hydrophobic leucine was included in the formulation to serve as a water

repellent to reduce the moisture uptake of the highly hygroscopic spray dried lactose, to reduce particle cohesiveness, and to improve particle morphology.

1.4.1.2. Nanocomposites

Nanocomposites are made by binding NP agglomerations with other excipients to form particles appropriate for pulmonary delivery and deep lung deposition. The main difference between nanocomposites and hollow nanoaggregates is that the former are not hollow particles, yet they possess the required aerodynamic characteristics for pulmonary delivery due to their porous texture. Nanocomposites can be formulated by spray drying, spray-freeze drying and controlled flocculation and milling.

- Spray drying

Tomoda et al. [139] studied the effect of inlet temperature and the weight ratio of NPs to excipients on nanocomposites made of PLGA NPs with a sugar (lactose or trehalose) binder. Their results demonstrated that the optimal inlet temperature depends mainly on the size range of the primary NPs; larger (400 nm) PLGA NPs showed a greater ability to tolerate elevated inlet temperatures, whereas smaller (200 nm) NPs formed nanocomposites that were not redispersible when the inlet temperature was at or above 80 °C. For the 400 nm NPs, the best nanocomposites were obtained using trehalose, an inlet temperature of 90 °C, and a 45% NP-to-excipient weight ratio. For the 200 nm NPs, the best results were obtained with trehalose and a 70 °C inlet temperature, regardless of the NP-to-excipient weight ratio. Another study found that lower inlet temperatures yielded PLGA nanocomposites with larger sizes but better redispersibility, and that the optimal inlet temperature was dependent not only on the size of NPs, but also on the type of binder used in the nanocomposites (80 °C for trehalose and 90 °C for lactose) [138].

The maximum tolerable inlet temperature during spray drying processes has been shown to be related to the glass transition temperature (Tg) of the polymer. In this regard, Yamamoto et al. [146] showed that PLGAs with a molecular weight (MW) of 20,000 or lower exhibited minimum heat tolerance, because the nanocomposites obtained at inlet temperatures higher than 45 °C showed no ability to redisperse to release original NPs. However, NPs made of a higher molecular weight polymer (120,000) were able to form redispersible nanocomposites at a higher inlet temperature (70 °C). The composition of the active ingredients may also require the use of low inlet temperatures. Jensen et al. [147] studied the spray drying of short interfering RNA (siRNA)-containing PLGA NPS using a very low inlet temperature (45 °C) in order to avoid the decomposition of the siRNA. This study showed that when using a low inlet temperature, the best nanocomposites were obtained using a high concentration of mannitol (30 mg/ml) and a low NP to excipient ratio (20%).

Muttil et al. reported that nanocomposites of PLGA NPs containing CRM-197, a diphtheria antigen [129], and PLGA/PEG NPs containing recombinant hepatitis B surface antigen [128] could be used as inhaled vaccinations. Nanocomposites prepared by Muttil et al. [128, 129] were obtained by spray drying a mixture of NPs dispersed with an L-leucine solution; the ratio of NPs to L-leucine was kept at 25:75 for PLGA NPs and at 10:90 for PLGA/PEG NPs. Other experimental settings of the spray drying procedure were: inlet temperature 95 °C and 80 °C, feed rate 30 ml/min, and air flow rates 100 and 98 kg/h for PLGA and PLGA/PEG NPs, respectively. Both nanocomposite powders (PLGA and PLGA/PEG) showed almost the same characteristics: the MMAD was approximately 5 μm and the FPF<5.8μm was around 50%. No redispersibility data were reported in either study.

To avoid rapid alveolar macrophage uptake and clearance upon pulmonary delivery, the nanocomposites should disintegrate rapidly and release the NPs at the site of action. Disaggregation is dependent on the solubility of the binder used during the spray drying process. Therefore, Lebhardt et al. [148] investigated the effects of using different excipients with different water solubilities on the redispersibility of nanocomposites. Compared to lactose and mannitol, PLGA nanocomposites produced with α-cyclodextrin were readily redispersed within 5 min by gently shaking; PLGA NPs within the size range of 200 nm were released.

- Spray-freeze drying

During the spray drying process, NPs are exposed to harsh physical conditions such as thermal stress during droplet drying, high shear stress in the sprayer nozzle, and high adsorption at the greatly expanded liquid/air interface of the spray solution [134]. These conditions might affect both the polymer matrix and the active ingredients of the NPs, as well as the redispersibility of the nanocomposites. Instead of solvent evaporation (as in spray drying), atomized droplets created by the spraying are instantly frozen in liquid nitrogen. The particles are lyophilized to remove the solvent and to create porous spherical particles suitable for inhalation. Alternatively, a cold gas can be used to both freeze and dry the particles [149].

Cheow et al. [150] reported a spray-freeze drying method to prepare nanocomposites of thermally sensitive polycaprolactone (PCL) NPs, because the low melting point of PCL limits the use of spray drying due to the high temperature requirement. Their results showed that nanocomposites produced by spray-freeze drying exhibited higher aqueous redispersibility than nanocomposites of the same formulation obtained by spray drying. Two different excipients were used to stabilize the nanocomposites during the spray-freeze drying process, mannitol and polyvinyl alcohol (PVA), with variable NP-to-excipient ratios (4:1, 3:2, and 3:7). Increasing the

mannitol concentration in the feeding solution from 0 to 70% enhanced the redispersibility from 30% to 85%. The best redispersible nanocomposites were obtained with high PVA concentrations (60% to 70%) in the feed solution.

- Controlled flocculation and milling

Controlled flocculation has been used to prepare nanocomposites of different active ingredients: budesonide [151], ciprofloxacin [152], paclitaxel [153], diatrizoic acid [154] and nifidipine [155]. NPs were prepared by antisolvent precipitation (budesonide, diatrizoic acid, paclitaxel, and nifidipine) or sonication of colloidal solution (ciprofloxacin). The main flocculating agents used to induce NP agglomeration were a solution of L-leucine (1%, w/v) and solid sodium chloride crystals. The amount of L-leucine added was adjusted to produce an AI-to-leucine ratio of 1:1. The L-leucine solution was added slowly to the NP suspension during homogenization, and then the flocculated NP suspension was lyophilized to a dry powder. The MMAD for budesonide nanocomposites prepared under the aforementioned experimental settings was 2.1 ± 1.8 μm, which is suitable for deep lung deposition [151]. The dissolution rates of nanocomposites in all studies were faster than those of unprocessed drug and slower than those of pure NPs.

Aillon et al. [156] reported a wet milling procedure to prepare nanoclusters of N1177 (a diatrizoic acid derivative) to be used through pulmonary delivery as a contrast agent for thoracic computed tomography (CT). Drug suspension samples were collected at different intervals of the milling procedure. The results showed that particles decreased in size within the first 30 min, yet increased in size over the next 2 hours. During this process, discrete NPs were not observed in the suspension, rather, they appeared to be agglomerated into low density clusters. No excipients other than the grinding media were used. The milling procedure was followed by lyophilization

to convert the nanocluster suspension into a dry powder for inhalation. The reported MMAD of the final nanoclusters was 4.2 ± 0.1 μm and the FPF<5.7μm was 75 ± 1%, characteristics suitable for deep lung deposition.

1.4.2. Microparticle carriers

Microparticle carriers can be used as vehicle for NPs for pulmonary delivery [157]. In this approach, deep lung deposition is achieved by loading NPs in microparticle carriers that possess optimal dispersibility and deposition properties. Sham et al. [158] reported a spray drying technique of loading different types of NPs, gelatin, and PIBCA into lactose microparticles. The MMAD of the resultant microparticles was 3.0 ± 0.2 μm and FPF<5.6μm was 40%, characteristics suitable for deep lung deposition. An NP size increase of about 30% was noticed after the spray drying process. The size of the NPs in the droplet, droplet size, droplet viscosity, drying temperature, gas flow rate, and the addition of surfactant all crucially affect the morphology of microparticle carriers produced by spray drying [159].

During the spray drying process, NPs are exposed to harsh physical conditions such as thermal stress during droplet drying, high shear stress in the sprayer nozzle, and high adsorption at the greatly expanded liquid/air interface of the spray solution [160]. These conditions might affect both the polymer matrix and the active ingredients of the NPs, and the redispersibility of the nanocomposites. Instead of solvent evaporation (as in spray drying), atomized droplets created by spraying are instantly frozen in liquid nitrogen, this process is called spray-freeze drying. The particles are lyophilized to remove the solvent and create porous spherical particles suitable for inhalation. Alternatively, a cold gas can be used to both freeze and dry the particles [149]. The main advantages of spray-freeze drying over spray drying are prevention of NP aggregation at an evaporation front during particle formation, and avoidance of elevated

temperatures which improves the stability of both the polymer and active ingredient [161]. Similar to spray drying, the freeze-drying process could destabilize NPs. During the freezing of a sample, there is a phase separation into ice and cryoconcentrate containing the NPs, which promotes NP aggregation [162]. Therefore, use of a cryoprotectant such as dextran is warranted during lyophilization to avoid NP aggregation. Different parameters of the spray process (such as type of polymer and pH of the aqueous dispersion) and their effects on the quality of the NP dry powder have been studied [163].

The purpose of the pharmaceutical formulations discussed above is to carry NPs and deposit them deep in the lungs. Thereafter, NPs are supposedly released and readily redispersed without a significant increase in size. Spray-drying or spray-freeze drying results in variable amounts of NP aggregation and, thus, a delay in the redispersibility process and an increase in NP size. Therefore, excipients such as a fast dissolving matrix (spray-dried lactose and mannitol, cyclodextrins) [134, 148], water-soluble polymers (PVA and PEG 6000) [158] , or different surfactants (pulmonary surfactant components and polysorbate-80) can be used to enhance redispersibility [140].

An approach developed by Ely et al. [164] depends on adding an effervescent pair in the formulation during the spray drying process. Upon spray drying, microcarrier particles that contain NPs will possess effervescent properties that allow them to actively release NPs once they are in contact with any source of water or humidity, such as the physiological fluids in the lungs. The effervescent components used were citric acid and anhydrous sodium carbonate. Citric acid was added to a PIBCA NP dispersion to form mixture (A), and ammonium hydroxide (ammonia) solution with anhydrous sodium carbonate was added to a solution of spray-dried lactose monohydrate to form mixture (B). Mixtures (A) and (B) were mixed immediately before

the spray drying process. The role of the ammonia solution was to inhibit the effervescent reaction prior to the spray drying process; it was later removed because of its low boiling point (about 38 ºC). SEM and confocal microscopy images showed microcarrier particles with diameters under 5 μm, spherical in shape, and with NPs distributed continuously throughout the matrix. The average MMAD for effervescent carrier particles smaller than 5.6 μm was 2.17 ± 0.42 μm, the FPF<5.6μm was approximately 46.47 ± 15% and the geometric standard deviation (GSD) was 2.00 ± 0.06. Upon exposure to humidity, the dry powder actively released NPs through gas bubbles with an average diameter of 30 μm, produced by the effervescent reaction as shown in Fig. 1. The size of the NPs was not affected by the spray drying technique, thus NPs released from the effervescent dry powder were similar in size to NPs observed before spray-freeze drying.

In order to avoid the disadvantages of spray drying, Azarmi et al. [165] used the same technique as described above, but replaced spray drying with spray-freeze drying and tested the tolerability of the effervescent powder *in vivo* using animal models. For this purpose, blank NPs were loaded in effervescent microparticles of lactose monohydrate using spray-freeze drying as shown in Fig. 2. The microcarrier particles showed optimum MMAD (4.80 ± 2.12 μm) and redispersibility properties (157 ± 12 and 162 ± 16 μm) before and after spray-freeze drying, respectively).

1.5. Toxicity of inhalable NPs

Inhalable nanotoxicolgy is an emerging field that focuses on the safety and tolerability of inhaled foreign nano-sized particles. The inhaled nano-sized particles could be part of the pharmaceutical treatment or as a result of air pollution and natural phenomena. The physio-

chemical characteristics of NPs make them potentially more reactive, raising concern about possible adverse effects in humans.

The delicate composition of the alveolar space should remain unchanged and be kept intact after delivery of any inhalable treatment including NPs. In the alveolar space, a thin film of lung surfactant composed of phospholipids and proteins covers the epithelium [166]. The main component of the film is 1,2-Dipalmitoyl-sn-Glycero-3-Phosphocholine (DPPC), a phosphatidylcholine with two saturated 16-carbon fatty acyl chains [167]. This phospholipid is a key factor for controlling the surface tension and the gas exchange process in the alveolar sacs [168]. Moreover, the ability of the lungs to function properly depends on the integrity of this surfactant layer [169]. An extremely relevant process is the interaction at the nano-bio interface. This interaction occurs primarily between NPs and proteins, the main biological molecules present in body fluids. The biological interface in the lungs consists largely of phospholipids, and is not static but described as being in continuous movement (association and dissociation of the molecules that at a certain point reach equilibrium)[170]. The analysis of the interaction between the pulmonary surfactant interface and NPs is of importance because dire consequences would result if such drug delivery systems were to destabilize the surfactant film coating the alveoli.

In vitro, lung-surfactant model systems have been developed to study the impact of NPs on the surfactant layer [171]. Using similar systems, the interaction of different NPs with the lung surfactant film was investigated [166]. In these experiments, a film of DPPC lipid monolayer was used to mimic the surfactant layer of the respiratory tract *in vitro*. The effect of NPs on the integrity of the surfactant film after deep lung deposition was investigated. Such interactions might cause dosage-form related incompatibilities and are important for the evaluation of the feasibility of pulmonary delivery of NPs. The incorporation of the particles into

the lipid film was dependent on their size and had a measurable impact on the surface tension of the lipid layer; however, the study also showed that NPs do not significantly destabilize the surfactant film reflecting a relative tolerability of inhalable NPs [166].

Changes in the surface pressure-area isotherms induced by NPs were recorded and might be used an indicator for interactions of NPs and components of the surfactant model [167]. The correlation between the *in vitro* and *in vivo* results has yet to be studied and established. Moreover, the tolerability of other additives that might be used to decorate or remodel the NPs should also be investigated.

Coating NPs with a hydrophilic surfactant such as polysorbate 80 has been used extensively to produce long-circulating NPs. Hydrophilic coating of NPs changes the physicochemical characteristics of NPs [93, 172]. This inhibits opsonization, which is the precipitation of antibodies and other proteins on the surface of NPs. This strategy was shown to successfully prolong the circulation time of NPs [173, 174] and also enhanced the distribution of NPs to some organs such as the brain [63]. Using polysorbate 80-coated NPs for pulmonary delivery may be associated with increased bioavailability since inhaled NPs may have a greater chance to evade alveolar macrophages; however, the delicate composition of the alveolar space should stay unchanged and kept intact after delivery of any inhalable treatment including NPs. Therefore, any pharmaceutical modification on an existing pulmonary delivery system has to be test for tolerability and safety

1.6. Distribution of inhalable NPs

After settling in the alveolar spaces, the fate of inhalable NPs is determined by their size and surface characteristics. A portion of the inhaled NPs—mainly the ultrafine NPs (about 20

nm)—evades macrophages and translocates out of the alveolar spaces to other lung tissues and to the general circulation [175]. Larger NPs are expected to be retained in the lung or cleared by alveolar macrophages, similar to other foreign objects brought into the lungs during breathing [176].

The distribution of the inhalable NPs after pulmonary delivery has been studied in healthy animal models. Inhalable rifampicin-loaded PLGA NPs showed a prolonged rifampicin presence in the lungs, with detectable drug levels up to 8 hours after pulmonary delivery in guinea pigs [122]. Tomoda et al. [177] studied the bodily distribution of TAS-103 (an anticancer agent) after pulmonary delivery in the form of nanocomposites; the TAS-103 concentration in the lungs was 13 times higher than the lung concentration after *i.v.* injection of the same dose. Another study found gold colloid particles, posinhalation, in endocytic vesicles, in alveolar epithelial cells (types I & II) and in phagocytotic vacuoles [178]. These results suggest the importance of both transcytosis of NPs across the alveolar epithelium and migration of particle-loaded alveolar macrophages to different parts of the lungs and to extrapulmonary organs. In one study, solid lipid nanoparticles (SLNs) were labeled using 99mTc and administered to the lungs using a nebulizer. The results showed that after 4 hours postinhalation only 25% of the total radioactivity was retained in the lung; the rest of the radioactivity was spotted mainly in the lymph nodes (para-aortic, axillary, and inguinal) followed by the MPS organs including the liver [130]. However, pulmonary disease, such as lung cancer and TB, is expected to affect the distribution and fate of inhalable NPs after pulmonary delivery [179].

The functionality and physiology of organs are altered due to chronic diseases. In cancer, there are essential changes that may affect the success of any treatment. Unlike normal cells, cancer cells multiply in a microenvironment associated with chronic inflammation that is

generally caused by inflammatory cytokines [180]. These cytokines attract alveolar macrophages that infiltrate the tumor tissue and turn them into tumor-associated macrophages (TAM) [181, 182]. Moreover, as mentioned earlier a tumor is associated with poor lymph draining due to the lack of a well-defined lymphatic system. This may delay the lymphatic uptake of the inhalable NPs and result in longer retention time in the lungs [52]. Therefore, investigating the bodily distribution of inhalable NPs after pulmonary delivery in a cancer-bearing animal model may help generate better understanding of the mechanism and the site of action. Moreover, the results could indicate if the formula used for the inhalable powder requires modification to enhance deep lung deposition and NPs redispersibility after pulmonary delivery.

1.7. Rationale, hypothesis and objectives

1.7.1. Rationale

Lung cancer is a leading cause of cancer death in men and women. According to the Canadian Cancer Society, it is expected that 25,600 Canadians will be diagnosed with different types of lung cancer and in 2015, unfortunately, 20,000 will not survive. Late diagnosis and the lack of effective treatments are responsible for the high mortality rate [183]. The design of a successful cancer treatment mandates a thorough understanding of the complexities of cancer including the cancer microenvironment and the numerous cellular interactions. Due to their appealing physiochemical characteristics, NPs are considered as a potential delivery system for cancer treatment. Nevertheless, after their *i.v.* administration NPs have to overcome several physiological and cellular barriers especially before they reach the site of action. In the case of lung cancer, it would be advantageous to deliver the medicated NPs as close as possible to the location of the cancer in the lung. A pulmonary route of administration would thus save NPs some physiological hurdles, such as wide bodily dissemination and interactions with a wide

variety of blood borne cells and enzymes. However, this route might also impose some difficulties such as achieving deep lung deposition, rapid cellular uptake by alveolar macrophages, tolerability and pulmonary toxicity.

As part of the MPS, the lungs are extremely rich with alveolar macrophages which form a portion of the organ's innate immunity [184]. It is therefore inevitable that inhalable NPs will become in contact with the alveolar macrophages located at the alveolar sacs. This interaction may consequently affect the efficacy of inhalable NPs in many ways. It has been shown that macrophages undergo cellular and metabolic changes before, during and after phagocytosis processes [185]. Moreover, it has been shown that translocation of NPs, intra and extra-pulmonary, is significantly attributed to macrophages [186]. Therefore, it is important to investigate the effect of macrophages and the macrophages cellular changes that are induced by NP exposure on cancer rejection.

In addition to cellular interactions and translocations, the delicate composition of the lungs at the alveolar level raises the concern of the tolerability and safety of any new inhalable delivery system. The integrity of the surfactant layer at the alveolar spaces is crucial to maintaining lung function and gas exchange during breathing [187]. Therefore, the pulmonary toxicity of any new inhalable delivery system and the physiochemical properties that might have an influence on this specific toxicity should be investigated [188]. The *in vivo* investigation of pulmonary toxicity is expensive, time consuming and demands substantial ethical attention. Therefore, new studies have utilized *in vitro* methods to assess the pulmonary toxicity of inhalable delivery systems, including those utilizing NPs [189]. One of the commonly used *in vitro* methods uses a Langmuir trough to study the changes in the Surface Pressure-Area Isotherm of a monolayer film before and after the addition of NPs [190, 191]. However, the

results of pulmonary toxicity obtained by *in vitro* methods have been not validated with *in vivo* animal models.

The importance of macrophage-NP interactions, and thus the effect of these interactions on the efficacy of any treatment delivery method utilizing NPs, raises the importance of real-time assessment. Additionally, the previously available methods for accessing macrophage-NP interactions require modification of the NP formulation to accommodate a fluorescent tag [192]. Therefore, it is essential to develop new methods that have the ability to both use unmodified NPs and evaluate the interactions dynamically. As discussed earlier, macrophages undergo metabolic changes during the phagocytosis processes, and obtain a different cellular heat exchange pattern. Isothermal microcalorimetry, when associated with proper cell-culture technique, may present as a potential universal analytical technique that can be utilized for this purpose.

After the *in vitro* investigation for the effect of NPs on macrophages and the tolerability of inhalable NPs, the next step is to carry these NPs to the site of action, the lungs. The potential of using inhalable NPs for lung cancer treatment can be limited by their inappropriate flowability properties [193]. In order to achieve deep lung deposition, NPs have to be loaded in a carrier with an appropriate MMAD. The pharmaceutical formulation procedures that are utilized for this purpose might result in NP agglomeration [194]. The agglomeration of NPs will change the preferable size and surface characteristics [195]. Therefore, the optimal delivery system for inhalable NPs should have appropriate flowability characteristics to achieve deep lung deposition, yet be able to release the NPs with insignificant changes in their physiochemical characteristics. Including an effervescent pair in the microparticles of lactose will help to actively release the NPs after deep lung deposition. Moreover, the efficacy of inhalable NPs should be

validated in an animal model, and the added benefit of adding effervescent technology to microcarrier particles should be compared with non-effervescent particles. Finally, the distribution of the NPs after pulmonary administration should be investigated with the results discussed in the light of the animal study.

1.7.2. Hypothesis

The present work was designed to test the following hypotheses:

(i) NPs have the ability to activate macrophages. This activation will benefit the efficacy of NPs for cancer treatment.

(ii) The tolerability of NPs is mainly related to the additives used in the NP formulation. Using changes in the Surface Pressure-Area Isotherm of DPPC monofilm may be valuable for screening the pulmonary toxicity of NPs *in vitro* before advancing to experiments in the animal model.

(iii) Different NP formulations will change the affinity of macrophages towards NPs. Isothermal calorimetry might be a potential technique to monitor NP-macrophage interactions, depending on the change of the thermal profile of the macrophages.

(iv) Inhalable NPs may be used as a potential treatment for lung cancer. Using effervescent technology may provide an added benefit to the efficacy of inhalable NPs.

(v) After pulmonary delivery, inhalable NPs are able to achieve deep lung deposition and are able to distribute over the lung.

1.7.3 Objectives

The specific objectives of the present work are:

(i) To study the ability of activated macrophages to decrease the viability of cancer cells using a co-culture system, and to compare the results with those using the naïve macrophages.

(ii) To investigate the mechanism by which activated macrophages exhibit cancer cell killing properties, by investigating two mechanisms: (a)- the ability of macrophages to release back NPs after phagocytosis, and (b)- changes in the cytokine releasing profile.

(iii) To study the tolerability of NPs after pulmonary delivery, *in vitro* using the Surface Pressure-Area Isotherm, and *in vivo* in an animal model. The effect of using polysorbate-80 as a coating material on the pulmonary toxicity will be investigated and correlated to the *in vitro* and *in vivo* results.

(iv) To study the capability of ITMC to study phagocytosis and to compare the results with flow cytometry. The changes in the formulation are achieved by coating NPs with polysorbate-80 or by using mannose to decorate the NP surface.

(v) To assess the efficacy and the cardiotoxicity of DOX-loaded inhalable NPs as a lung cancer treatment in an animal model. Moreover, to compare the results obtained from effervescent and non-effervescent microparticle carriers.

(vi) To study the distribution of inhalable DOX-loaded NPs after pulmonary delivery using whole body autoradiography and confocal microscopy.

CHAPTER 2 – MATERIALS AND METHODS

2.1 Secondary cytotoxicity of NPs mediated by alveolar macrophages

2.1.1 NP preparation and characterization

PIBCA NPs were prepared using an emulsion polymerization method described previously [88, 196]. 100 mg of dextran was added to 10 mL of 0.01 N hydrochloric acid, then 100 µL of isobutyl cyanoacrylate monomer was added under continuous stirring at 500 rpm. The final NP dispersion was filtered using a 0.8-µm-nucleopore® membrane filter from Whatman (Ontario, Canada) under vacuum. Concentrations of the NP dispersions were determined using a gravimetric method. Then, 1 mL of NP dispersion was placed in a porcelain dish and the sample was heated at 60 °C until it was dry, and the difference in weight was used to calculate the NP dry matrix weight [196]. DOX-loaded NPs were prepared by adding 2.4 mg of DOX in a 2 mg/mL solution 30 min after addition of the monomer. The mixture was stirred continuously for 4 h in the dark. The loading efficiency was determined by calculating the difference between the added amount of DOX and the unbound fraction of DOX. The unwashed NP dispersion was centrifuged at 17,000 rpm for 10 min using a 5415C® microcentrifuge from Eppendorf (Hamburg, Germany). The supernatant was separated and analyzed for free DOX. The centrifuged NP pellets were separated and dried, and the weight was used to calculate the loading capacity. The loading efficiency was 80% and the loading capacity was 9.6 mg/100 mg of NPs. These values are in agreement with which was reported previously [54, 197]. The loading capacity value was used later to calculate the DOX concentration for the primary toxicity study. Particle size and zeta potential were measured by photon correlation spectroscopy using a Zetasizer HAS 3000 from Malvern (Worecestershire, UK). The Z-average value was used to express the mean hydrodynamic particle size in nm, and the polydispersity index was used to

indicate the width of distribution. The final NP preparations were tested for endotoxin presence using an E-Toxate™ Kit (Sigma, Canada).

2.1.2. Cell culture

Murine alveolar macrophages (MH-S) and human non-small cell lung carcinoma cells (H460) were cultured in 25-ml ventilated flasks (Corning, USA) using RPMI-1640 medium supplemented with 0.11% sodium pyruvate, 1% nonessential amino acids, 1 mM HEPES buffer, 0.15% sodium bicarbonate, 100 IU/ml penicillin, 10 μg/ml streptomycin, and 10% heat inactivated fetal bovine serum. Cells were maintained in a humidified incubator at 37 °C in an atmosphere containing 5% CO_2.

2.1.3. Primary cytotoxicity and EC_{50} values of treatments

The primary cytotoxicity of four different treatments, DOX solution, blank NPs, mixture of blank NPs and DOX solution, and DOX-loaded NPs, on both MH-S and H460 cells was assessed using MTT assay. Briefly, the cells grown in flasks were washed with phosphate-buffered saline (PBS) and trypsinized using 1% trypsin–EDTA. The cells were centrifuged, the supernatant was discarded, and the cells were resuspended in RPMI-1640 complete medium. Approximately 5000 cells were counted using a hematocytometer and seeded in each well of a 96-well plate. The plates were incubated for 24 h at 37 °C under 5% CO_2. After 24 h, the wells were rinsed with PBS, and different treatments were added in serial concentrations. The DOX concentration value was used to indicate the primary cytotoxicity of DOX-loaded NPs and DOX solution. NP concentration, determined based on the dry weight of PIBCA polymer, was used to refer to the primary toxicity of blank NPs. Blank NPs had the same concentration based on dry weight as DOX-loaded NPs for comparison purposes. The treatment was washed off after 1 h,

and the cells were rinsed with PBS three times. Then, 100 µl of 0.5 mg/ml MTT was added to each well. After 2 h, the MTT solution was removed, 100 µl of isopropanol was added to the plates, and the plates were shaken for 1 h. The color intensity of the wells was measured at 550 nm using a bio-Tek EL 312e microplate reader (Winooski, VT). The EC50 of each treatment was calculated using a linear best-fit line.

2.1.4 Secondary cytotoxicity mediated by macrophages

A 24-mm transwell® co-culture system (Costar Inc., USA) was used to evaluate the ability of murine macrophages to mediate the secondary cytotoxicity of different treatments on H460 cells. Each transwell® plate contained 6 wells and 6 inserts, each insert and well were separated by a 0.4-µm porous membrane. Approximately 1 × 105 H460 cells were implemented into the lower compartment of each well, and plates were incubated for 24 h. Aliquots containing EC50 concentrations of different treatments were added to MH-S cells grown in separate flasks. After 1 h, MH-S cells were washed 3 times with PBS, trypsinized, centrifuged, washed again, counted, and then added to the upper compartment. The following macrophage/cancer cell ratios were tested in the co-culture system: 1:10, 1:5, 1:1, 5:1, and 10:1. No treatment of any kind was added to the upper compartment; only macrophages were seeded in the upper compartment. Naïve macrophages, not previously treated, were seeded in the upper compartment, and results were used as control. The viability of the cancer cells in the lower compartment of each well was tested at 1, 8, and 24 h using the MTT assay previously mentioned.

2.1.5 Sample collection

Using the same co-culture system, macrophages incubated with different treatments were seeded into the upper compartment. Samples were collected from the lower compartment, filled with medium after 1, 8, and 24 h, and analyzed for DOX and changes in the cytokine secreting profile.

2.1.6. HPLC analysis

Each sample was added to 250 µl of water, vortexed for 30 s, and centrifuged at 17,000 rpm. Aliquots from the supernatant were analyzed by HPLC. The HPLC system consisted of a 851-AS® auto sampler (Jasco Co., Tokyo, Japan), a LC-600® isocratic pump (Shimadzu Co., Tokyo Japan), and a lichosphere®100 RP18e (5 µm) cartridge (Lichocart, Merck, Germany). Samples were eluted with a mixture of water, acetonitrile, methanol, and phosphoric acid (540:290:170:2) at a flow rate of 1 ml/min. DOX was detected with an FP-920® fluorescence detector (Jasco Co., Tokyo, Japan) adjusted to 460-nm excitation wavelength and 550-nm emission wavelength. This analysis detected free DOX in the samples as PIBCA NPs are not water soluble. To analyze the total DOX—free DOX and DOX attached to NP fragments—samples were treated with 250 µl of acetonitrile and the mixture was vortexed for 2 min to ensure that the cyanoacrylate polymer was totally dissolved before the samples were centrifuged as above, and aliquots of the supernatants were injected into the HPLC system [198]. Appropriate calibration curves were prepared using appropriate serial concentrations of DOX solution. The experiments were repeated three times with two technical duplicates in each experiment.

2.1.7. Cytokine analysis

Changes in cytokine secreting profiles, induced by different treatments, were assessed using a Raybio® cytokine antibody array (Ray biotech Inc., USA). Membranes covered with primary antibodies were incubated with the collected samples overnight at 4 °C in a plastic plate included in the kit, then washed using the buffer provided in the kit. After the antibody–cytokine complexes were formed, membranes were incubated with biotinylated secondary antibodies and then with labeled streptavidin. The membranes were exposed to X-ray film for 5 s, and the film was developed. The intensity of the signal of each spot representing a specific cytokine was evaluated using ImageJ software. The experiments were repeated three times with two technical duplicates in each experiment. Each membrane contained six control spots located on the left-upper and right-lower of each membrane to confirm that the membranes were treated correctly throughout the different experiments. The average reading of the six control spots was used to normalize the reading in each membrane separately. In order to confirm that the cytokines detected in this experiment were excreted from macrophages and were not an artifact of the cell-culturing medium, a cytokine-free RPMI-1640-conditioned medium was used.

2.1.8. Statistical analysis

Statistical analysis was performed using a single factor ANOVA test or T test, as appropriate, with a 0.05 level of significance.

2.2 Pulmonary toxicity of polysorbate-80-coated inhalable NPs

2.2.1 Surface Pressure-Area Isotherm

Experiments were carried out using a custom built small-scale Langmuir trough from Accurion (Göttingen, Germany), changes in surface pressure was measured using a pressure sensor (model PS4, Nima, Coventry, UK) based on the Wilhelmy principle at the air-water interface using the Nima517 software from Nima (Coventry, UK). In the lungs, the surfactant layer exists at the gaseous-surfactant interface with an aqueous subphase [166]. Therefore, in order to simulate this situation, this study was designed to have NPs suspended in the aqueous subphase of the trough with DPPC monolayer film spread on top at the air-water interface. NPs concentration was determined using an evaporation method; a known volume of NPs suspension was taken, the solvent was totally evaporated, the residues were weighted, and the value was used to calculate NPs concentration. Dilutions of NPs dispersion were made to obtain a subphase solution of 1 mg/mL of NPs in purified water. Calculated amount of DPPC from Avanti Polar Lipids (Alabaster, AL, USA) was dissolved in chloroform (ACS grade, Thermo Fisher, Toronto, Canada) to obtain a concentration of 0.75 mg/mL. Drops of DPPC solution were added to the top of the NPs-containing subphase and the solvent was allowed to evaporate for 10 min before recording isotherms. All experiments were performed at 5 cm^2/min compression rate. The trough was cleaned between experiments with acetone, methanol, hexane, and chloroform followed by purified water for several times. Data was transferred to Microsoft Excel and plotted as area ($Å^{2/}$molecule $\times 10^3$) versus surface pressure milli-Newton per meter (mN/m) [171]. The surface pressure-area isotherms of DPPC on the top of subphase of purified water alone or purified water containing polysorbate 80 at concentration of 0.01 mg/ml were recorded and considered as

controls for further comparison. Each experiment was repeated five times and average values were reported.

2.2.2. Animal study

The animal study was approved by the Animal Care Committee at the Cross Cancer Institute. Coated and non-coated inhalable NP powders were administered to 6-7 week-old Balb/c nude mice. The animals were divided into two different treatment groups and one control group, each treatment group received either:

1 mg non-coated inhalable NPs powder (n = 4)

1 mg polysorbate-80-coated inhalable NPs powder (n = 4)

Control group mice (n = 4) received 0.25 mL of air which is the same volume used for powder insufflation in the treatment groups for each mouse. Animals were anesthetized with intraperitoneal injections of 0.15 ml of a mixture of ketamine/acepromazine/saline. After being anesthetized, each animal was positioned against an angled restraining stand and 1 mg of the designated inhalable NP powder, coated or non-coated, was administered using a DP-4M insufflator (Penn-Century Inc., Philadelphia, PA, USA). In order to accurately determine the amount of the inhalable NPs powder delivered, the insufflator was weighed before and after powder filling, as well as after powder administration. With the help of a fiber optic light, the tip of the insufflator was positioned near the carina (first bifurcation) so that the delivered dose of powder could penetrate deep into the lung. DP-4M device was calibrated to use 0.25 mL of air for each puff. Each mouse was assigned a number according to the group and the type of treatment used. After the administration of inhalable NPs, animal morbidity was closely

monitored using a morbidity score that focuses on changes in breathing pattern. The animals were observed continuously for the first 2 h after administration, then every hour for the following 6 h, then every 8 h for the following day and daily thereafter. Animals were sacrificed when the compiled morbidity score reached a value higher than 10 or any individual item scored a value higher than four. All other animals were sacrificed after 14 days.

2.2.3. Histopathological study

The euthanized mice were dissected, lungs were collected and inflated with 1 ml of 10% neutral buffered formalin and fixed for a minimum period of 24 h. Following fixation, lung tissues were trimmed with a scalpel to a thickness of 2-3 mm and a section of the lung was placed in tissue cassette. These tissues were processed into paraffin, embedded in a paraffin block, sectioned on a microtome to a thickness of 5 μm, placed on a microscope slide, and stained with hematoxylin and eosin stain. A board-certified veterinary pathologist examined the slides and each tissue section was either recorded as normal, or a description was made of any abnormalities. The pathologist was blinded in term of the type of treatment administered previously to each mouse.

2.2.4. Statistical analysis

Data are presented as mean ± standard error of the mean. A one-way ANOVA was used to test for differences among the collapse pressure values of five duplicates for each experiment. The collapse pressure values were compared using Student's t test. NPs characteristics such as size, zeta potential, and MMAD were compared using Student's t test. A result was considered statistically significant at a value $p < 0.05$.

2.3. Microcalorimetric method to assess phagocytosis: macrophage-NP interactions

2.3.1. Cell culture

MH-S cells, a continuous cell line of murine alveolar macrophages, were cultured in 25 mL ventilated flasks (Corning, USA) using DME medium supplemented with 100 mM sodium pyruvate solution, 100 mM non-essential amino acid solution, 1 mM HEPES buffer, 17.8 mM sodium bicarbonate, 100 IU/mL penicillin, 10 μg/mL streptomycin, and 10% (v/v) heat inactivated fetal bovine serum. Macrophages were maintained at 37°C in a 5% CO_2 humidified incubator. In order to prepare the cell culture glass slabs to receive macrophages, the surface of each slab was covered with 250 μL of collagen dissolved in isopropyl alcohol. The glass slabs were left under the laminar flow hood until the alcohol totally evaporated. After the cell culture slabs were prepared, passage #12 of macrophages, cultivated previously in flasks, were trypsinized, counted, and seeded on the surface of the glass slabs; each glass slab received approximately 250,000 cells to achieve a density of about 50,000 cell/cm^2. The glass slabs, with macrophages seeded on the surfaces, were placed in Petri dishes filled with 15 mL of DME medium and maintained in a cell culture incubator for 24 h.

2.3.2. Preparation and characterization of NPs

PIBCA NPs were prepared using an emulsion polymerization method as described in paragraph 2.1.1. Polysorbate-80-coated PIBCA NPs were prepared by adding 0.1 mg of polysorbate-80 to previously prepared uncoated PIBCA NPs under continuous stirring for 4 h [63].

Gelatin NPs were prepared using a two-step desolvation method [199]. 2.5 g of gelatin was dissolved in distilled water under constant stirring (500 rpm) and heating (40°C). The high

molecular weight fraction of gelatin was precipitated in the first desolvation step using acetone. The supernatant was discarded and the precipitated gelatin was dissolved again using distilled water. The pH of the high molecular weight gelatin solution was adjusted to 2.5 using 0.1 M hydrochloric acid and acetone was added dropwise until NPs formed. One hundred microliters of an 8% aqueous solution of glutaraldehyde was added as a cross-linker to stabilize the in situ formed NPs. Acetone remaining in the gelatin NP dispersion was removed by evaporation under vacuum followed by dialysis for 48 h. Mannosylated gelatin NPs were synthesized using the gelatin NP dispersion prepared previously. The synthesis process includes the ring opening of mannose followed by Schiff's base formation [87]. Briefly, a calculated amount of d-mannose was dissolved in 0.1 M acetate buffer (pH 4.0) and added to a gelatin NP dispersion to form a 1:1 w/w ratio. The mixture was shaken continuously at room temperature for 48 h to insure reaction completion. Excess unreacted mannose was removed by dialysis against double distilled water using dialysis tubing (12–14 KDa molecular weight cut-off) for 48 h. The synthesis of mannosylated NPs was confirmed with IR spectroscopy (Nicolet Magna 550 IR spectrometer). After freeze-drying, a small amount of mannosylated gelatin NPs powder was ground with potassium bromide crystals using a mortar and pestle to form a fine, homogeneous powder. A small portion of the mixture was mechanical pressed to form a translucent, thin film. The film was held using two discs of potassium bromide and inserted in the IR spectrometer.

The concentration of NPs dispersions was determined using a gravimetric method. A 1 ml volume of NP dispersion was placed in a porcelain pan and the sample was heated until totally dry. The weight of NPs was calculated by subtracting the weight of the pan from the total weight of pan plus dried NPs. Appropriate dilutions were made to maintain the four different types of NP dispersions at a concentration of 0.1 mg/mL. The size, polydispersity index, and zeta

potential of all types of NPs were assessed using a Zetasizer HSA 3000 (Malvern, Worecestershire, UK). Four different NP formulations were labeled with FITC by adding FITC-dextran during the first step of preparation procedure. The amount of FITC-dextran was calculated to be 1% of the dry weight of the final NPs. Excess free FITC-dextran was removed by dialysis against double distilled water using dialysis tubing (12–14 KDa molecular weight cut-off) for 48 h. The loading efficiency of FITC-dextran was calculated according to the fluorescence difference between the supernatant separated after NP precipitation and the unwashed NP dispersions at 488 nm excitation wavelength and 530 nm emission wavelength.

2.3.3. ITMC and thermal activity

A TAM III was calibrated using a stainless steel ampoule filled with 3 mL of DME medium and the baseline was adjusted accordingly. A cell culture glass slab with macrophages seeded on the surface was transferred to the stainless steel ampoule of the titration cell. The ampoule was filled with 3 mL of DME medium and sealed to the shaft of the titration cell, then inserted gradually in the TAM III channel according to the manufacture's recommendations. The average ($n = 3$) thermal activity recorded during this experiment was considered to be the basic thermal activity of the macrophages. To assess the thermal activity associated with phagocytosis, 100 μL of different NP dispersions of equal concentrations was titrated at 50 μL/min to the ampoule in order to be in direct contact with the macrophages seeded on the surface of the glass slab. This was performed with a Hamilton syringe filled with 250 μL of NP dispersion and connected to the stainless steel ampoule of the titration cell. The experiment was repeated for the four different types of NP-PIBCA (coated and uncoated) and gelatin (mannosylated and non-mannosylated). Each experiment was done in triplicate. The average ($n = 3$) heat exchange associated with each NP formulation was used to calculate the relative interactive coefficient as

described later. Control experiments were performed by (1) titrating the same amount of NPs to a stainless steel ampoule containing a glass slab with no macrophages seeded on the surface and (2) titrating 100 μL of phosphate buffered saline (PBS) into the stainless steel ampoule containing macrophages seeded on a glass slab. The control experiments measured the heat flow associated with the titration process itself, effects of the titration on the thermal activity of macrophages, and side reactions unrelated to macrophage–NP interactions, such as dissolution effect. The thermal activity of control experiments was excluded from the total thermal activity before calculating the relative interactive coefficient. Four positive control experiments were performed using the following mixtures: (1) uncoated PIBCA NPs mixed with 1% w/w of polysorbate-80 for 1 min and used directly, (2) 1% w/w polysorbate-80 solution in distilled water, (3) a 1:1 w/w mixture of mannose and gelatin NPs not chemically bonded, and (4) 0.1 mg/mL mannose solution.

Experiments that included different NP formulations were repeated under the same conditions after adding $2.5 \times 10{-}6$ M Cyto B to the medium in the stainless steel ampoule. This amount of Cyto B was shown previously to inhibit phagocytosis by 50% [200].

The total heat exchange for each experiment was determined by calculating the area under the curve of the thermal activity profiles using the TMA III assistant® program. The relative interactive coefficient of each NP formulation toward macrophages was calculated using the same program after subtracting the basal thermal activity of non-treated macrophages and the thermal activity of other control experiments. In the present study macrophage-nanoparticle interactions were described by the following equation:

$$M + nL \leftrightarrow MLn$$

Where M stands for macrophages and L for NPs.

The interaction between one macrophage with one or more NPs can be considered to proceed in an overall or stepwise reaction path. An overall reaction path is given by:

$M + L \leftrightarrow ML_1$ ß1, ΔH1

$M + 2L \leftrightarrow ML_2$ ß2, ΔH2 where $\beta 1 = \frac{[ML_1]}{[M][L]}$ $\beta 2 = \frac{[ML_2]}{[M][L]^2}$ $\beta n = \frac{[MLn]}{[M][L]^n}$

$M + nL \leftrightarrow MLn$ ßn, ΔHn

Where ßn refers to the overall affinity constant and ΔHn is the reaction enthalpy for the overall reaction.

A stepwise reaction path is given by:

$M + L \leftrightarrow ML_1$ K_1, ΔH_{1s}

$ML_1 + L \leftrightarrow ML_2$ K_2, ΔH_{2s} where $K1 = \frac{[ML_1]}{[M][L]}$ $K2 = \frac{[ML_2]}{[ML_1][L]}$ $Kn = \frac{[MLn]}{[ML_{n-1}][L]}$

$ML_n + L \leftrightarrow ML_n$ K_n, ΔH_{ns}

Where K_n is the stepwise affinity constant and ΔH_{ns} is the reaction enthalpy for the stepwise reaction.

The relation between the stepwise and the overall affinity constants can be found by comparing K_n and $ß_n$:

$ß_1 = K_1$ $ß_2 = K_1K_2$ $ßn = K_1K_2\ K_n\text{-}1K_n$

The relation between the reaction enthalpies for stepwise and overall reactions is described by:

$\Delta H_{1s} = \Delta H_1$ $\Delta H_{2s} = \Delta H_2 - \Delta H_1$ $\Delta H_{ns} = \Delta H_n - \Delta H_{n-1}$

NP concentration and initial cell count were input in the TMA III assistant® program to calculate the affinity constant.

2.3.4. Flow cytometry analysis

The cellular uptake of different NP formulations by macrophages was assessed using flow cytometry. Appropriate dilutions of FITC-labeled NPs were made to obtain the four different types of labeled NP dispersions at a concentration of 0.1 mg/ml using cell culture media. Five milliliter of each diluted FITC-labeled NP dispersion were added MH-S alveolar macrophages cultivated in 75 ml vented flasks. The treatment was discarded after 1 h and macrophages were washed three times with PBS and trypsinized using 1% trypsin-EDTA to obtain a single-cell dispersion. The cells were centrifuged, the supernatant was discarded, and the cells were resuspended in 2 mm EDTA-PBS solution. The final cell suspensions were counted using trypan blue and hemocytometer and the counts were adjusted to 1×10^6 cell/ml. Cell suspensions were filtered with BD Falcon, 5 mL polystyrene round-bottom tube with cell-strainer cap (BD biosciences, USA), and injected into the FACSCalibur. Flow cytometric analyses were performed using a FACSCalibur flow cytometer equipped with a 15 mW argon ion laser emitting at 488 nm for excitation. FITC was detected using FL1 detector, 530 ± 15 nm band-pass filter. Cells were gated according the forward scattering and side scattering to exclude dead cells and cell debris from the analysis. Auto-fluorescence of untreated macrophages on flow

cytometric analysis was used as negative control. All parameters were collected as logarithmic signals. The intensity cut-off of fluorescence was set so that 99% of the untreated macrophages auto-fluorescence was considered negative. The percentage of the macrophages that show positive fluorescence properties was expressed by counting the macrophages that exceed the cut-off value. Data analysis was carried out with CellQuest software obtained from BD Biosciences. Generally, a total of 20,000 cells were analyzed for each one of the four NP dispersions.

2.3.5. Statistical Analysis

Data were expressed as mean ± standard deviation. A one-way ANOVA was used to test for differences among heat exchange and relative interactive coefficient values for different NP formulations. NP characteristics, particle size, and zeta potential were compared using the Student's t test. A result was considered statistically significant at $P < 0.05$.

2.4. Inhalable nanoparticles as lung cancer treatment in mouse model

2.4.1. Preparation of characterization of NPs

Blank and DOX-loaded NPs were prepared and characterized as described in paragraph 2.1.1.

2.4.2. Determination of drug loading efficiency and capacity

The loading efficiency was determined by calculating the difference between the added amount of DOX and the unbound fraction of DOX as previously reported [201]. The unwashed NP suspension was centrifuged at 100,000 g for 10 min using an Airfuge (Beckman, CA, USA). The supernatant was separated and analyzed for free doxrubicin by HPLC. The HPLC system consisted of a 851-AS auto sampler (Jasco Co., Tokyo, Japan), a LC-600 isocratic pump (Shimadzu Co., Tokyo Japan), and a lichosphere 100 RP18e (5 ml) cartridge (Lichocart, Merck,

Germany). Samples were eluted with a mixture of water, acetonitrile, methanol, and phosphoric acid (540:290:170:2) at a flow rate of 1 mL/min. DOX was detected with an FP-920 fluorescence detector (Jasco Co., Tokyo, Japan) adjusted to 460-nm excitation wavelength and 550-nm emission wavelength. The centrifuged NP pellets were separated and dried, and the weight was used to calculate the loading capacity.

2.4.3. Preparation of effervescent carrier particles

Effervescent carrier particles were prepared as described previously [165]. 250 mg sodium carbonate (Sigma, Canada) and 1000 mg spray dried lactose monohydrate (FlowLac 100, Meggle, Germany) were dissolved in 3 mL distilled water and 300 μL ammonium hydroxide 28–30% (Sigma, Canada) was added. The solution was kept in a tightly closed container. Before spray–freeze drying, 200 mg citric acid (Sigma, Canada) powder and 10 mL of nanoparticle suspension were added to the solution. The suspension was spray–freeze dried as following: a two-fluid nozzle (Spraying Systems Co., Wheaton, IL, USA) utilizing gaseous nitrogen at a flow rate of 0.6 scfm was used to atomize the nanoparticle suspension, which was supplied at a flow rate of 37 mL/min using a peristaltic pump (CTP-A, Chem-Tech, Punta Gorda, FL, USA). The nozzle was placed ~ 15 cm above a 600 mL flask containing 300–400 mL of liquid nitrogen. Following spraying, the flask contents were transferred to a Pyrex vacuum beaker, and the liquid nitrogen was allowed to evaporate. The vacuum container was attached to a freeze-dry system (Labconco Corp., Kansas City, USA) operating at 0.004 mbar with a collector at −52 °C. The powder in the flask was held at subzero temperature for 7 h, followed by 41 h at 23 °C. The powder was collected and stored in a sealed vial at 4 °C.

2.4.4. Preparation of non-effervescent carrier particles

For the preparation of nanoparticle loaded non-effervescent carrier particles, 1200 mg spray dried lactose monohydrate (FlowLac 100, Meggle, Germany) was added to the nanoparticle suspension. The suspension was spray–freeze dried as described in paragraph 2.5.3.

2.4.5. Measurement of MMAD

The MMAD of the powder was measured as described previously [165] using a Mark II Anderson Cascade Impactor (Graseby Anderson, Smyrna, GA, USA) with effective cut-off points recalibrated at 60 L/min. A passive dry powder inhaler that utilizes cyclonic action as well as mechanical impaction to disperse powder particles was used to de-agglomerate and deliver the powder [202]. The flow rate was monitored with a pneumotachometer (PT 4719, Hans Rudolph Inc., Kansas City, MO, USA).

2.4.6. Animal studies

Animal studies were approved by the animal ethics committee of the Alberta Cancer Board.

2.4.6.1. Implantation of lung cancer cells

Female 4–5 week old BALB/c nude mice were purchased from Charles River Laboratories (Senneville, Quebec, Canada). The human non-small cell lung carcinoma cell line NCl-H460 obtained from American Type Culture Collection (Rockville, MD, USA) was cultured in RPMI 1640 medium supplemented with 10% fetal bovine serum and antibiotics. On the day of inoculation, cultured cells were trypsinized, washed, and suspended in 0.9% saline. Each mouse received 100 μL of tumor cells with > 95% viability at a concentration of 2×10^6 cells per 1 μL using a 27 gauge needle through the tail vein of anesthetized mice.

2.4.6.2 Treatment protocol

Tumor bearing mice with 5% weight loss were randomized into five different control and treatment groups (as listed below). For administration via inhalation, the animals were anesthetized with ketamine/acepromazine, positioned against an angled restraining stand, and treated once a week for 4 weeks by either:

(i) 1 mg inhalable effervescent nanoparticle powder containing 30 μg DOX (*n* = 16)

(ii) 1 mg inhalable non-effervescent nanoparticle powder containing 30 μg DOX (*n* = 16).

A DP-4M insufflator (Penn-Century Inc., Philadelphia, PA, USA) was used to administer the inhalable powders. The insufflator was weighed before and after powder filling as well as after administration of the powder to determine the delivered dose. The tip of the insufflator tube was positioned near the carina (first bifurcation of the pulmonary tracts) so that the measured dose of powder could penetrate deep into the lung. A fiber optic light (Nikon Inc., USA) was positioned on the animal's chest to visualize the location of the DP-4M device in the animal. For powder delivery, 0.25 mL of air was puffed through the DP-4M device.

For *i.v.* injection, animals were anesthetized by isoflurane and injected via tail vein by one of:

(i) 100 μL of 0.9% normal saline (negative untreated control) (n = 16)

(ii) 30 μg DOX in 100 μL of normal saline (positive control) (n = 8)

(iii) NP suspension containing 30 μg DOX in normal saline (positive control) (n = 8).

Two other control groups were included in the study:

(i) 1 mg inhalable lactose powder containing 30 μg DOX powder (n = 8)

(ii) 1 mg blank inhalable nanoparticle powder (n = 4).

2.4.6.3. Animal monitoring

In order to assess a predetermined level of tumor burden in the lung, during the study period animals were monitored three times a week for weight loss and inactivity in addition to signs of morbidity such as scruffy appearance, listlessness, and compromised breathing. A morbidity scoring sheet was used as previously described [165]. Animals exhibiting higher morbidity scores (> 10 out of 14) were euthanized according to the approved protocol. The study duration was 140 days, at which time the statistical endpoints of survival differences were reached according to the approved study protocol.

2.4.6.4. Histopathological study

During the gross postmortem examination, a set of organs was removed from each animal. Removed tissues were immediately immersed in 10% neutral buffered formalin and fixed for a minimum period of 24 h. Following fixation, tissues were trimmed with a scalpel to a thickness of 2–3 mm and a section of each organ was placed in a tissue cassette. Tissues in cassettes were processed into paraffin, embedded in a paraffin block, sectioned on a microtome to a thickness of 5 microns, placed on a microscope slide and stained with hematoxylin and eosin stain, following standard histology techniques. Slides were examined by a certified veterinary pathologist and each section of tissue was either recorded as normal, or a description was made of abnormalities or findings.

2.4.6.5. MRI imaging

Three mice from each treatment group were selected randomly and MRI imaging was performed to establish the location of the tumor burden. MRI images were acquired with a 9.4 T 21.5-cm horizontal bore magnet equipped with a 12.0-cm inner diameter gradient set (Magnex

Scientific, Oxford, UK) interfaced to a TMX console. A 44-mm inner diameter birdcage coil was used for radiofrequency (rf) excitation and reception. The images are T1 weighted, and transverse spin echo scans were recorded with the following parameters: Echo time (TE)/repetition time (TR) was 13/1500 ms, the bandwidth (BW) was 50 kHz, the field of view (FOV) was 26×26 mm with 128 × 128 matrix, the number of averages was 4, and the thickness was 0.5 mm.

2.4.6.6. Cardiac toxicity of inhaled DOX

To evaluate the effect of local lung delivery of free DOX inhalable powder, an inhalable DOX powder was prepared using a spray–freeze drying technique. Cancer-free mice were treated in the same way as mentioned in paragraph 2.4.6. The animals were divided into 3 groups and treated with either:

(i) 1 mg effervescent DOX inhalable nanoparticle powder containing 30 μg DOX(n = 3)

(ii) 1 mg DOX in lactose inhalable powder containing 30 μg DOX (n = 3)

(iii) Control group (n = 3), untreated.

Effervescent DOX inhalable nanoparticle powder was chosen for this study as it was proven to be the most effective treatment as it will be discussed later in the (Result) section.

To investigate cardiac toxicity, three enzymes that are indicators of cardiac toxicity—aspartate transaminase (AST), alanine transaminase (ALT) and creatine phosphokinase (CPK)—were measured in blood. Blood samples were collected 1 h after insufflation of designated treatment in heparinized glass tube and sent to IDEXX laboratories (Edmonton, Canada) to be analyzed.

2.4.7. Statistical calculation and analysis

The number of mice in each group was calculated to obtain a statistical power of at least 0.8. The Kaplan–Meier curves of the different groups were compared via log-rank tests (Mantel–Cox test). Another statistical analysis was performed using a single factor ANOVA test or Student T test, as appropriate, with a 0.05 level of significance using SSPS Statistics® program (SPSS Inc. Illinois, USA).

2.5. Distribution of inhalable effervescent NPs

2.5.1. NPs and inhalable NPs

Preparation of DOX-loaded PIBCA NPs was performed as described in paragraph 2.1.1. For the preparation of radiolabelled NPs, the DOX solution was substituted with a mixture of regular DOX and radiolabelled ^{14}C DOX (GE Pharmaceuticals, Canada) (10:1) with the total DOX concentration adjusted to 2.5%. The total radioactivity was adjusted to obtain 0.2 MBq/mg in the final inhalable NP powder after a spray-freeze drying process described later. The final nanoparticle dispersion was filtered through a 0.8 μm membrane filter (Nuclepore Track-Etch membrane, Whatman, USA) and stored at 4 °C.

For the preparation of FITC-labelled NPs, dextran was substituted with FITC-dextran during the first step of NP preparation. Excess free FITC-dextran was removed by dialysis against double distilled water using dialysis tubing (12–14 kDa molecular weight cutoff) for 48 hours 15 [192].

The loading efficiencies of ^{14}C-labelled DOX and FITC-dextran were determined by calculating the difference between the added amounts of unbound fractions of ^{14}C DOX and FITC for radiolabelled and fluorescent NPs, respectively. The unwashed NP suspension was centrifuged at 100,000 g for 10 min using an Airfuge (Beckman, CA, USA). Pellets were

separated and the supernatant was analyzed for radioactivity (^{14}C) with a liquid scintillation counter or for fluorescence (FITC) with a fluorescence spectrometer (SPEX FluoroMax-3, Horiba, USA).

Effervescent carrier particles were formulated as described in paragraph 2.5.3. To confirm the radioactivity of the final ^{14}C-labelled effervescent inhalable NP powder, 1 mg of the powder was suspended in 10 ml of scintillant for low energy beta emitters and the activity was measured in a liquid scintillation counter (Packard Tri-Carb, Perkin-Elmer, USA). Sample radioactivity was approximately equivalent to 0.2 MBq/mg.

2.5.2. NPs and inhalable NP characterization

All preparation methods reported in the previous section were replicated using regular DOX to determine NP size and zeta potential and to characterize the mass MMAD of the effervescent inhalable NP powder. Particle size and zeta potential were characterized using a Zetasizer HAS 3000 from Malvern (Worcestershire, UK). 100 μL of the nanoparticle suspension was mixed in 4 mL deionized water and sonicated for 1 min at 25 °C.

The MMAD of the final inhalable powder was measured using a Cascade Impactor (Mark II Anderson, Graseby Anderson, Smyrna, GA, USA) with effective cut-off points recalibrated at 60 L/min. For powder delivery, a passive dry powder inhaler was used. The passive inhaler disperses powder through cyclonic action as well as mechanical impaction. The flow rate was monitored with a pneumotachometer (PT 4719, Hans Rudolph Inc., Kansas City, MO, USA).

2.5.3. Animal studies

Approval of the Animal Ethics Committee of the Alberta Cancer Board was obtained before the study was initiated.

Implantation of lung cancer cells: 9 female 4–5 week old BALB/c nude mice (Charles River Laboratories, Senneville, Quebec, Canada) were used as an animal model. Each mouse was injected with 100 μL of a cell suspension of the human nonsmall cell lung carcinoma cell line NCl-H460 at a concentration of 2×10^6 cells per 1 μL using a 27 gauge needle through the tail vein of anesthetized mice. To prepare the cell suspension, H460 cells were cultured in RPMI 1640 complete medium. On the inoculation day, cancerous cells were trypsinized, washed, and suspended in 0.9% saline for injection.

2.5.4. Inhalable NP administration

Two weeks after inoculation with cancer cells, the mice were divided into three groups: group 1 (3 mice) received 1 mg of inhalable radioactive (0.2 MBq) effervescent DOX-loaded NPs (equivalent to 30 μg of DOX); group 2 (3 mice) received FITC-labelled effervescent inhalable DOX-loaded NPs; and group 3 (3 mice) received 0.2 MBq of ^{14}C-labelled DOX solution. The inhalable NPs in groups 1 and 2 were administered via a pulmonary route and the DOX solution was administered via tail vain injection.

For pulmonary administration of inhalable NPs, animals were anesthetized with katemine/acepromazine, and then positioned against an angled restraining stand. Inhalable NP powder was administered to the lungs using a DP-4M insufflator (Penn-Century Inc., Philadelphia, PA, USA); the insufflator was calibrated to deliver 0.25 ml of air per 1 puff . To ensure the accuracy of the delivered dose, the insufflator was weighed before and after powder filling and after administration of the powder to determine the delivered dose. The tip of the insufflator tube was inserted through the trachea of anesthetized mice and held near the carina (first bifurcation of the pulmonary tract) to ensure the delivery of the total dose of inhalable powder. The position of the insufflator tip was visualized with the aid of a fiber optic light

(Nikon Inc., USA). For *i.v.* injection, animals were anesthetized by isoflurane and the injection was applied using a using a 27 gauge needle through the tail vein of anesthetized mice. Animals in different groups were euthanized by intraperitoneal injection of sodium thiopental solution 1, 8, and 24 hours after treatment. Euthanized animals were handled according to group number. In groups 1 and 3, the whole animal was positioned sagittally in a block of cryoprotective gel of carboxymethylcellulose (Invitrogen, Canada) and flash-frozen in liquid nitrogen. Group 2 mice were dissected and the lungs were isolated and inflated with a cryoprotective gel of carboxymethylcellulose, flash-frozen in liquid nitrogen, and stored at -20 °C for confocal microscopy imaging.

2.5.5. Whole-body autoradiography

In order to sample all tissues, 20 to 25 pairs of sections of 50 µm thickness were collected on tape at different levels in each block with a specially designed cryomicrotome (CM3600, Leica, Canada) cooled at -25 °C. After 32 h of dehydration at -25 °C, the sections were exposed on phosphor screens for one week and then scanned with a Cyclone Phosphor Imager (Perkin-Elmer, USA) [203, 204]. The ^{14}C activity in tissues was scanned as digital light unit per mm^2, with the software OptiQuant v4.0 (Perkin-Elmer, USA).

2.5.6. Confocal laser scanning microscopy

The isolated lungs of group 2 mice were sectioned using a microtome cooled at -25 °C. The tissue cryosections (about 8 µm) were placed on microscope slides (1 × 3 in), mounted with glycerin, and covered with glass covers. Images were recorded with a Zeiss LSM 510 confocal microscope (Oberkochen, Germany) coupled with argon-ion (488 nanometer line), violet diode (405 nanometers), and green helium-neon (543 nanometers) lasers. During the processing stage,

individual image channels were pseudocolored with red, green, and blue (RGB) values corresponding to each of the fluorophore emission spectral profiles.

CHAPTER 3 – RESULTS

3.1 Secondary cytotoxicity of NPs mediated by alveolar macrophages

3.1.1. NP properties

The prepared blank NPs had an average size of 137.22 ± 1.53 nm, the polydispersity index was 0.12, and the zeta potential was −23.5 ± 0.41 mV. No significant changes were observed with DOX-loaded NPs as the average particle size observed was 140 ± 1.98 nm, the polydispersity index was 0.21 and the zeta potential was −21.56 ± 0.32 mV. An E-Toxate™ test indicated that tested NP preparations were endotoxin free.

3.1.2. Primary toxicity and EC50

Fig. 1 shows the primary cytotoxicity of different treatments on MH-S and H460 cells. As expected, DOX-loaded NPs exhibited the highest primary cytotoxicity in both cell lines. Moreover, the EC50s of DOX-loaded NPs were similar, 0.24 μg/ml and 0.26 μg/ml for MH-S and H460 cells, respectively. Furthermore, the primary cytotoxicity of DOX-loaded NPs in both cell lines was higher than an equal mixture of blank NPs and DOX solution. The effect of the mixture was less than the additive cytotoxicity of the individual components. Therefore, the mixture of blank NPs and DOX solution was excluded from secondary toxicity experiments. Although both cell lines, MH-S and H460, showed almost the same sensitivity toward DOX-loaded NPs, blank NPs showed higher cytotoxicity for macrophages than for lung cancer cells, as indicated in Table 1. DOX solution showed significant cytotoxicity in both cell lines; however, MH-S cells were less sensitive than H460 cells.

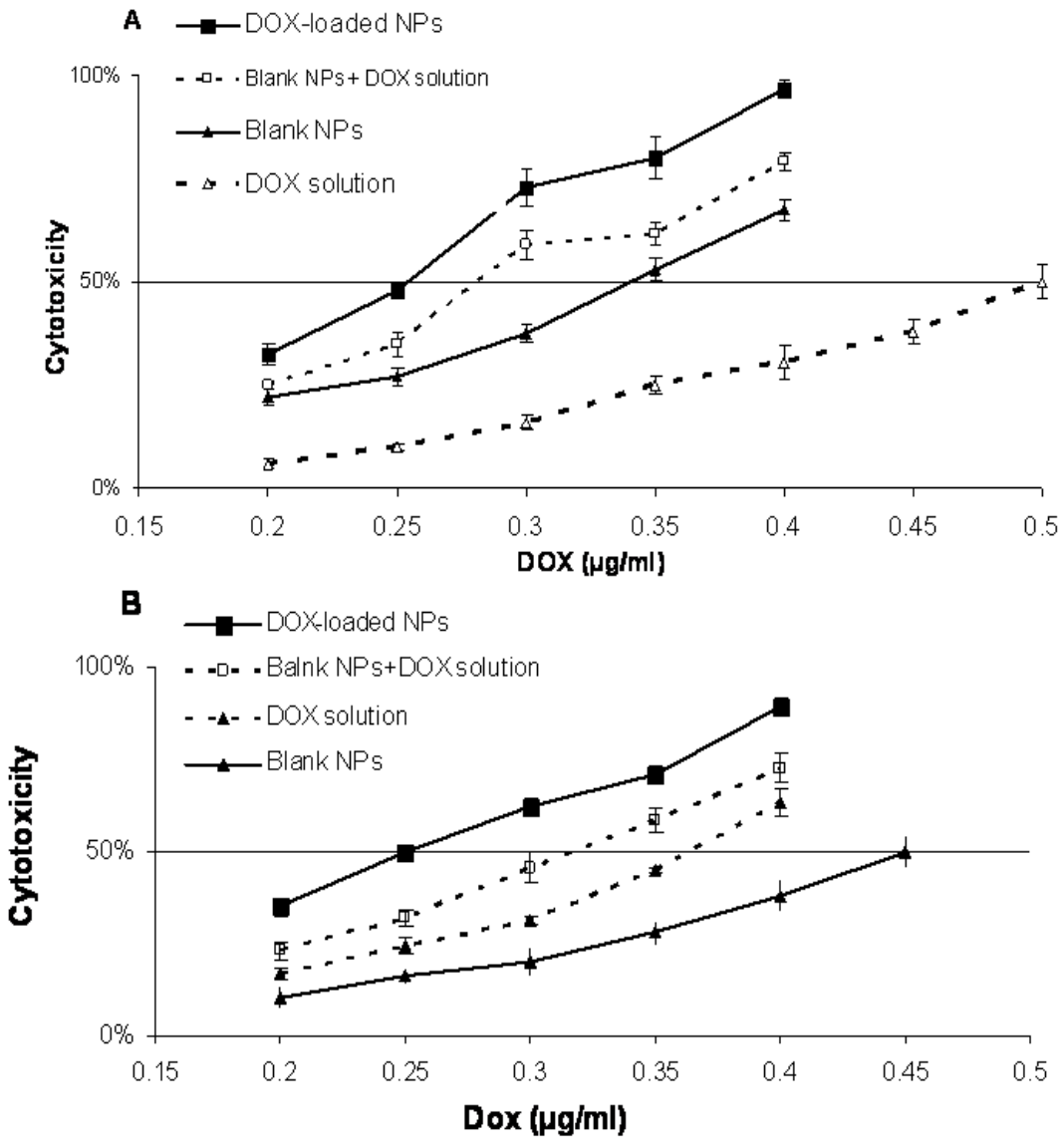

Fig. 1. Primary cytotoxicity of four different treatments: DOX solution, blank NPs, mixture of blank NPs and DOX solution, and DOX-loaded NPs, on MH-S (murine alveolar macrophages) (A) and H460 (human non-small cell lung carcinoma) cells (B). Each data point represents the average of six wells and three separate experiments. The concentration of DOX solution and DOX-loaded NPs was calculated according to the DOX concentration (µg/ml). NP loading capacity value was used to correlate between NP dry matrix and DOX concentration. Reprinted with permission of ©Elsevier publisher

Table 1. The EC_{50} values of different treatment on MH-S cells (macrophages) and H460 cells (lung carcinoma).

	DOX solution	**Blank NPs**	**DOX-loaded NPs**
MH-S cells	EC_{50} of DOX = 0.52 ± 0.02 µg/ml ***** NP dry matrix (N/A)	Blank NP matrix to exert EC50 = 3.54 ± 0.12 µg/ml ***†** EC_{50} of DOX (N/A)	EC_{50} of DOX = 0.24 ± 0.01 µg/ml Equivalent to NP dry matrix of 2.5 µg/ml
H460 cells	EC_{50} of DOX = 0.35 ± 0.01 0.µg/ml NP dry matrix (N/A)	Blank NP matrix to exert EC50 = 4.79 ± 0.18 µg/ml EC_{50} of DOX (N/A)	EC_{50} of DOX = 0.26 ± 0.02 µg/ml Equivalent to NP dry matrix of 2.71 µg/ml

* $P < 0.05$ for the same treatment on different cell lines, † NPs concentration was calculated depending on the value of loading capacity. Reprinted with permission of ©Elsevier publisher

3.1.3. Secondary cytotoxicity of NPs mediated by macrophages

Secondary cytotoxicity was defined as an acquired cytotoxicity exerted by phagocytotic cells on cancerous cells. This special cytotoxicity is described as acquired because it is a result of macrophage exposure to NPs and to the fact that this property was not expressed by naïve macrophages. Alveolar macrophages were proved able to mediate secondary cytotoxicity on H460 cells. The extent of secondary cytotoxicity was dependent on both the type of treatment and the cell ratio used in the two-compartment co-culture system. Low MH-S to H460 cell ratios failed to produce any significant secondary cytotoxicity. The cytotoxicity started to be detectable at a 1:1 cell ratio, but the results were more significant at 5:1 and 10:1 ratios. The last two ratios showed almost the same extent of cytotoxicity with a better reproducibility obtained with a 5:1 cell ratio. Therefore, a 5:1 ratio was chosen for further investigation.

Fig. 2 shows the secondary cytotoxicity induced by different treatments and mediated by macrophages at different time points using a MH-S:H460 5:1 cell ratio. As shown, the DOX solution did not induce alveolar macrophages to cause any secondary toxicity at any time point. On the other hand, macrophages treated with blank or DOX-loaded NPs showed an acquired toxicity against cancer cells after 8 and 24 h. Naïve macrophages did not exert any secondary cytotoxicity against cancer cells and the viability of cancer cells in the lower compartment was comparable with results obtained when no macrophages were added to the upper compartment.

3.1.4. DOX released from macrophages

To further investigate the mechanistic causes of the observed secondary cytotoxicity, samples were collected from the lower compartment and analyzed for both free and total DOX. Total DOX consisted of the free DOX existing in the sample and the fraction of DOX still attached to NP fragments. When macrophages were incubated with DOX solution and seeded in

the upper compartment, no DOX was detected in the sample collected from the lower compartment, whereas free and NP-attached DOX was detected in the samples when macrophages were previously treated with DOX-loaded NPs. This indicated that NP fragments were released from macrophages after DOX-loaded NPs were phagocytized. Fig. 3 shows the amount of free and total DOX detected in the samples collected from the lower compartment after treating macrophages with DOX-loaded NPs.

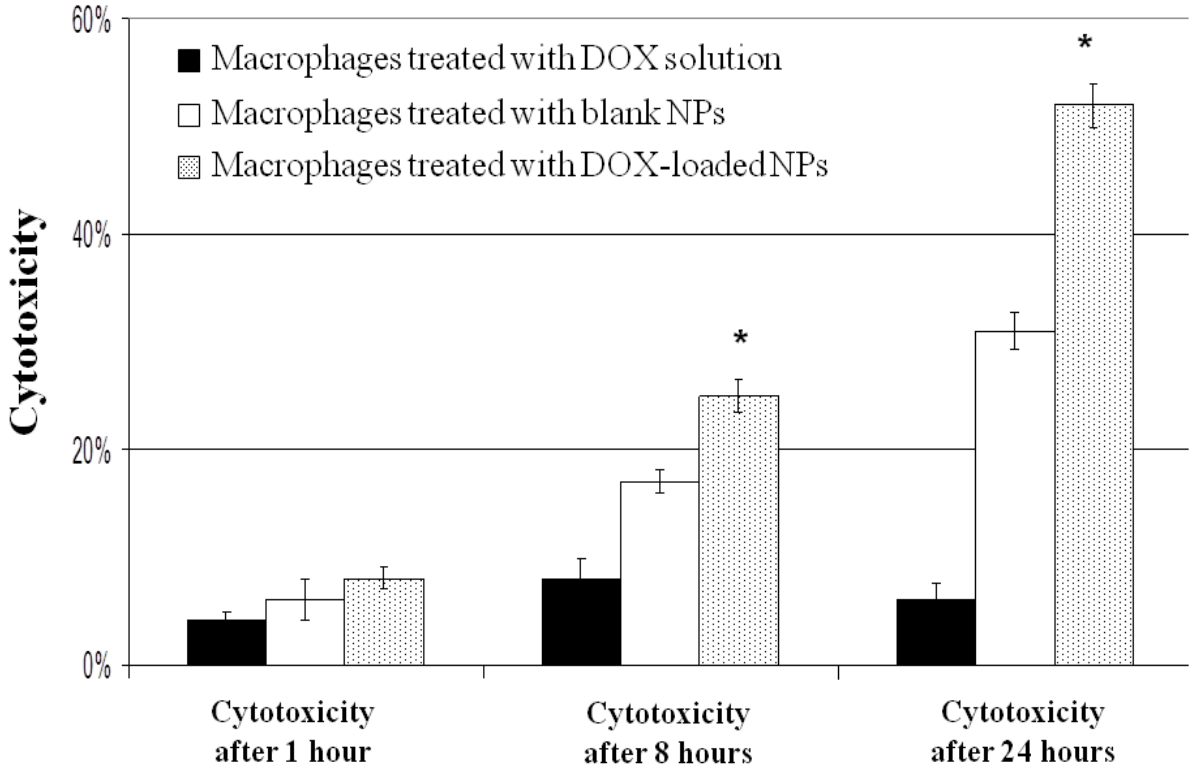

Fig. 2. The secondary cytotoxicity mediated by murine alveolar macrophages (MH-S) on human non-small cell lung carcinoma cells (H460) at a 5:1 MH-S:H460 cell ratio. Macrophages were incubated with EC_{50} aliquots of different treatments for 1 h before being added to the upper compartment of the transwell® co-culture system. Each value represents the average of two wells and three independent experiments (*P<0.05). Reprinted with permission of ©Elsevier publisher

Almost equal amounts of free DOX were detected at all time points with no significant increase after 24 h, whereas no attached DOX was observed in samples collected after 1 h as the total DOX was equal to the free DOX detected. On the other hand, a significant increase in total DOX was detected after 8 and 24 h (Fig. 3).

3.1.5. Cytokine secreting profile

Changes in the cytokine secreting profile of macrophages were investigated after macrophages were exposed to different treatments. The type and the amount of cytokines were closely related to both the type of treatment and the sampling time point. The results showed a significant increase in the secretion of Th1-type cytokines which are known to induce acute inflammation and cell-mediated immune response.

The increase in cytokine secretion was observed after 8 and 24 h and was limited to macrophages treated with blank and DOX-loaded NPs. Monocyte chemoattractant protein-1 (MCP-1), macrophage inflammatory protein-1 (MIP-1), tumor necrosis factor α (TNF-α), and interferon gamma (IFN-γ) all belong to the group of Th1 cytokines (Fig. 4). MCP-1, followed by MIP-1, was the main cytokine triggered by NPs; the increase was about threefold compared with control samples collected at 24 h (Fig. 5). No changes in cytokine secreting profiles were observed over time in naïve macrophages used as control, or in macrophages previously incubated with DOX solution. No significant difference in cytokine secreting profile was observed between macrophages treated with blank or DOX-loaded NPs. Table 2 shows a complete list of the cytokines included antibody array test

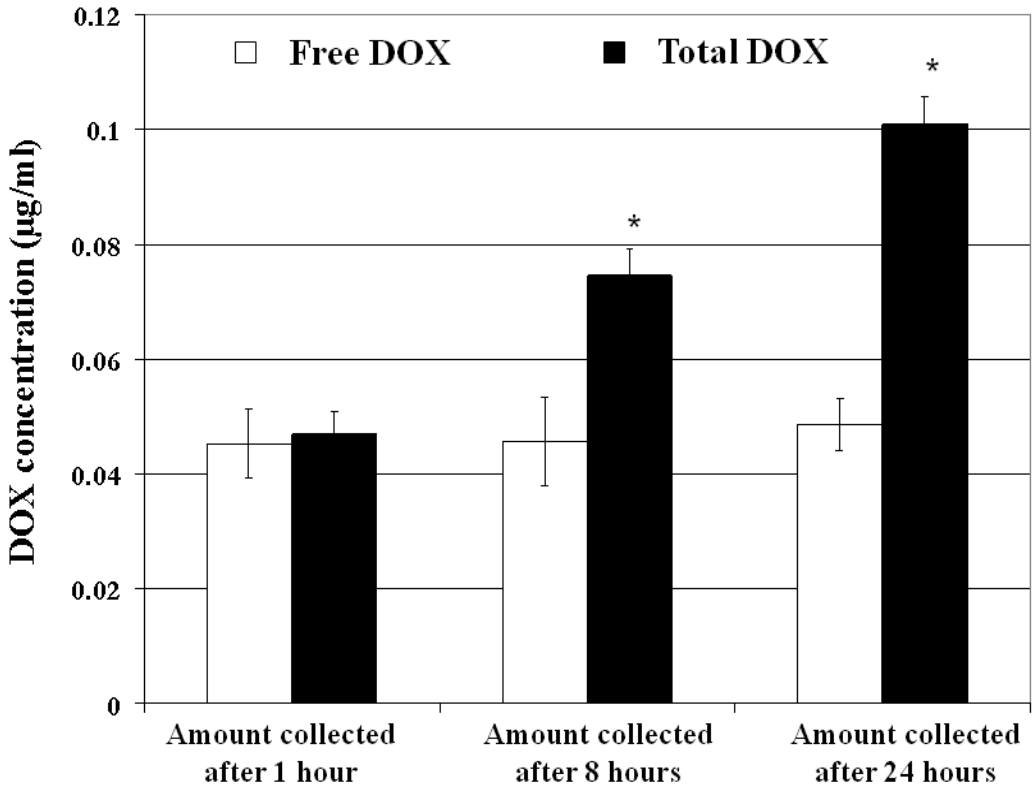

Fig. 3. The amount of free and total DOX detected in samples collected from macrophages treated with DOX-loaded NPs at different time points. Each value represents the average of two technical repetitions of three separate experiments (*P<0.05). Reprinted with permission of ©Elsevier publisher

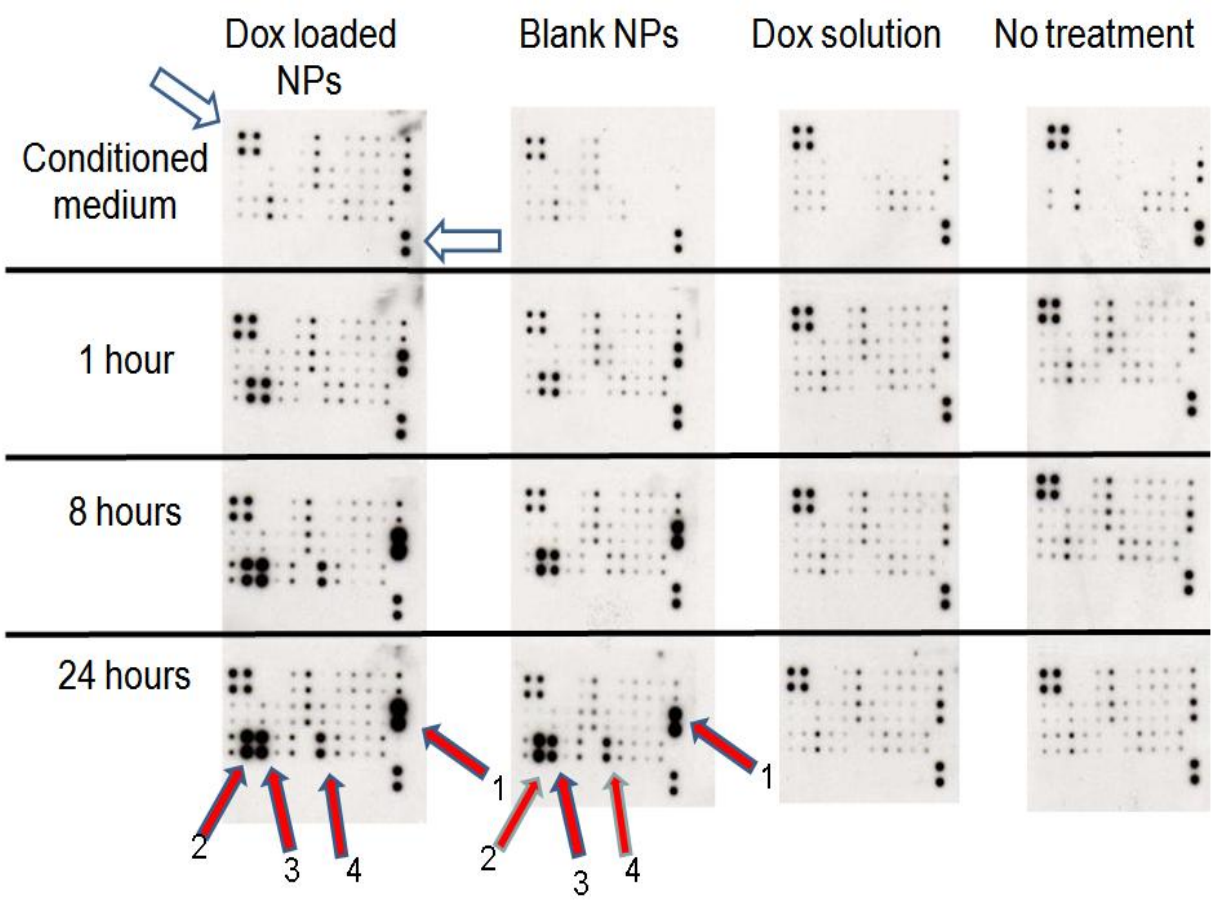

Fig. 4. Blots of the cytokines antibody-array membranes of naïve macrophages (no treatment) and macrophages treated with three different treatments at different time points. Filled arrows point to four different cytokines: MCP-1 (1), MIP-1 (2), TNF-α (3), and IFN-γ (4). Empty arrows point to the control spots in one of the membranes. Reprinted with permission of ©Elsevier publisher

Table 2: A complete list for cytokines included in the antibody array test in Fig.4

Pos	Pos	Neg	Neg	6Ckine	CTACK	Eotaxin	IL-1α	IL-1β	IL-2	IL3	IL4
Pos	Pos	Neg	Neg	6Ckine	CTACK	Eotaxin	IL-1α	IL-1β	IL-2	IL3	IL4
IL-5	IL-6	IL-9	IL-10	IL-12-P70	IL-12	IL13	IL17	TIMP1	KC	Leptin	MCP-1
IL-5	IL-6	IL-9	IL-10	IL-12-P70	IL-12	IL13	IL17	TIMP1	KC	Leptin	MCP-1
MCP-5	MIP-1	TNF-α	RANTES	SDF-1α	TCA-3	IFN-γ	TECK	STNFRI	TARC	Thrombo-poietin	VEGF
MCP-5	MIP-1	TNF-α	RANTES	SDF-1α	TCA-3	IFN-γ	TECK	STNFRI	TARC	Thrombo-poietin	VEGF
blank	blank	blank	blank	lank	blank	blank	blank	blank	blank	blank	Pos
blank	blank	blank	blank	blank	blank	blank	blank	blank	blank	blank	Pos

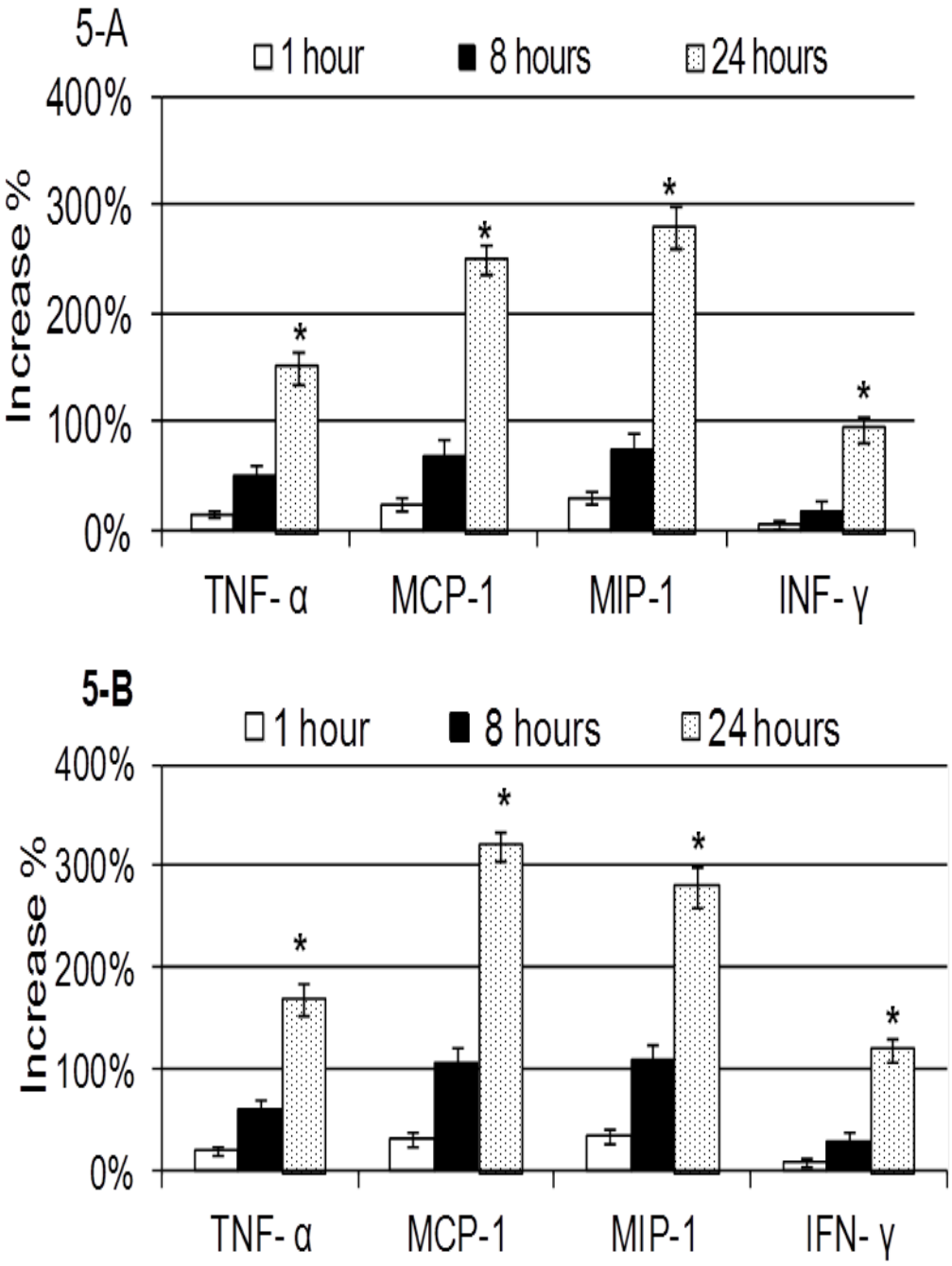

Fig. 5. The increase in cytokine secretion induced by blank NPs (A) and DOX-loaded NPs (B) at different time points. Values are expressed relative to the negative control (conditioned medium). Each value represents the average of two technical repetitions of three separate experiments (*P<0.05). Reprinted with permission of ©Elsevier publisher

3.2. Pulmonary toxicity of polysorbate-80-coated inhalable NPs

3.2.1. NP characteristics

No significant difference was observed between polysorbate-80-coated NPs and non-coated NPs in terms of size and zeta potential. The average size of non-coated NPs was 137.2 ± 1.5 nm, the polydispersity index was 0.12 ± 0.03 and the zeta potential was -23.5 ± 0.4 mV. Coated NPs showed almost the same values for average size and zeta potential, 145.4 ± 3.2 and -24.7 ± 0.2 mV, respectively. The MMAD of the inhalable microparticles loaded with coated and non-coated NPs was 3.2 ± 0.2 and 3.3 ± 0.7 μm, respectively, with 60% as fine powder fraction. These results were similar to those reported previously.

3.2.2. Surface pressure-area isotherm of DPPC film over different subphases

Fig. 6 shows the surface pressure-area isotherms of DPPC monolayers spread on top of different subphases. The subphase varied between purified water, purified water containing 0.01 mg/ml polysorbate 80, or purified water containing1 mg/ml of polysorbate 80 coated or non-coated NPs. The reported data are the average of five duplicates. The surface tension values at different points were statistically compared. Those points were chosen at the beginning and end of different phases of the isotherm. All experiments were reproducible with no significant difference between five runs. The surface pressure-area isotherm of DPPC using purified water as subphase (Fig. 6.a) shows that as compression increases, the monofilm stays in the gas phase until around 95 $Å^{2/}$molecules. This is indicated by the zero surface pressure increase recorded as the molecular area decreased from around 115 to 95 $Å^{2/}$molecules. The increase in the surface pressure detected after 95 $Å^{2/}$molecules is correlated to the rearrangement of DPPC molecules to from a so-called liquid expanded phase.

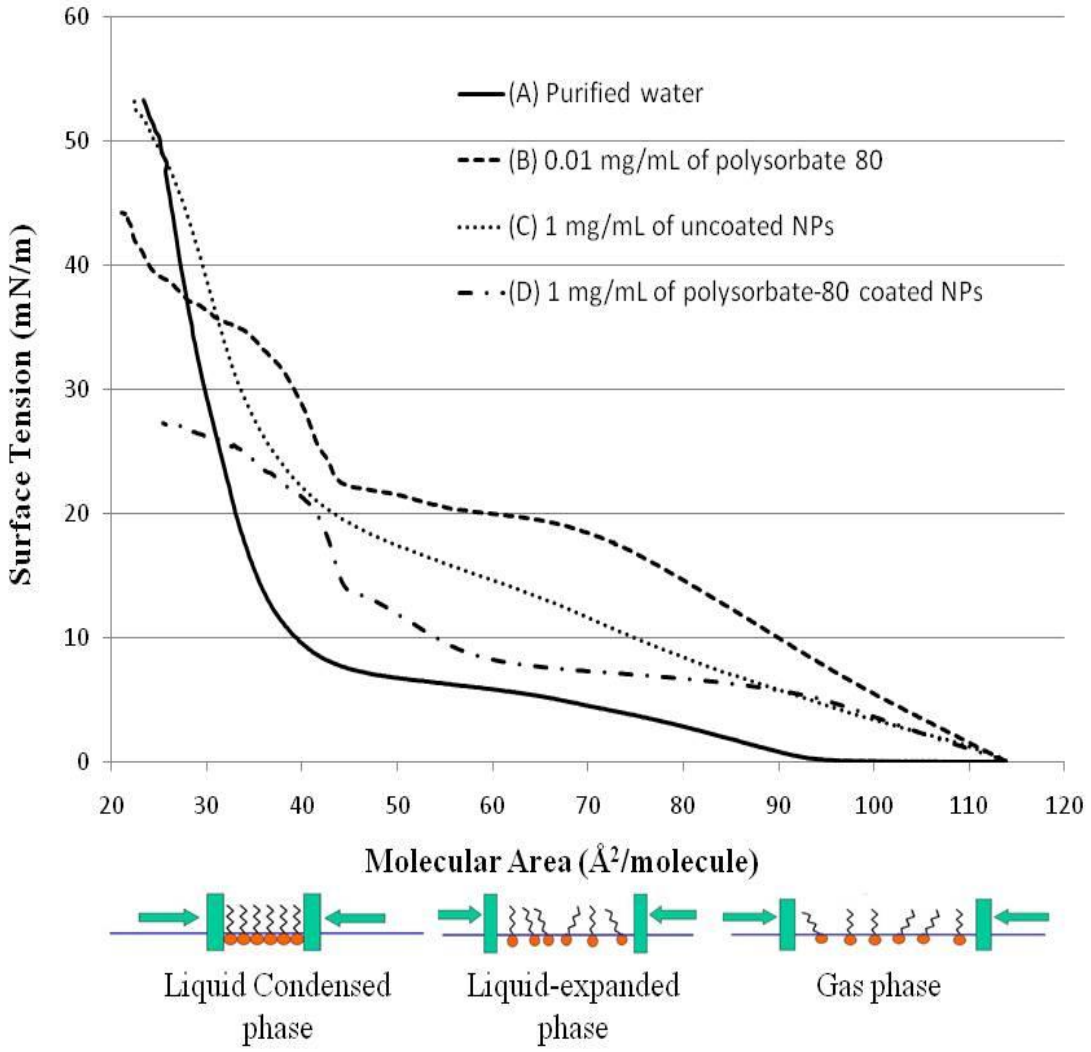

Fig. 6. Surface pressure-area isotherms for 0.75 mg/mL 1,2-Dipalmitoyl-sn-Glycero-3-Phosphocholine (DPPC) on the top of subphase containing **a** purified water, **b** 0.01 mg/mL of polysorbate-80, **c** 1 mg/ml of uncoated nanoparticles, and **d**1 mg/ml of polysorbate 80-coated NPs. Reprinted with permission of ©Springer publisher

A plateau region was seen approximately at 4 mN/m with molecular area of 75 $Å^{2/}$molecule. This plateau region indicates the coexistence of both a liquid expanded and a liquid condensed phase. Further compression shows a steep increase in the pressure as the lipid molecules get packed tightly to an area of about 25 $Å^{2/}$molecule whereby the maximum pressure is reached around 53.4 ± 3.7 mN/m, after which the DPPC monolayer collapsed. Adding polysorbate 80 to the subphase changed the onset of DPPC monolayer phase formation under progressive compression. As shown in (Fig. 6.b), a gradual increase in the surface pressure was recorded directly until a value of 20 mN/M was reached. This immediate response in the surface pressure to the compression indicates that the DPPC molecules are not in a gaseous status but they shift directly upon compression to the liquid expanded phase. Moreover, the addition of polysorbate 80 resulted in a less distinguished plateau region which was also formed at much higher surface pressure (18 and 22 mN/m), when compared to the of additive-free DPPC isotherm. After the plateau phase, the surfaced pressure started to increase sharply in a similar way to what was observed with the DPPC isotherm. The collapse pressure was 45.3 ± 3.1 mN/m. The addition of polysorbate 80 resulted in small difference in the collapse pressure when compared with the DPPC alone, 45.3 ± 3.1 and 53.4 ± 3.7 mN/m, respectively. The isotherm of DPPC monolayer spread on top of a subphase containing non-coated NPs showed different behavior (Fig. 6.c). Neither gas phase nor plateau region were detected which is in agreement with previously published reports [171]. More specifically, an initial increase in the surface pressure was recorded between 0 and 20 mN/m as the molecular area decreased from 115 to 43 $Å^{2/}$molecule. This reflects the formation of a liquid-expanded phase. The initial increase of the surface pressure was followed by a second, but sharper increase to a liquid-condensed phase before a collapse pressure of 53.1 ± 2.4 mN/m was reached. The collapse pressure was not

significantly affected by the addition of non-coated NPs at concentration of 1 mg/ml. Similar to what was observed with both polysorbate 80 and non-coated NPs, the addition of polysorbate-80-coated NPs resulted in a missing gas phase (Fig. 6.d). In contrast to polysorbate 80 and non-coated NPs, the addition of polysorbate-80-coated NPs resulted in a more distinct plateau region of the surface pressure. This plateau region was similar to what was observed with the DPPC isotherm. The plateau region expanded over molecular area values of 95 and 60 $Å^{2/}$molecule with a surface pressure between 7 and 9 mN/m. The coated NPs caused a huge decrease in the collapse pressure as shown in (Fig. 6.d). The recorded collapse pressure value of the DPPC mono-film after the addition of coated NPs was 27.3 ± 2.2 mN/m, which is almost half of what recorded with DPPC film alone. This value was significantly lower than all other recorded.

3.2.3. *In vivo* pulmonary toxicity

According to the approved animal protocol, compiled morbidity scored higher than 10 or any individual morbidity score of 4 requires that the animal will be instantly euthanized to avoid unnecessary suffering. Three mice, out of four, treated with polysorbate 80-coated NPs reached the critical value of 4 within 1 h of administration, and after 2 h for the fourth mouse. These mice exhibited very shallow breathing pattern with slower than 50% of the normal breathing rate. The controlled group and the group treated with uncoated NPs experienced slight changes in the breathing pattern for a very short time and they totally recovered within 3 h, none of these animals had an individual score higher than 2. These mice had no other significant changes in their morbidity scores, e.g., body weight, food intake, or behavioral signs over the duration of the study.

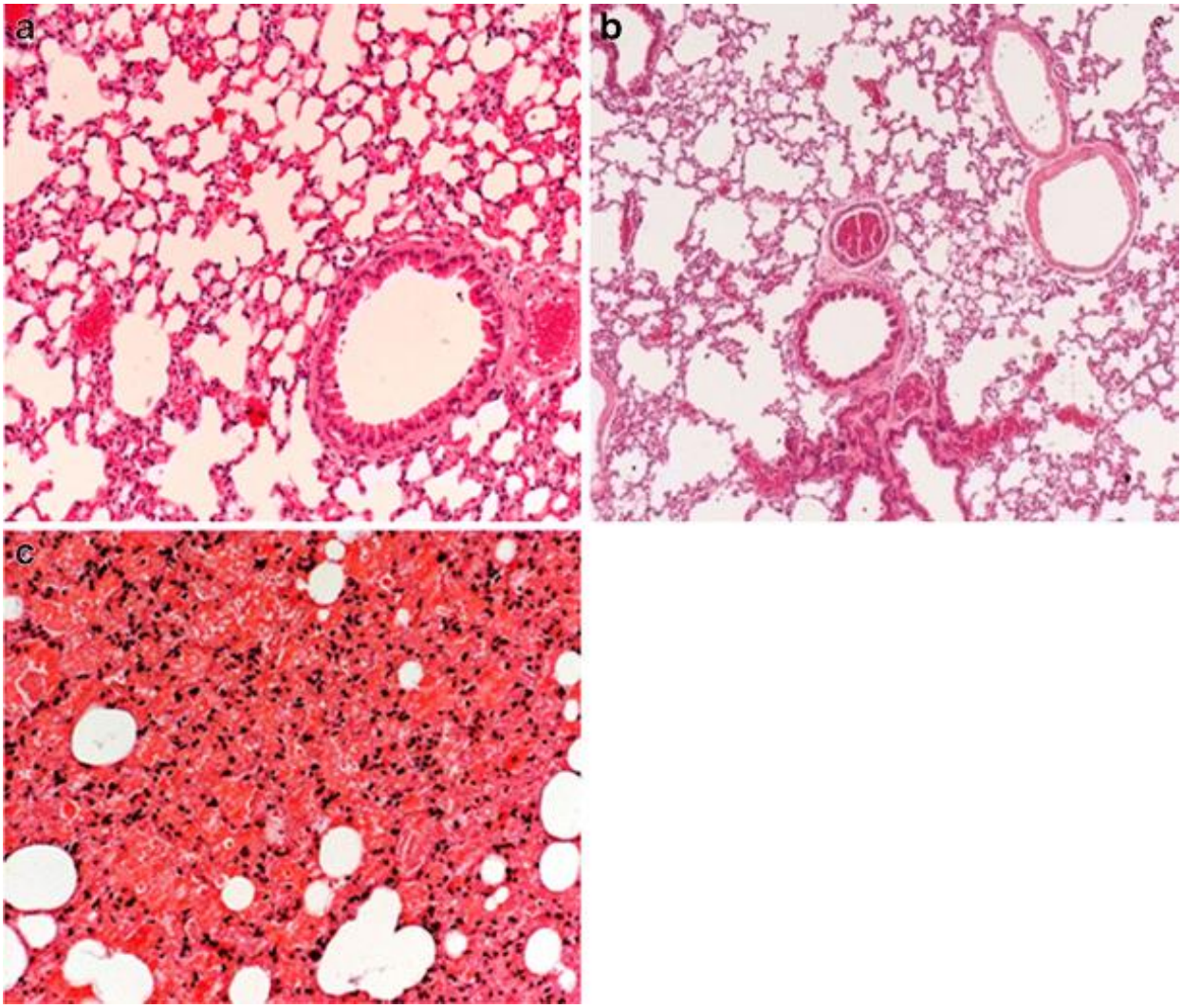

Fig. 7. Lung tissue section taken from **a,** a control mouse treated with 0.25 ml air, **b,** mice treated with non-coated inhalable NPs, and **c** mice treated with polysorbate-80-coated inhalable NPs. (×200 magnification). Reprinted with permission of ©Springer publisher

Fig. 7.a shows a tissue section taken form a lung of a control animal and examined under the microscope at ×200 magnification. The section did not exhibit any abnormalities. The alveolar sacs are well defined with no signs of hemorrhage, flooding, or collapse of the alveolar spaces which all can be defined as a manifestation of pulmonary toxicity. Tissue sections taken from animal treated with non-coated inhalable NPs (group 1) appeared very similar to what was seen in the control group (Fig. 7.b). Again, the histological examination indicated the absence of pulmonary toxicity in this group.

All mice that received coated inhalable NPs had to be euthanized with 1 h of the administration time due to breathing difficulties. These animals expressed very shallow breathing pattern followed by 50% reduction in the breathing rate. Moreover, the histopathological results associated with polysorbate-80-coated inhalable NPs powder were totally different from what was seen in all other groups. Fig. 7.c shows that alveolar sacs were deflated and there was an acute terminal microhemorrhage from the alveolar capillaries accompanied by local flooding of many alveoli with a protein-rich fluid. An increased number of neutrophils were present in the fluids of the affected alveoli. There were also large perivascular sacs filled with edema fluid around some of the large pulmonary vessels. These changes were consistently associated with all animals treated with polysorbate-80-coated NPs. Pathology reports along with the observed high morbidity scores prove the connection between polysorbate-80-coated NPs and the observed pulmonary toxicity.

3.3. Microcalorimetric method to assess phagocytosis: macrophage-NP interactions

3.3.1. NP characteristics

Table 3 shows the physical characteristics of different NP formulations. Loading efficiency of FITC-dextran was about 90% in all NP formulations with no significant difference

between them. Fig. 8 is the IR of mannosylated gelatin nanoparticles. The stretches between 1505- 1550 and 1465-1500 that correspond to secondary amines groups and Schiff's base (-C=N-), respectively, which confirm the synthesis of mannosylated gelatin NPs.

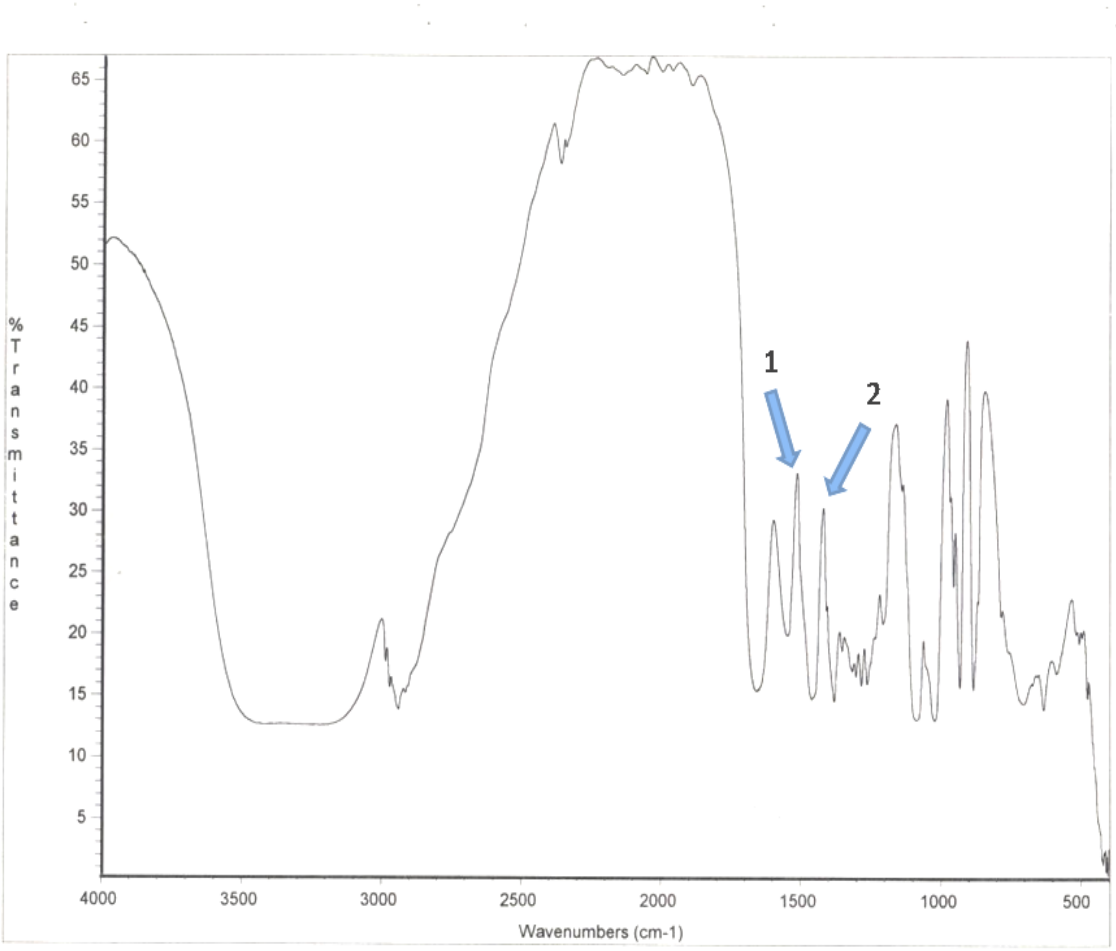

Fig. 8. The IR spectrum of mannosylated gelatin nanoparticles. arrow 1 and 2 point to the stretches between 1505- 1550 and 1465-1500 that correspond to secondary amines groups and Schiff's base (-C=N-), respectively. Reprinted with permission of ©Springer publisher

Table 3. Characteristics of poly (isobutyl cyanoacrate) and gelatin nanoparticles.

NP formulation	Particle size (nm) ± SD	Polydispersity ± SD	Zeta potential (mV)
Uncoated PIBC NPs	137 ± 19	0.082 ± 0.009	-25.64 ± 0.32
Polysorbate-80-coated NPs	140 ± 25	0.073 ± 0.011	-24.25 ± 0.41
Gelatin NPs	225 ± 23	0.098 ± 0.013	12.21 ± 0.25
Mannosylated gelatin NPs	305 ± 35	0.125 ± 0.015	7.32 ± 0.12

Values are mean ± SD (n=3). Reprinted with permission of ©Springer publisher

3.3.2. Thermal activity of macrophages

The thermal activity profiles of macrophages alone and after titration with 100 μL of uncoated PIBCA NPs and polysorbate-80-coated NPs are shown in Fig. 9. The thermal activity of macrophages alone (Fig. 9.a) consists of two main phases, ascending and descending. The ascending phase extends for the first 37 h and comprises two subphases, the first subphase is a linear increase in heat production for the first 10 h followed by an exponential incline in the thermal exchange for the rest of the ascending phase to reach a maximum of 221 μW after 37 h. The descending phase shows a sharp linear decline for the first 5 h followed by a slower exponential decline that extends to near stagnation. The total heat exchanged during the 100 h was 9.8 ± 2.3 J.

The thermal activity of macrophages recorded after 100 μL of uncoated PIBCA NPs were titrated is shown in Fig. 9.b. Although two main ascending and descending phases are also present, the linear increase of the exothermic phase has a higher slope, which reflects a faster increase in heat production. The exponential subphase of the heat exchange has a slower start, resulting in a shift of the whole heat flow profile to the right, with a maximum heat flow of 386 μW after 60 h. The total heat exchanged during 100 h was 37.6 ± 5.6 J, which is significantly higher than what was observed with macrophages alone, 9.8 ± 2.3 J ($P < 0.05$). The relative interactive coefficient of uncoated PIBCA NPs toward macrophages was calculated to be $4{,}356 \pm 350$ M^{-1}.

The results of using polysorbate-80-coated PIBCA NPs instead of uncoated NPs are shown in Fig. 9.c. The thermal activity of polysorbate-80-coated PIBCA NPs falls between values of the thermal activity of macrophages alone and after titrating uncoated NPs. The total heat exchanged during 100 h after titrating coated NPs (15.2 ± 3.4 J) was significantly less than

what was observed using uncoated NPs (37.6 ± 5.6 J) and higher than the thermal activity of macrophages alone (9.8 ± 2.3 J). Coating the surface of PIBCA NPs with polysorbate-80 resulted in a significantly lower relative interactive coefficient (890 ± 120 M−1) compared with the relative interactive coefficient of uncoated NPs ($P < 0.05$). Titrating the same concentration of uncoated NPs after mixing them with 1% w/w of polysorbate-80 for only 1 min resulted in a thermal activity profile very similar to what was observed with uncoated NPs. Similarly, titration of 100 μL of 1% w/w polysorbate-80 solution in PBS resulted in a thermal activity profile very similar to that observed with macrophages alone. Adding Cyto B to the cell culture medium produced macrophage thermal activity profiles as shown in Fig. 10. The thermal activity profile of macrophages alone (Fig. 10.a) was significantly different from the thermal activity of macrophages in the presence of Cyto B. The thermal activity profile of macrophages plus Cyto B was shorter in time (60 h) and lower in terms of heat exchange (3.9 ± 1.3 J) than when the experiment was performed with macrophages alone (9.8 ± 2.3 J). Moreover, the presence of Cyto B in the medium inhibited cellular responses of macrophages toward coated or uncoated NPs (Fig. 10.b, c). The total heat exchange after titrating NPs in the presence of Cyto B was not significantly different from the heat exchange of titrating macrophages alone.

Fig. 11 shows the thermal activity profile of macrophages alone after titrating 100 μL of gelatin NPs and mannosylated gelatin NPs. Similar to what was seen with uncoated PIBCA NPs, non-mannosylated gelatin NPs (Fig. 11.b) induced a significant increase in the total thermal activity when compared with macrophages alone, 45.5 ± 8.2 J and 9.8 ± 2.3 J, respectively. The relative interactive coefficient of non-mannosylated gelatin NPs was significantly higher than the relative interactive coefficient of uncoated PIBCA NPs, $5{,}120 \pm 410\ M^{-1}$ and $4{,}356 \pm 350\ M^{-1}$, respectively (Table 4).

This can be attributed to the difference in NP characteristics (size and zeta potential) and to their polymer nature. Mannosylated gelatin NPs changed the thermal activity profile and the total heat exchange dramatically (Fig. 11.c). The thermal activity of macrophages increased from 0 to almost 100 μW in less than 1 h. The thermal activity associated with mannosylated gelatin NP titration, 75.4 ± 7.5 J was not predicted by experiments performed previously. The high amount of heat produced resulted in a significantly higher relative interactive coefficient, $9{,}269 \pm 630$ M^{-1}, for mannosylated NPs. Fig. 12 shows the heat production associated with the titration of 100 μL of a 1:1 w/w mixture of not chemically bonded mannose and gelatin NPs (A) and 100 μL of 0.1 mg/mL mannose solution (B). The thermal activity recorded with not chemically bonded mixture of mannose and gelatin NPs (Fig. 12.a) was similar to what was observed with mannosylated NPs, which are chemically bonded (Fig. 11.c). However,

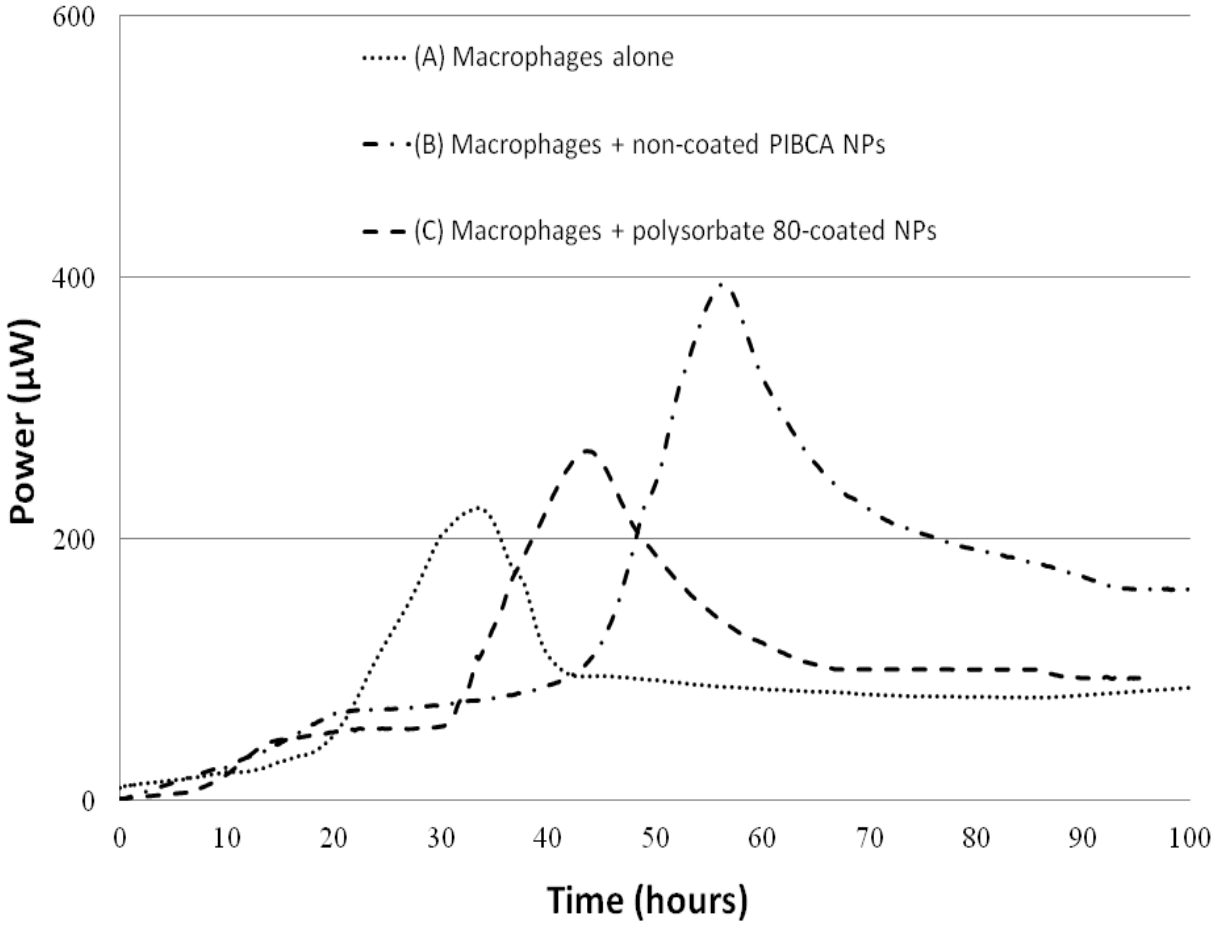

Fig. 9. The thermal activity profiles of *A* macrophages alone, *B* macrophages after titration of 100 µL of uncoated poly(isobutyl cyanoacrylate) nanoparticles, and *C* macrophages after titration of 100 µL of polysorbate-80-coated poly(isobutyl cyanoacrylate) nanoparticles. Reprinted with permission of ©Springer publisher

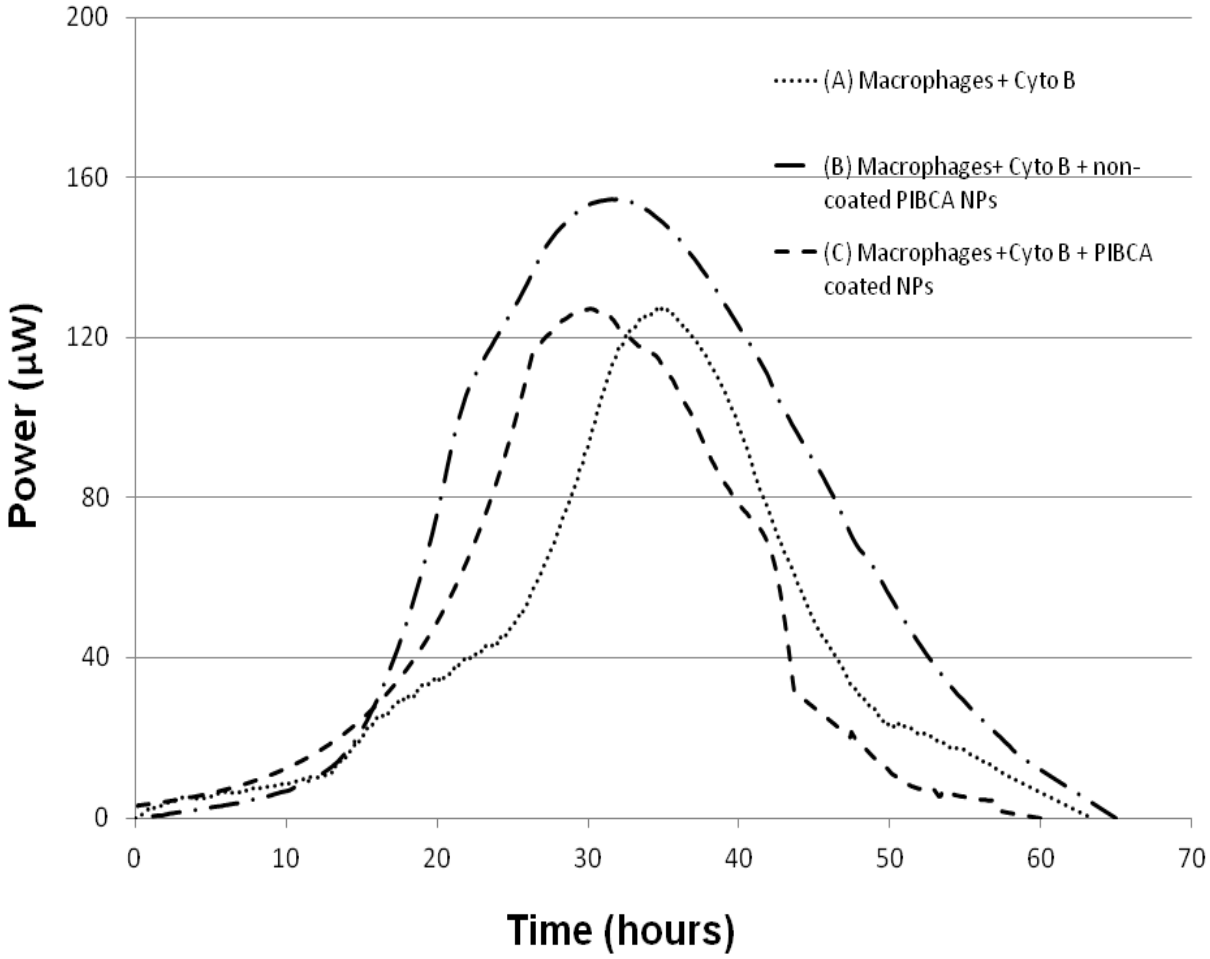

Fig. 10. The thermal activity profiles of *A* macrophages alone, *B* macrophages after titration of 100 μL of non-coated poly(isobutyl cyanoacrylate) nanoparticles, and *C* macrophages after titration of 100 μL of polysorbate-80-coated poly(isobutyl cyanoacrylate) nanoparticles after the cytochalasin B was added at the same concentration ($2–5 \times 10^{-6}$ M) to the medium used in all experiments. Reprinted with permission of ©Springer publisher

using mannose solution resulted in a different thermal activity profile (Fig. 12.b). The same early, sharp increase in heat production was noticed (Fig. 12.b), but the rest of the thermal profile was very similar to what was observed with macrophages alone.

Adding Cyto B to the cell culture medium resulted in phagocytosis inhibition of mannosylated gelatin NPs. However, it did not affect the sharp increase in the heat production associated with ligand–receptor interaction of mannose and mannose receptor as shown in Fig. 12.c.

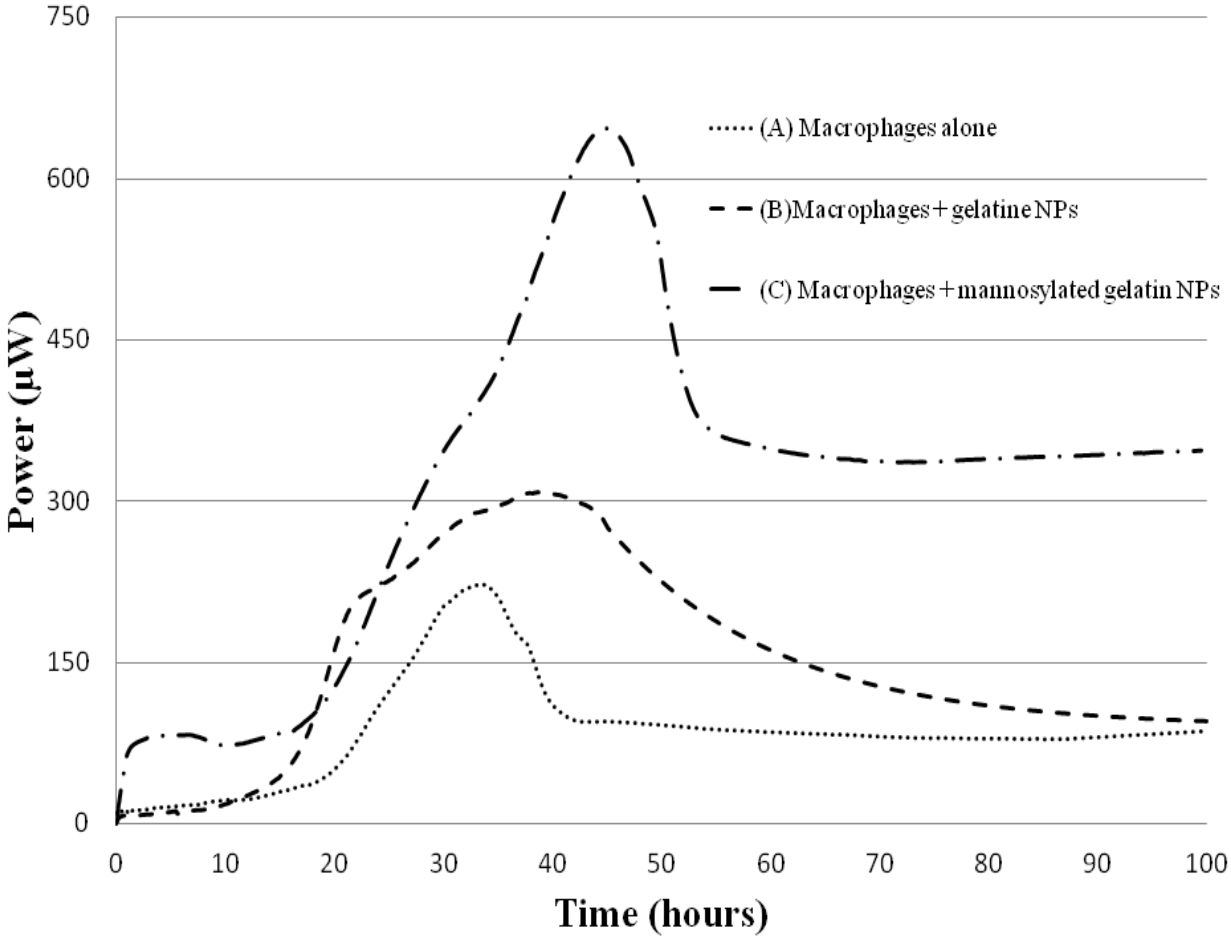

Fig. 11. The thermal activity profiles of A macrophages alone, B macrophages after titration of 100 µl of gelatin nanoparticles, and C macrophages after titration of 100 µl of mannosylated gelatin nanoparticles. Reprinted with permission of ©Springer publisher

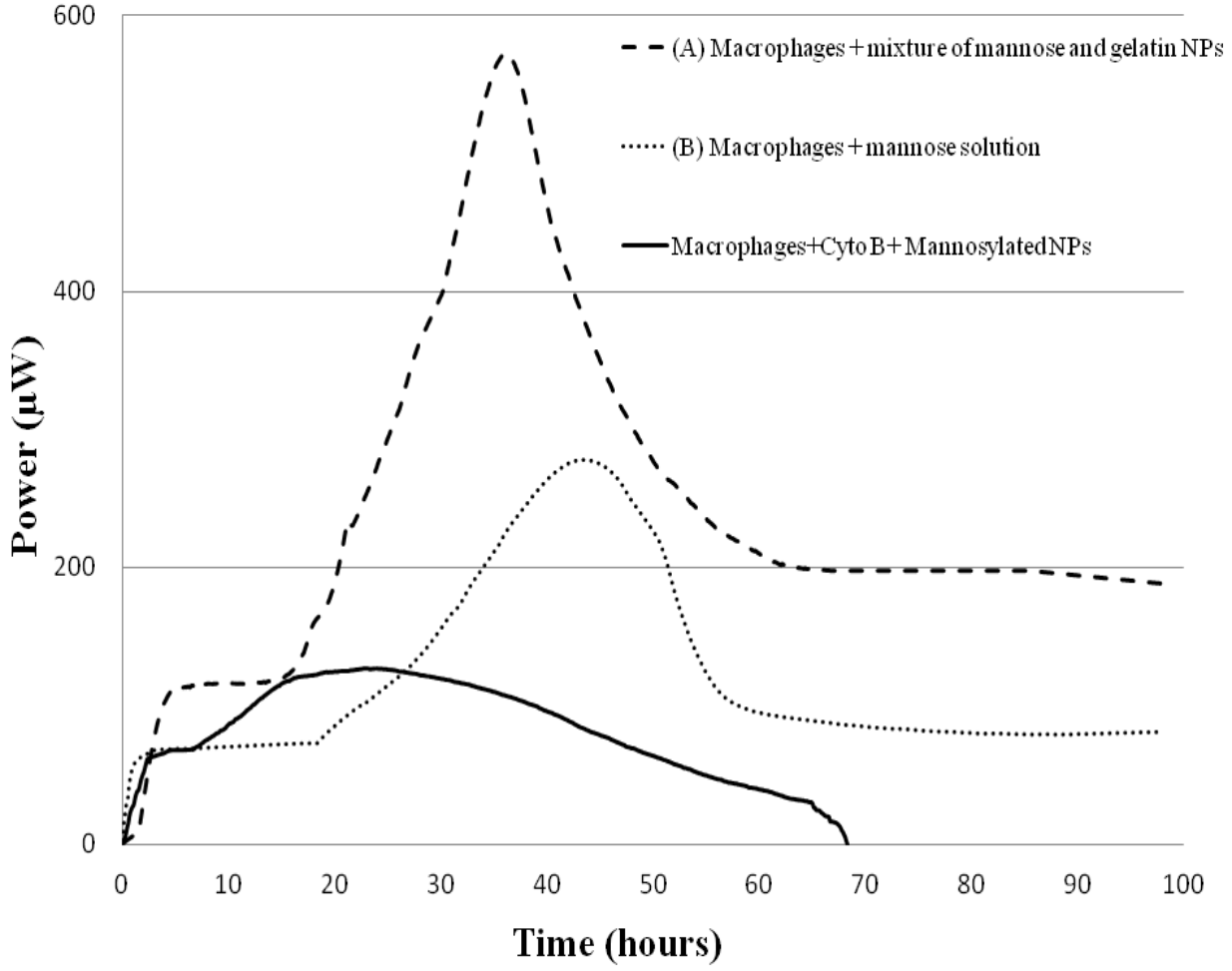

Fig. 12. The thermal activity profiles of A macrophages after titration 100 µl of 1:1 mixture of gelatin nanoparticles and mannose, B macrophages after titrating 100 µl of mannosylated solution of 0.1 mg/ml, and C macrophages after titration of 100 µl of mannosylated gelatin nanoparticles with cytochalasin B added to the cell culture medium. Reprinted with permission of ©Springer publisher

Table 4. Values of total heat exchange and the affinity constant of different NP formulations.

NP formulation	Total heat exchange (J)	Affinity constant (1/M)
Macrophages alone	9.8 ± 2.3	NA
uncoated PIBCA NPs	37.6 ± 5.6	4356 ±350
Polysorbate-80-coated NPs	15.2 ± 3.4	890 ± 120
Gelatin NPs	45.5 ± 8.2	5120 ± 410
Mannosylated gelatine NPs	75.4 ± 7.5	9269 ± 630

Values are mean ± SD (n=3). Reprinted with permission of ©Springer publisher

3.3.3. Flow cytometry analysis

Representative dot plots and histograms of four different FITC-labeled NP formulations along with the negative control are shown in Figs. 13 and 14, respectively. More than 99% of the untreated macrophages are located mainly in the lower left (LL) quadrant and showed a mean fluorescence intensity (MFI) of 3.19 on an arbitrary channel as shown in Figs. 13.a and14.a, respectively. After treating macrophages with polysorbate-80-coated PIBCA only 1% of these macrophages were detected in the lower right (LR) quadrant Fig. 13.b with low MFI value of 5.07. 14.12% of macrophages were shifted to the LR quadrant when they were exposed to the uncoated PIBCA NPs; the MFI was 16.8 as shown by Figs. 13.c and 14.c.

A higher percentage (54.96%) of macrophages were detected in the LR when gelatin NPs were used as treatment with MFI value of 18.39 as shown in Figs. 13.d and 14.d, respectively. Mannosylated gelatin NPs were associated with highest uptake as shown by Figs. 13.e and 14.e. 58.69% of macrophages were shifted to the LR quadrant and the MFI was 46.08 on an arbitrary channel.

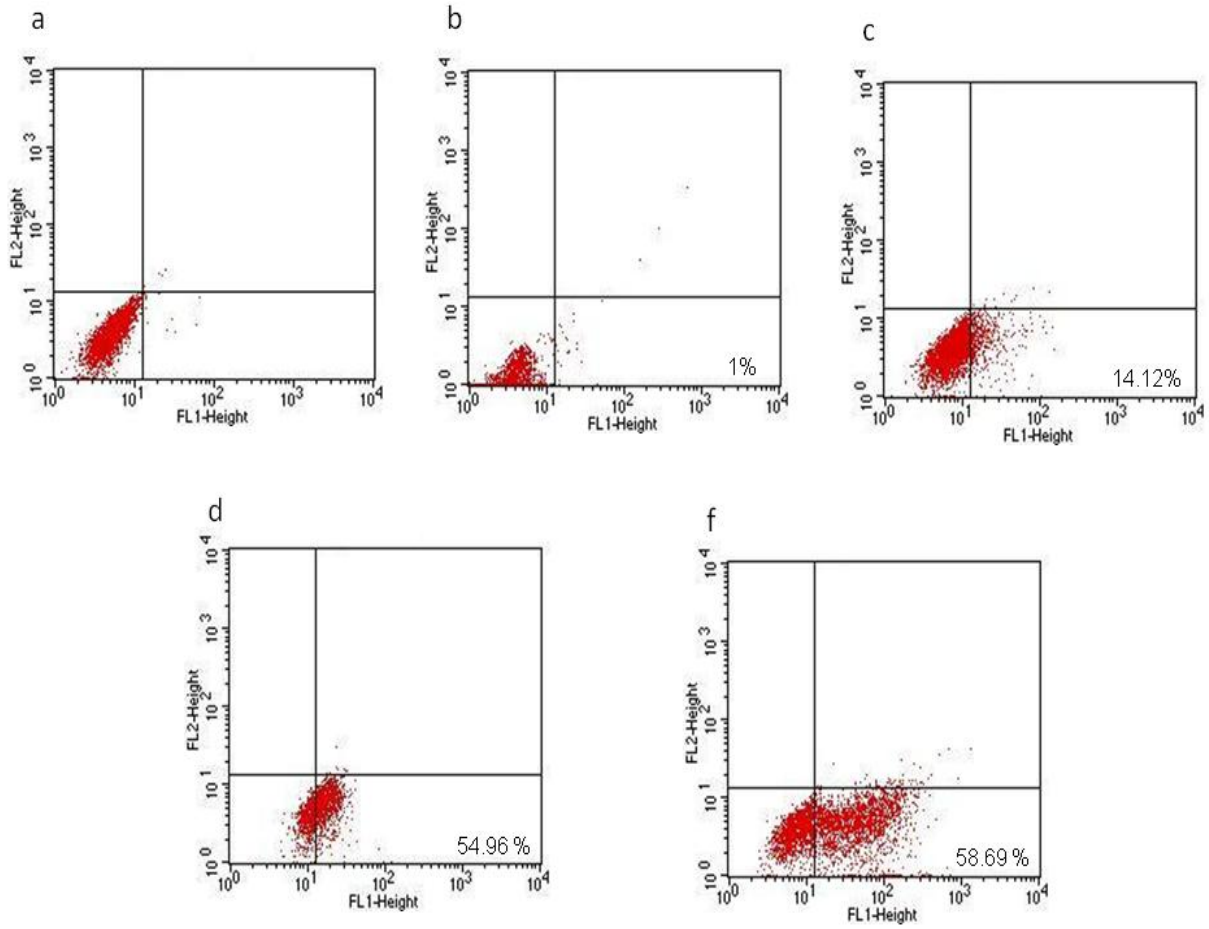

Fig. 13. Flow cytometric dot plots of (a) untreated macrophages, (b) macrophages treated with polysorbate-80-coated PIBCA nanoparticles, (c) macrophages treated with uncoated PIBCA nanoparticles, (d) macrophages treated with gelatin nanoparticles and (e) macrophages treated with mannosylated gelatin nanoparticles. Reprinted with permission of ©Springer publisher

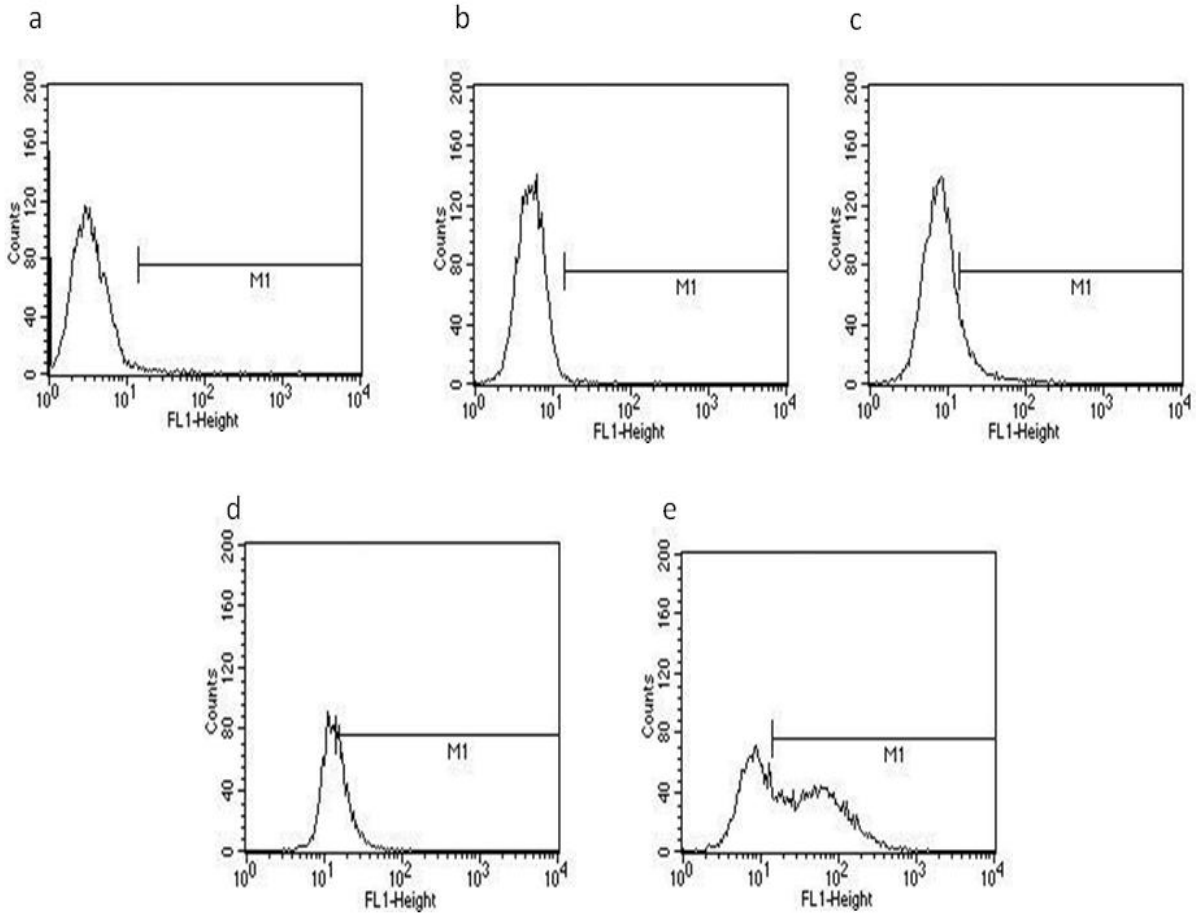

Fig. 14. Flow cytometric analysis of the macrophage uptake of nanoparticles: (a) represent the macrophages auto-fluorescences MFI=3.19. The horizontal line was set to calculate the percentage of positive cells, (b) poysorbate-80 coated PIBCA nanoparticles MFI=5.07, (c) uncoated PIBCA nanoparticles MFI=16.81, (d) gelatin nanoparticles MFI=18.39 and (e) mannosylated gelatin nanoparticles MFI=46.08. Reprinted with permission of ©Springer publisher

3.4. Inhalable nanoparticles as lung cancer treatment in a mouse model

3.4.1. NPs and inhalable NPs characteristics

The loading efficiency of DOX in NPs was 85% and the loading capacity was 9.6 mg of DOX/100 mg of NPs. These values are in agreement with those reported previously [37, 88]. The prepared NPs had an average size of 137.22 ± 1.53 nm, the polydispersity index was 0.12, and the zeta potential was −23.5 ± 0.41 mV. The loaded amount of DOX in the carrier particles after spray–freeze drying was calculated to be 30 μg/mg powder. The mean particle size of DOX-loaded NPS after redissolution was 145 ± 20 nm and 256 ± 29 of the effervescent and non-effervescent spray–freeze dried powder, respectively (n = 6). The Student T test indicated that the increase in the size of NPS after redissolution was only significant with the non-effervescent formula. The MMAD of carrier particles loaded with blank and DOX NPs were 3.45 ± 0.11 and 3.41 ± 0.22 μm, respectively (n = 6). The GSD were 1.99 and 1.91, respectively.

3.4.2. Treatment efficacy and animal survival data

The animal survival data are shown in Fig. 15. All mice in the no-treatment control group (group iii) died or were euthanized during the first 45 days due to reaching the predetermined morbidity scores for euthanizing. The no-treatment control group showed significant weight loss after 3 to 4 weeks. The sacrificed or deceased animals had massive tumors in their lungs which showed metastasis to the liver, heart, and bone. For evaluating the effect of blank NPs (NPs without DOX), a group (vii) of animals was treated with 1 mg blank nanoparticle inhalable powder. In this group nearly 90% of the mice died or were sacrificed within 50 days. The animals in this group also showed significant weight loss after 3 to 4 weeks. Similar to the no-treatment group, massive tumor burden was found in lungs, liver, heart, and bone.

Fifty percent of the mice treated with 30 μg DOX solution as *i.v.* injection (group iv) died or were sacrificed within 40 days and all died or were sacrificed in less than 50 days. This group showed body weight loss after 28 days.

The positive control group injected intravenously with a suspension of NPs containing 30 μg DOX (group v) survived comparably to animals injected intravenously with DOX solution (group iv); all the animals died or were sacrificed in less than 50 days.

Groups of mice treated via inhalation with 1 mg nanoparticle effervescent powder containing 30 μg DOX (group i) or 1 mg non-effervescent powder containing 30 μg DOX (group ii) showed different results. The animals treated with inhalable non-effervescent nanoparticle powder containing 30 μg DOX showed longer survival times compared to the no-treatment groups and the groups injected intravenously with DOX as solution or NPs suspension (groups iv and v) (p values compared to either group were smaller than 0.0001). Fifty percent of the animals treated with inhalable non-effervescent NPs containing 30 μg DOX (group ii) survived over 70 days and 30% of the mice survived until the termination of the study at day 140. The animals treated with inhalable effervescent nanoparticle powder containing 30 μg DOX (group i) showed a significantly longer survival time compared to all other groups ($p < 0.05$). Seventy percent of the animals in this group survived 140 days.

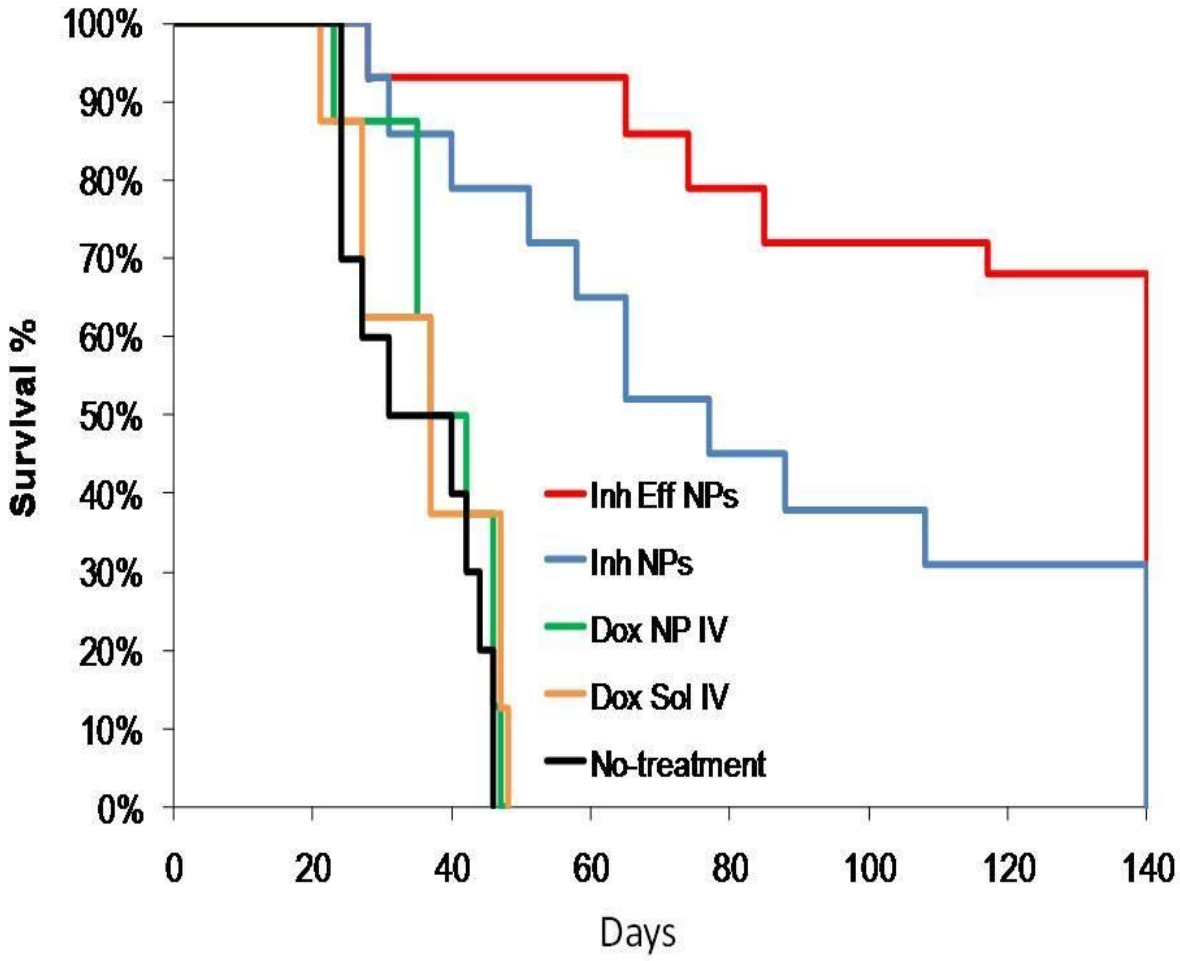

Fig. 15. Percent animal survival versus time. Animals were treated either with effervescent inhalable doxorubicin nanoparticle powder (Inh Eff NPs), inhalable doxorubicin nanoparticle powder (Inh NPs), doxorubicin-loaded nanoparticles *i.v.* (Dox NP IV), and doxorubicin solution (Dox Sol IV) or non-treated control group (No-treatment). Reprinted with permission of ©Elsevier publisher

3.4.3. Histology results

During the postmortem examination, three animals were randomly selected from each group and lungs, liver, and heart were removed for a pathology study. One representative picture is shown from each treatment group. Fig. 16 shows a section of a mouse lung representative of the no-treatment group (group 3). The sections of lung revealed multiple large and often confluent tumor masses in the parenchyma. There were also numerous smaller metastases throughout the alveolar septa. The central core of some of the larger masses was necrotic. The tumor cells were undifferentiated and mitoses were common.

Fig. 17 shows the heart of the animal of Fig. 16, showing tumors in the ventricular lumen. In the heart, there were large masses of tumor cells growing within and occupying most of the lumen of the right atrium and half of the lumen of the right ventricle. In addition to the primary metastases seen grossly in the lung, there were numerous secondary metastases also present.

Fig. 18 shows a representative lung section of an animal injected intravenously with DOX. This animal showed multiple pulmonary tumor metastases. The tumor masses in the lungs were of the same size as those in non-treated mice but they were not as numerous. Microscopic examination confirmed the presence of multiple pulmonary tumor metastases.

Fig. 19 shows a representative histopathology of a lung belonging to a mouse treated via inhalation with non-effervescent DOX nanoparticle powder (group ii). This mouse showed multiple pulmonary tumor metastases. The metastases in the lungs of this animal were fewer in number compared to non-treated animals and mice injected intravenously with a DOX solution (group iv). A small number of fairly uniform individual metastases were randomly located in the lungs. Fig. 20 shows a representative histopathology of the lung of a mouse treated via inhalation

with effervescent DOX nanoparticle powder (group i). Metastases in the lungs were few and small. The lungs of this animal had only a few small metastases present.

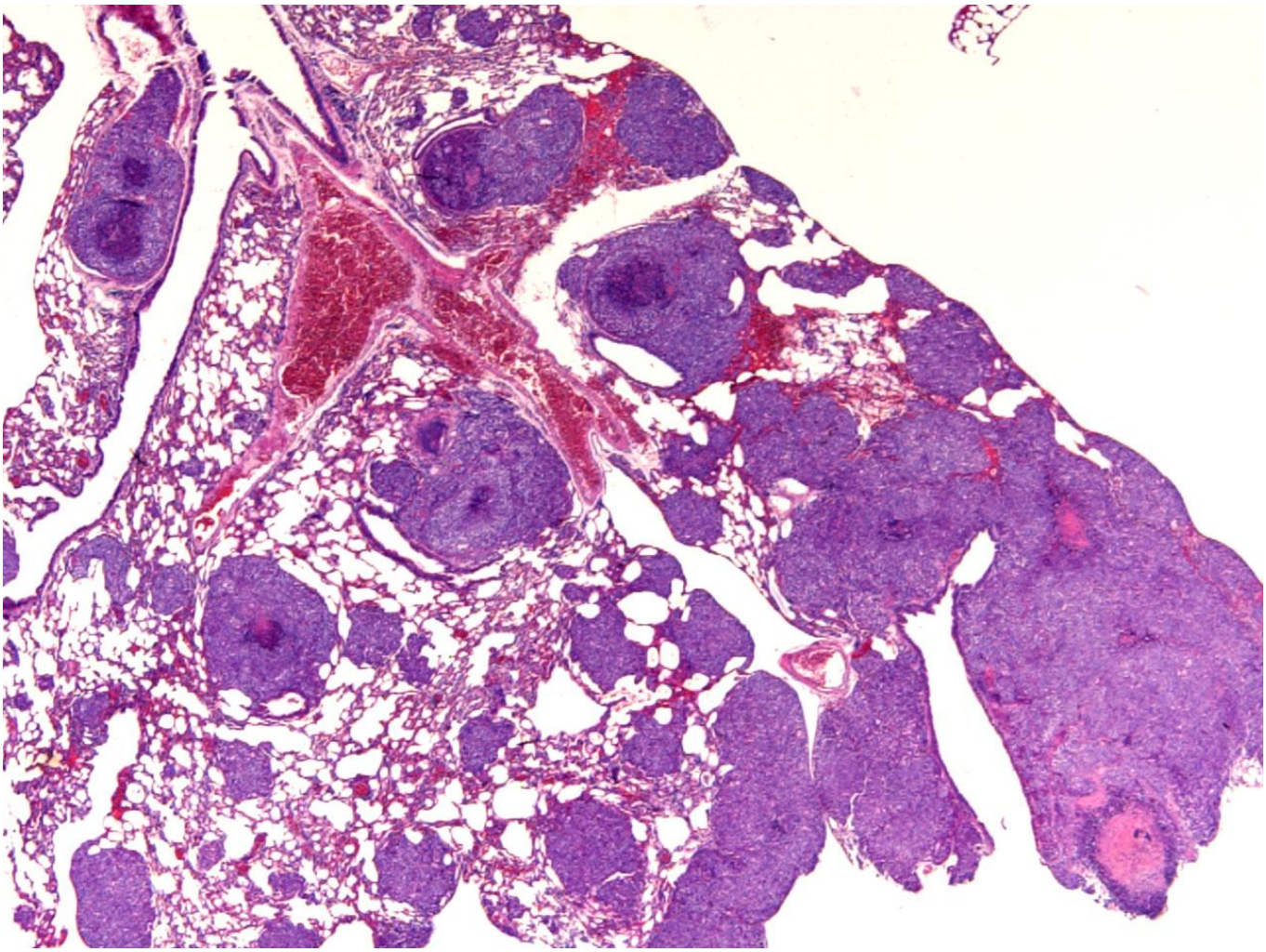

Fig. 16. Lung section of mouse from the non-treatment group. (20× magnification hematoxylin and eosin staining). Discrete tumor nodules are easily observed in the lung parenchyma. Reprinted with permission of ©Elsevier publisher

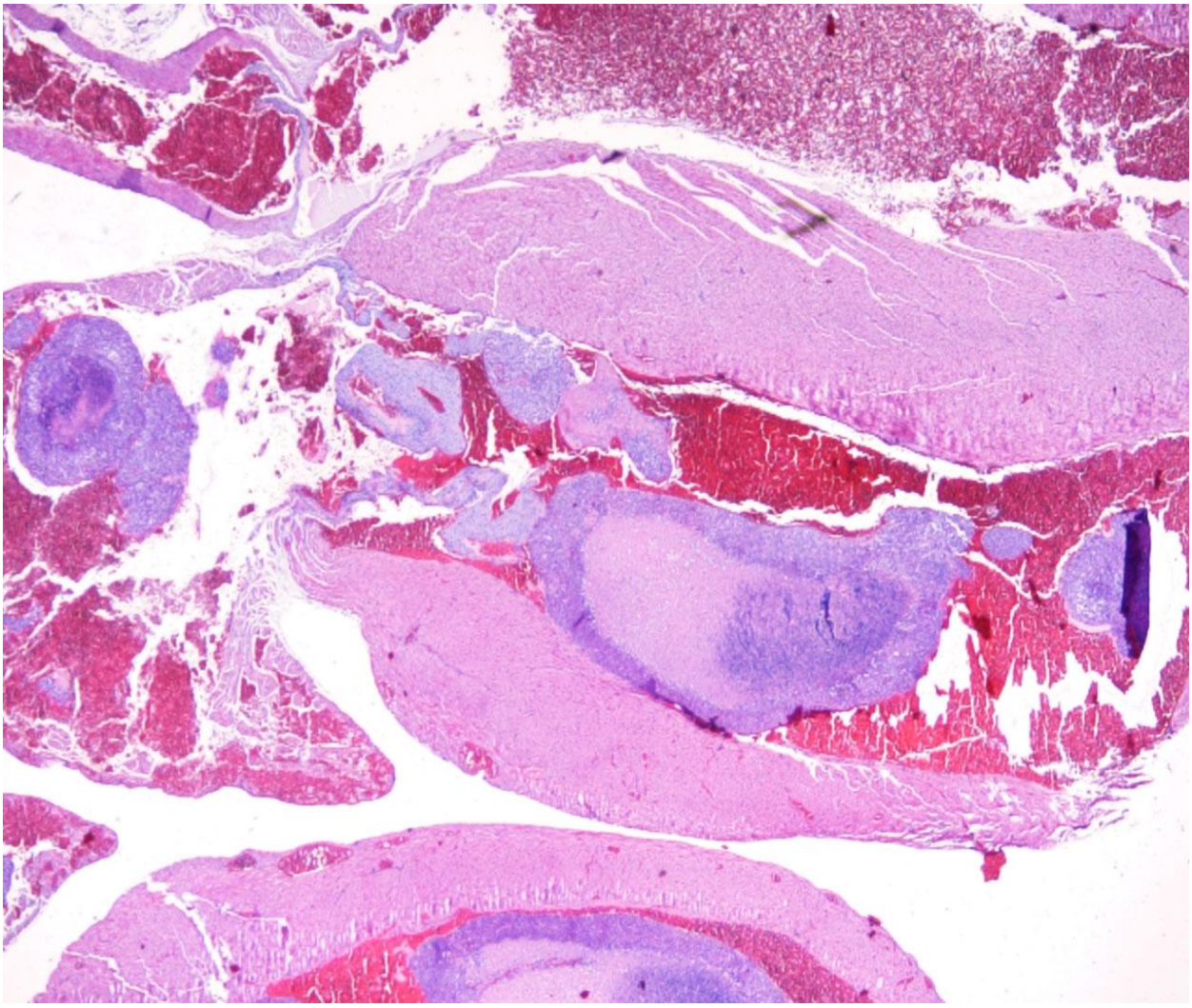

Fig. 17. Heart section of the animal in Fig. 16 showing growth of tumor in the ventricular lumen. (20× magnification hematoxylin and eosin staining). Reprinted with permission of ©Elsevier publisher

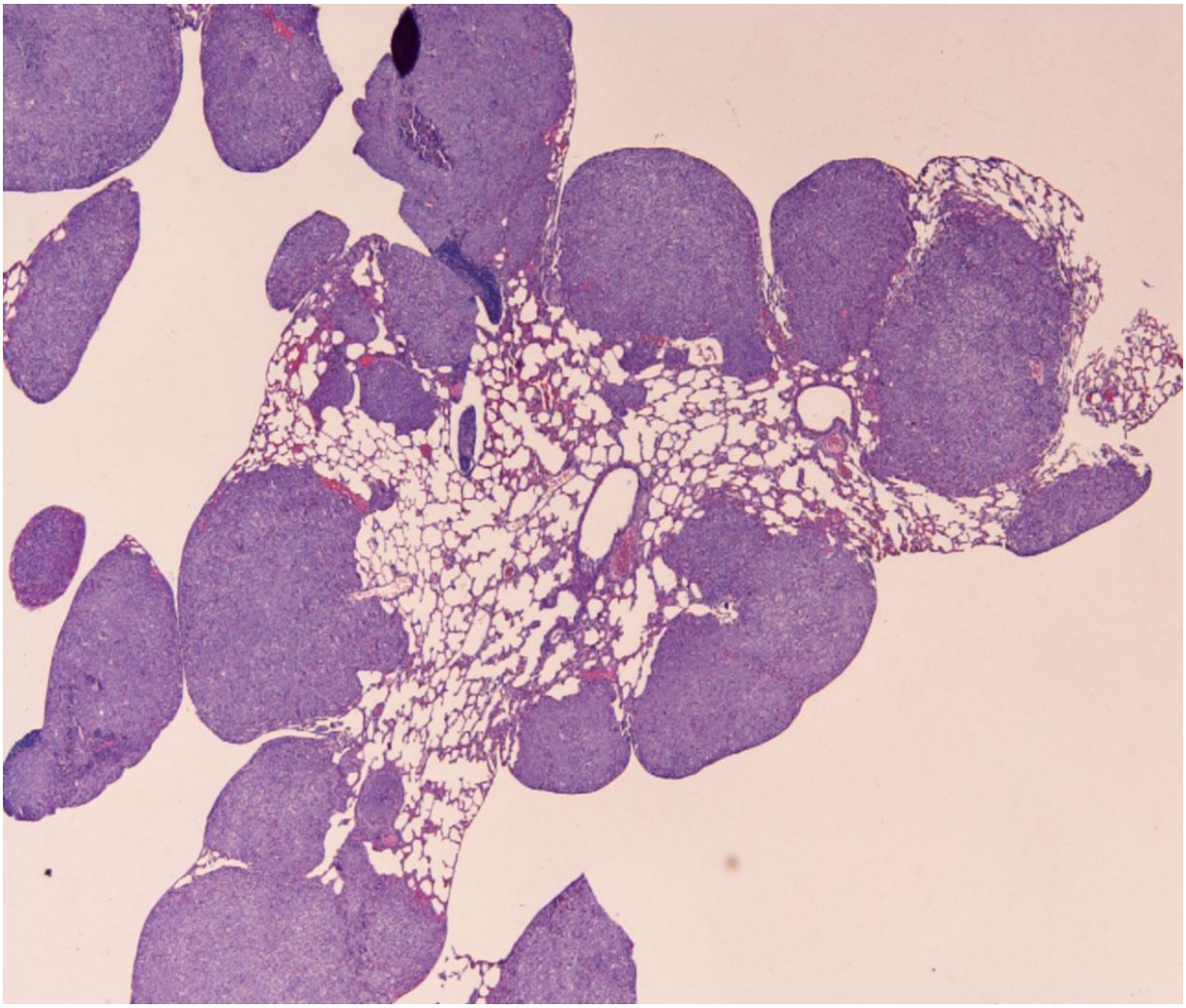

Fig. 18. Lung section of a mouse treated with doxorubicin solution intravenously. Bulky tumor nodules are easily observed. (20× magnification, hematoxylin and eosin staining). Reprinted with permission of ©Elsevier publisher

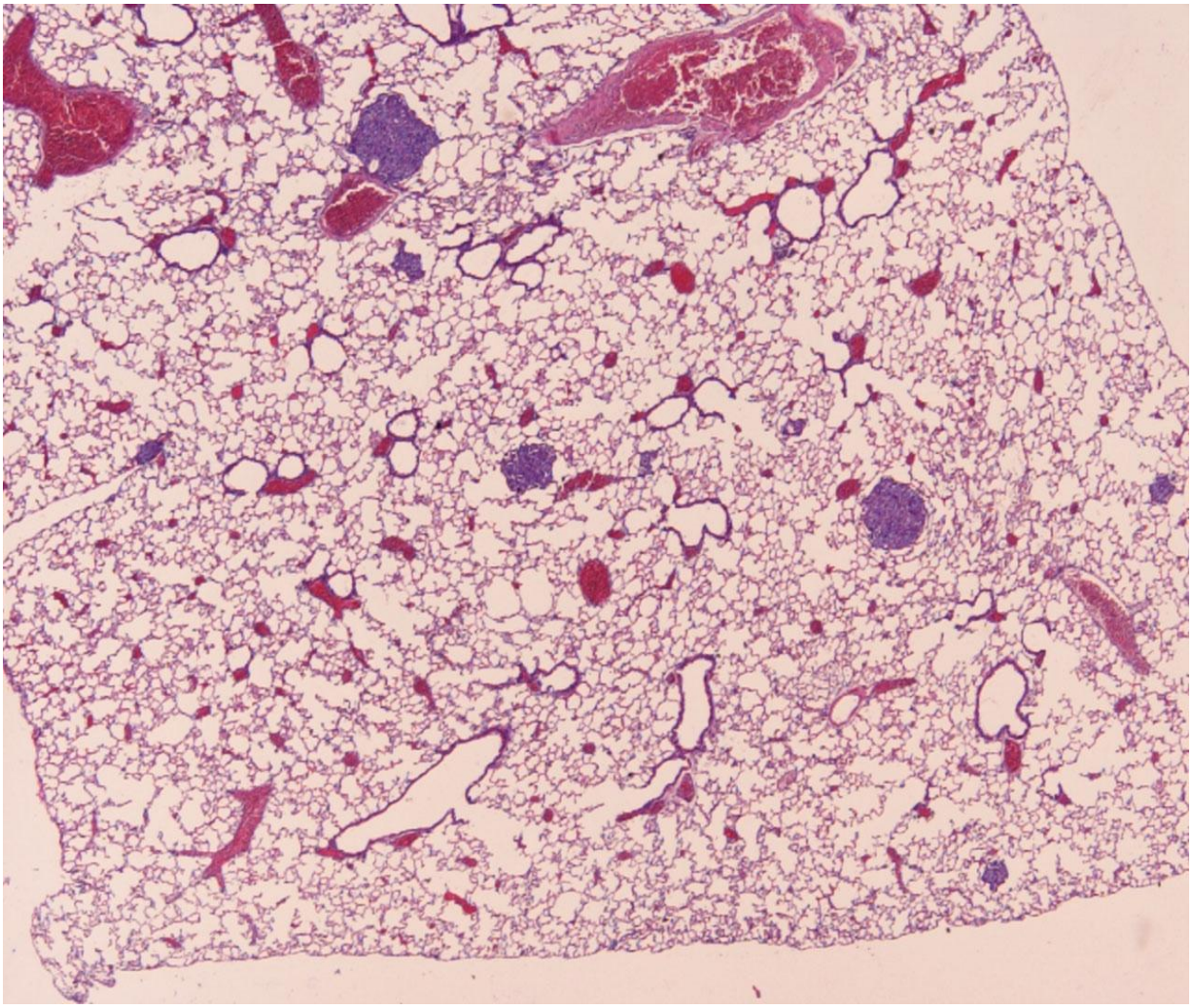

Fig. 19. Lung section of a mouse treated with non-effervescent doxorubicin nanoparticle powder. Small tumor nodules are observed. (20× magnification, hematoxylin and eosin staining). Reprinted with permission of ©Springer publisher

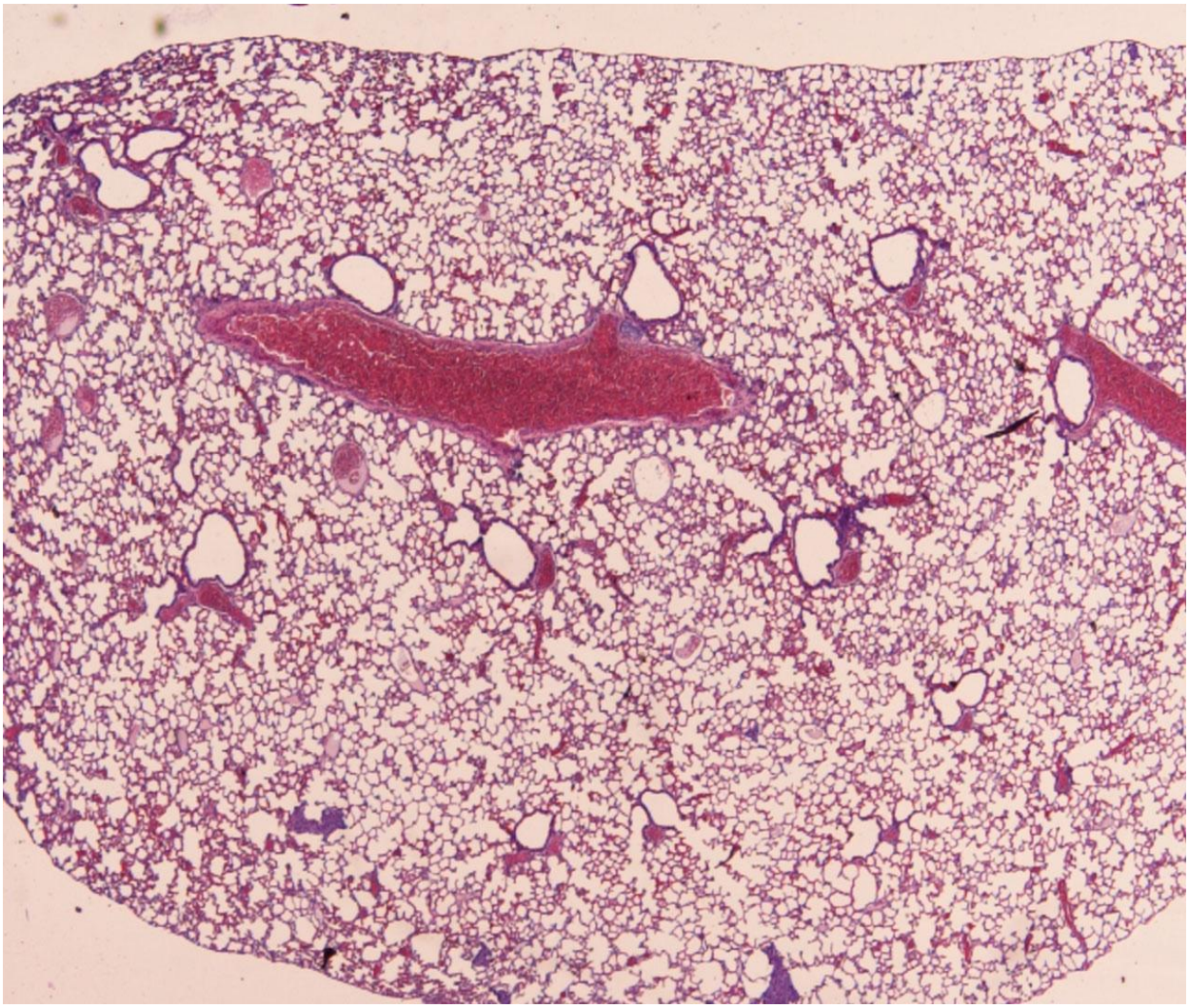

Fig. 20. Lung section of mouse treated with effervescent doxorubicin nanoparticle powder. (20× magnification, hematoxylin and eosin staining). Reprinted with permission of ©Elsevier publisher

3.4.4. MRI results

The MRI images demonstrated an excellent soft tissue contrast which enabled the localization of intra-thoracic lung cancer and any extra cancerous manifestations. Fig. 21.a is a T1 weighted, transverse spin echo scan of an untreated mouse 4 weeks after cancer inoculation. Tumor masses showed intense signals relative to adjacent tissues such as normal lung, and tumor boundaries were well delineated. Fig. 21.a shows big tumor masses (arrow 1) with the involvement of the visceral and mediastinal pleura (arrow 2), chest wall (arrow 3), parietal pericardium, and the heart (arrow 4). The sections of lung isolated from the same animal revealed multiple large and often confluent tumor masses in the parenchyma with numerous metastases throughout the alveolar septa; the tumor cells are undifferentiated and mitoses are common. In the heart, there were large masses of tumor cells growing within and occupying most of the lumen of the right atrium and half of the lumen of the right ventricle (Fig. 16 and Fig. 17). Fig. 21.b and c show MRI scans of mice treated via inhalation with 1 mg of effervescent DOX nanoparticle powder (group i) and a control mouse (not injected with cancer cells), respectively. The MRI images of the mouse treated with inhalable effervescent DOX nanoparticle powder (group i) showed no signs of intra-thoracic lung cancer. The MRI results were consistent in each group and one representative image was chosen. The animal study results showed a good correlation between MRI and histology data, as all tumor manifestations detected in MRI were confirmed later by histology.

3.4.5. Cardiac toxicity of inhaled doxorubicin

To investigate the cardiac toxicity, three enzymes, AST, ALT and CPK were measured in blood samples collected 1 h after insufflation of inhalable powder. Table 5 shows the concentration of AST, ALT and CPK in treatment and control groups. The results show a

significant increase in all enzyme concentrations where animals were treated with inhalable DOX powder compared to inhalable effervescent DOX-loaded NPs or non-treated. No significance difference in the enzyme levels were observed between animals treated with inhalable DOX NPs and non-treated mice.

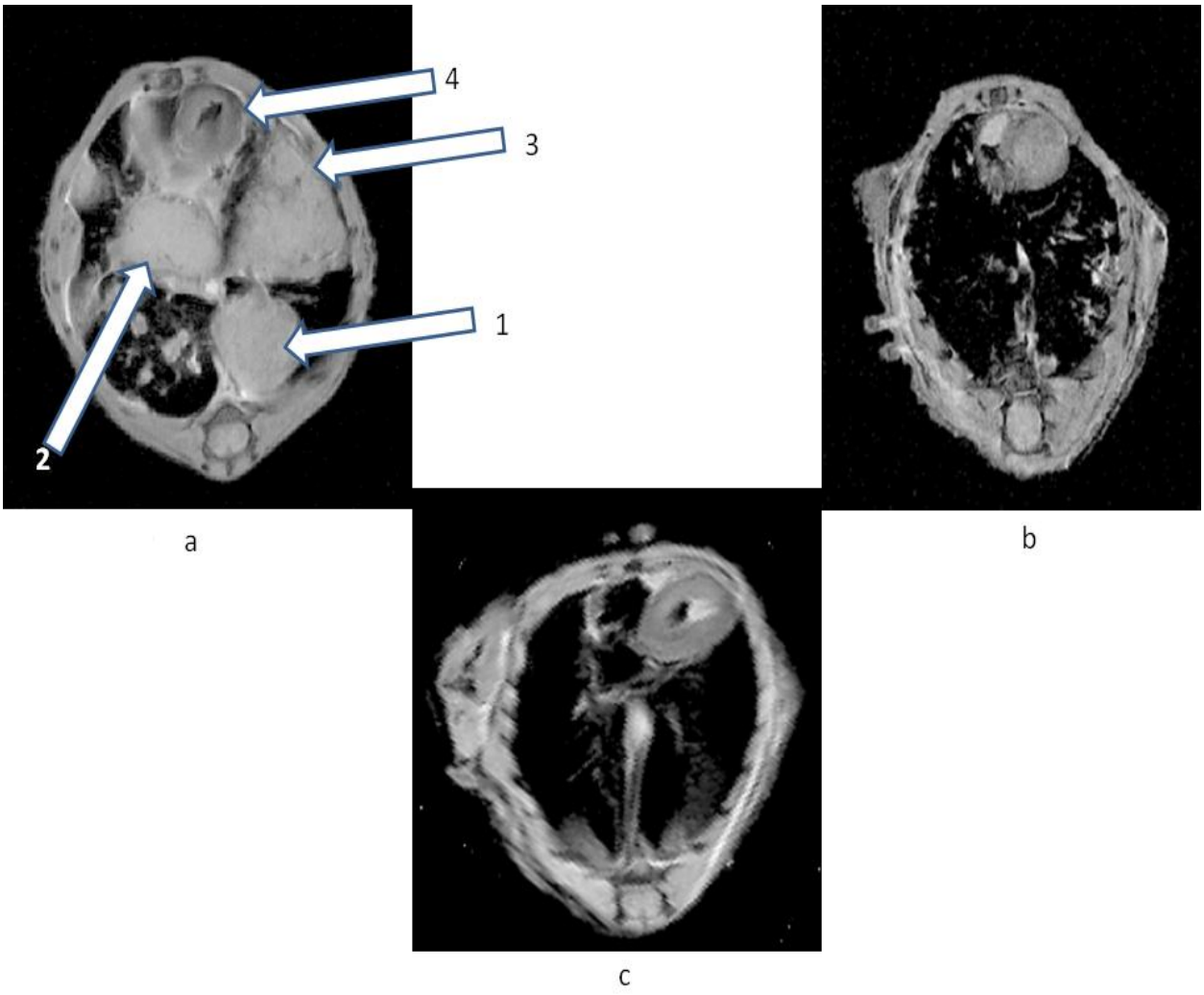

Fig. 21. T1 weighted, transverse spin echo scans (TE/TR = 13/1500 ms, BW = 50 KHz, the FOV = 26 X 26 mm with 128 × 128 matrix, thickness = 0.5 mm) of; (a) control non-treated mouse, (b) mouse treated with effervescent doxorubicin nanoparticle powder, and (c) control mouse (not injected with cancer cells). Reprinted with permission of ©Elsevier publisher

Table 5. Blood concentration of AST, ALT and CPK in control mice and mice treated with either 1 mg nanoparticle powder containing 30 µg doxorubicin or 1 mg doxorubicin powder containing 30 µg doxorubicin. All values are expressed in IU/L.

	Control	**1 mg Dox inhalable effervescent NPs (contains 30 µg of DOX)**	**1 mg Dox inhalable powder (contains 30 µg of DOX)**
AST	141±22	160±27	1356±249
ALT	67±3.9	70±12	767±156
CPK	524±56	600±71	4359±1663

3.5. Distribution of inhalable effervescent NPs

3.5.1. NPs and inhalable NP characterization

The loading efficiencies in NPs were 85% for ^{14}C-labelled DOX and 90% for FITC dextran. Prepared NPs had a diameter of 137 nm, a polydispersity index of 0.11, and a zeta potential of -24 mV. The MMAD of carrier particles loaded with DOX-NPs was 3.55 μm and the GSD was 1.92. These values agreed with values previously reported [125, 192, 201].

3.5.2. Results of whole-body autoradiography confocal laser scanning microscopy

The whole-body autoradiographic method was used to assess the biodistribution of radiolabelled effervescent inhalable NPs after pulmonary delivery. Representative autoradiograms were selected from mice euthanized after 1, 8, and 24 hours. One autoradiogram was selected to represent the *i.v.* radiolabelled DOX solution of the mouse euthanized 8 hours postinjection. Fig. 22.a is a photoscan image of a cryosection of a mouse that received inhalable NPs and was euthanized 1 hour after inhalation. Fig. 22.b shows the image of the same section scanned by the phosphor imager and Fig. 22.c is an overlay of images in Figures 22.a and 22.b performed with Photoshop Element 7® (Adobe, USA). Fig. 22.b shows that the radioactivity was detected as a cloud in one location only; there is a total absence of radioactivity at other locations or organs. The overlay of images in Fig, 22.c shows that the cloud of radioactivity was located in the lungs. Fig. 23.a is a photoscan image of a cryosection of a mouse that received inhalable NPs and was euthanized 8 hours after inhalation. Eight hours after pulmonary delivery of NPs, the autoradiogram (Fig. 23.b) shows that the radioactivity disseminated to larger areas in the lungs with some deposition in the trachea.

Some hot spots of radioactivity were detected outside the lungs. These spots are outlined with red circles in Fig. 23.c.

The autoradiogram (Fig. 24) of the mouse euthanized 24 hours after NP inhalation shows radioactivity over the whole lung area with traces of radioactivity in the intestinal loop.

Fig. 25 shows the distribution of DOX solution 8 hours after a tail vain injection of radioactivity. The radioactivity associated with DOX was detected in almost all tissues and organs with no specificity.

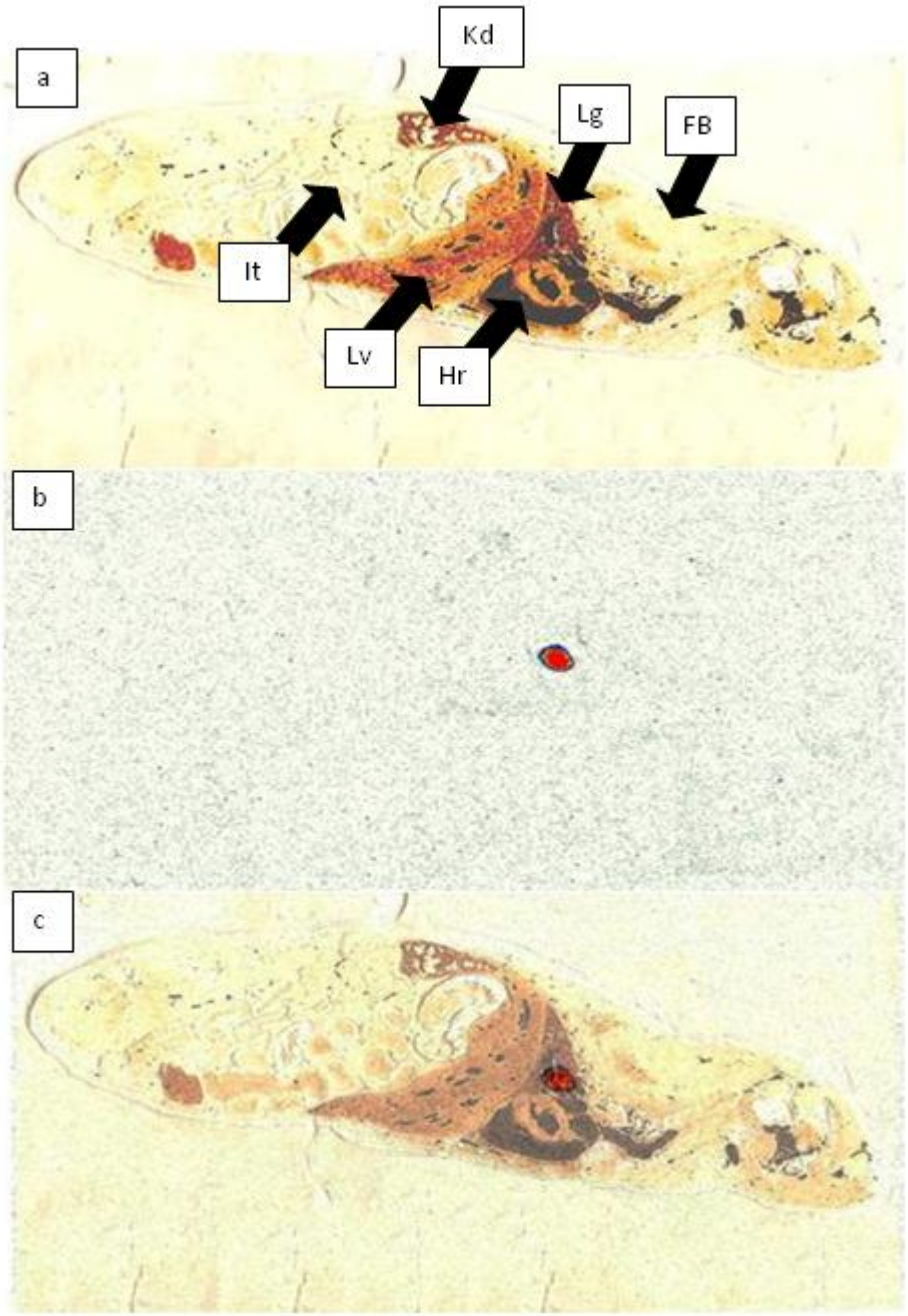

Fig. 22. 22-a: a simple photoscan of a freeze-drying cryosection taken from a mouse that received a single dose of effervescent inhalable NPs and euthanized 1 hour post-inhalation, 22-b: whole body autoradiogram of the distribution of ^{14}C from the same section, 22-c: an overlay of Fig. 22-a and 22-b. Major organs are marked on the Fig. 1-a as following (FB): fatty brown, (Hr): Heart, (Lg): lung, (Lv): liver, (Kd): kidney and It: intestine. Reprinted with permission of ©Future sciences publisher

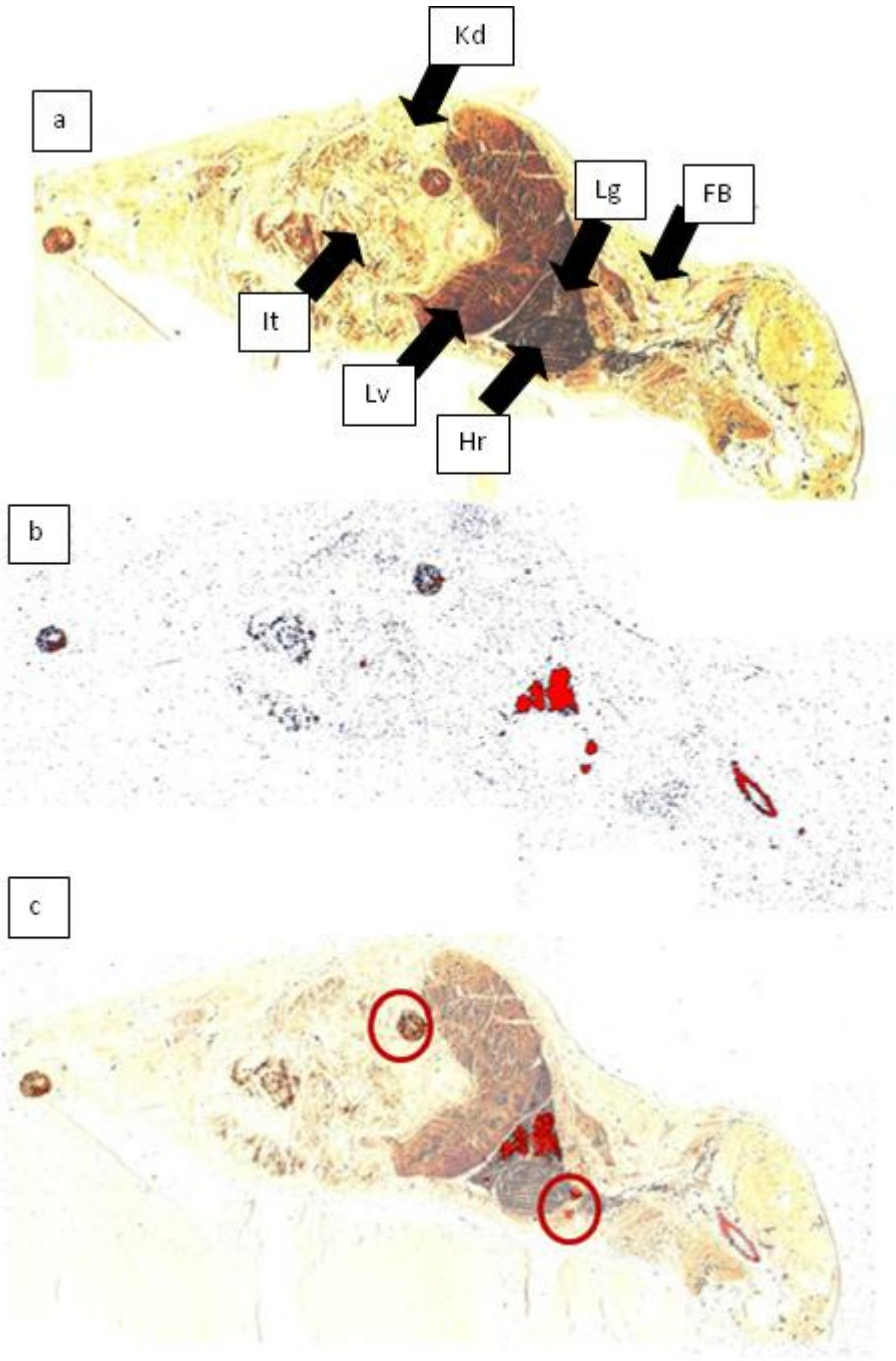

Fig. 23. 23-a: a simple photoscan of a freeze-drying cryosection taken from a mouse that received a single dose of effervescent inhalable NPs and euthanized 8 hours post-inhalation, 23-b: whole body autoradiogram of the distribution of ^{14}C from the same section, 23-c: an overlay of fig. 23-a and 23-b. Major organs are marked on the Fig. 22-a as following (FB): fatty brown, (Hr): Heart, (Lg): lung, (Lv): liver, (Kd): kidney and It: intestine. Reprinted with permission of ©Future sciences publisher

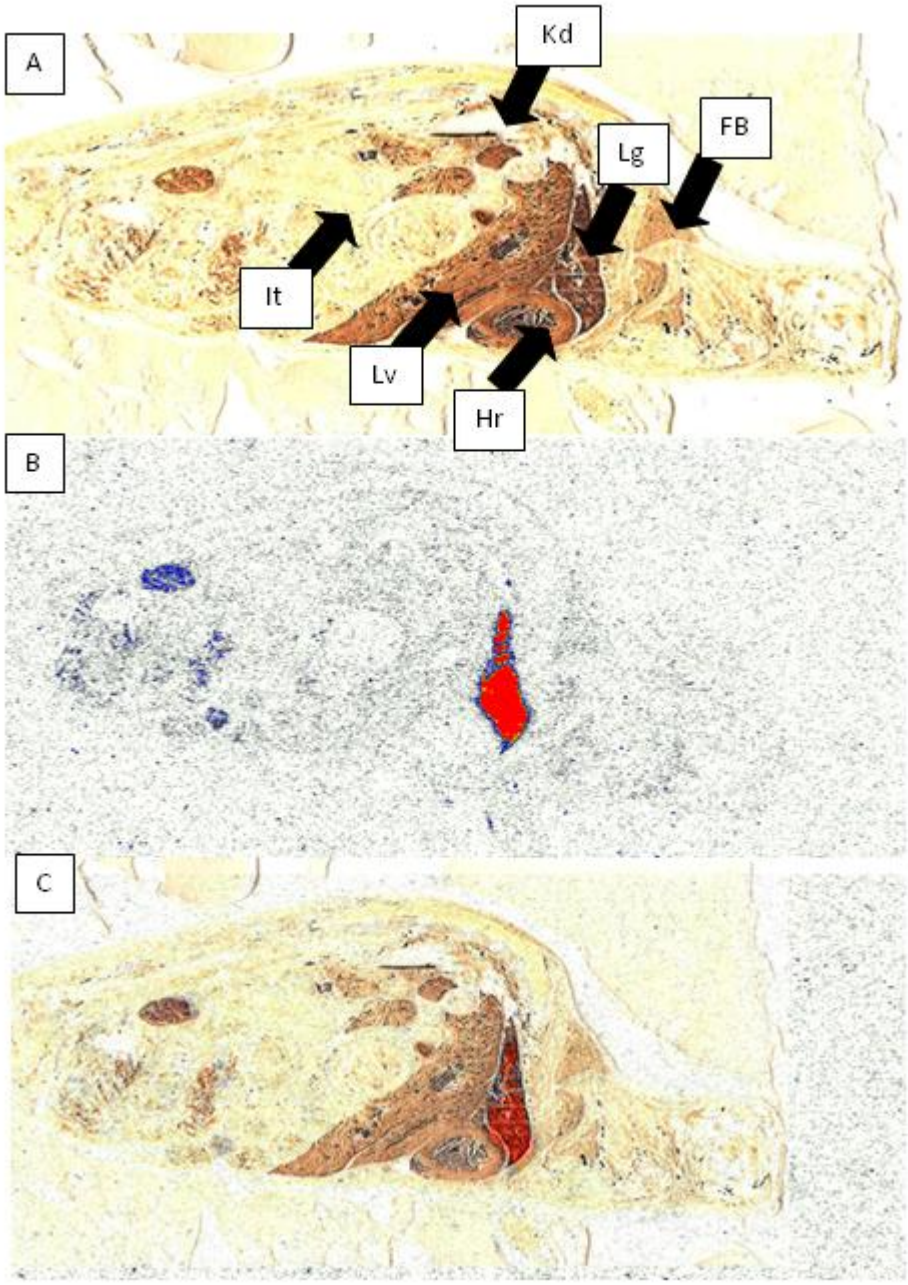

Fig. 24. 24-a: a simple photoscan of a freeze-drying cryosection taken from a mouse that received a single dose of effervescent inhalable NPs and euthanized 24 hours post-inhalation, 24-B: whole body autoradiogram of the distribution of ^{14}C from the same section, 3-C: an overlay of fig. 24-a and 24-b. Major organs are marked on the Fig. 24-b as following (FB): fatty brown, (Hr): Heart, (Lg): lung, (Lv): liver, (Kd): kidney and It: intestine. Reprinted with permission of ©Future sciences publisher

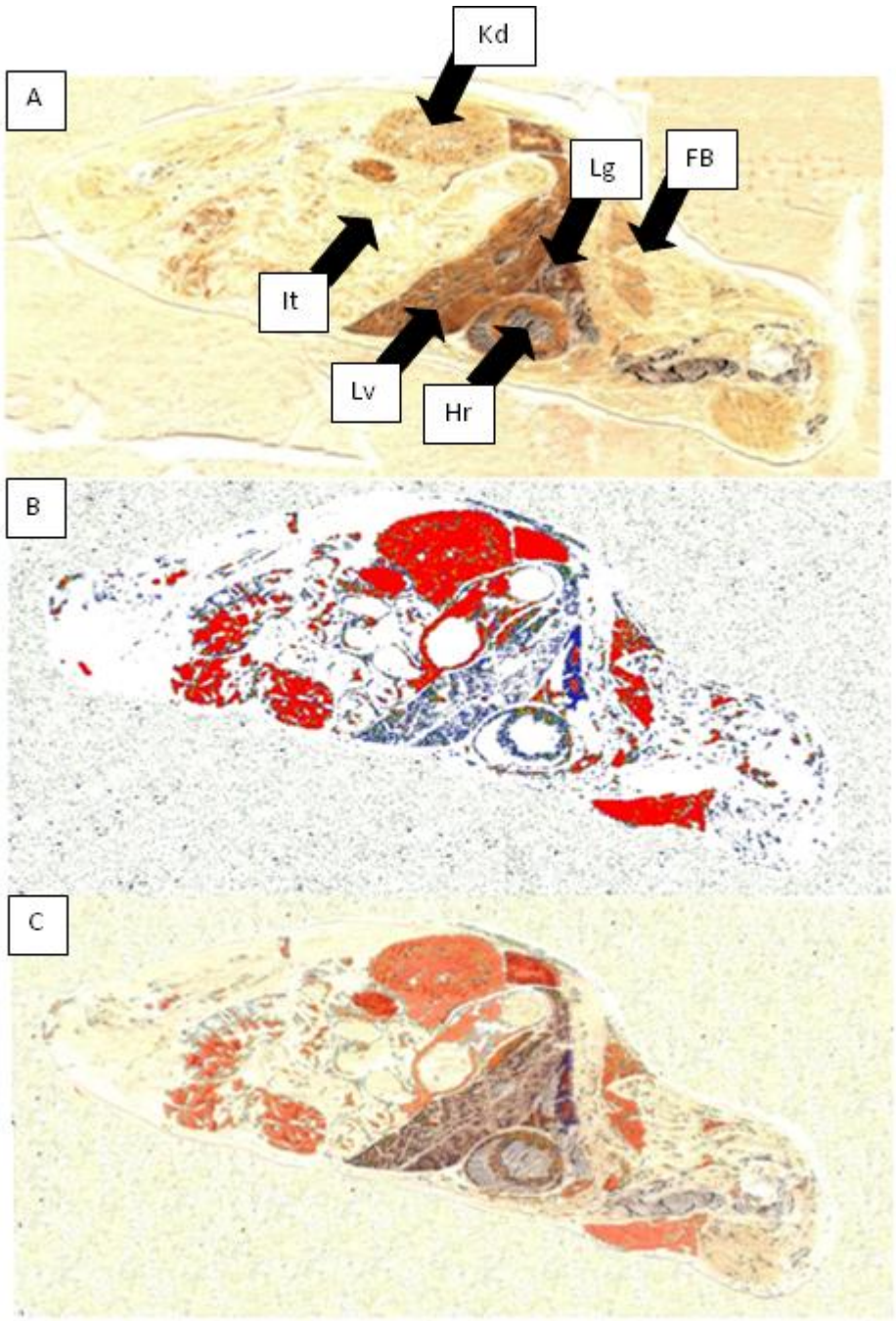

Fig. 25. 25-a: a simple photoscan of a freeze-drying cryosection taken from a mouse that received a single dose of DOX solution intravenously and euthanized 8 hours post-administration, 25-b: whole body autoradiogram of the distribution of ^{14}C from the same section, 25-c: an overlay of fig. 25-a and 25-c. Major organs are marked on the Fig. 25-c as following (FB): fatty brown, (Hr): Heart, (Lg): lung, (Lv): liver, (Kd): kidney and It: intestine. Reprinted with permission of ©Future sciences publisher

3.5.3. Results of confocal laser scanning microscopy

Confocal microscopy images of cryosections of isolated lungs of mice that received inhalable NPs labelled with FITC-dextran (group 2) are shown in Fig. 26. Images in columns a and b were collected at 530 nm for green FITC and at 650 for red DOX, respectively; images in column c are overlays of the images in columns a and b. The presence of NPs in the recorded confocal images is indicated by the overlay of green and red (orange) in column c.

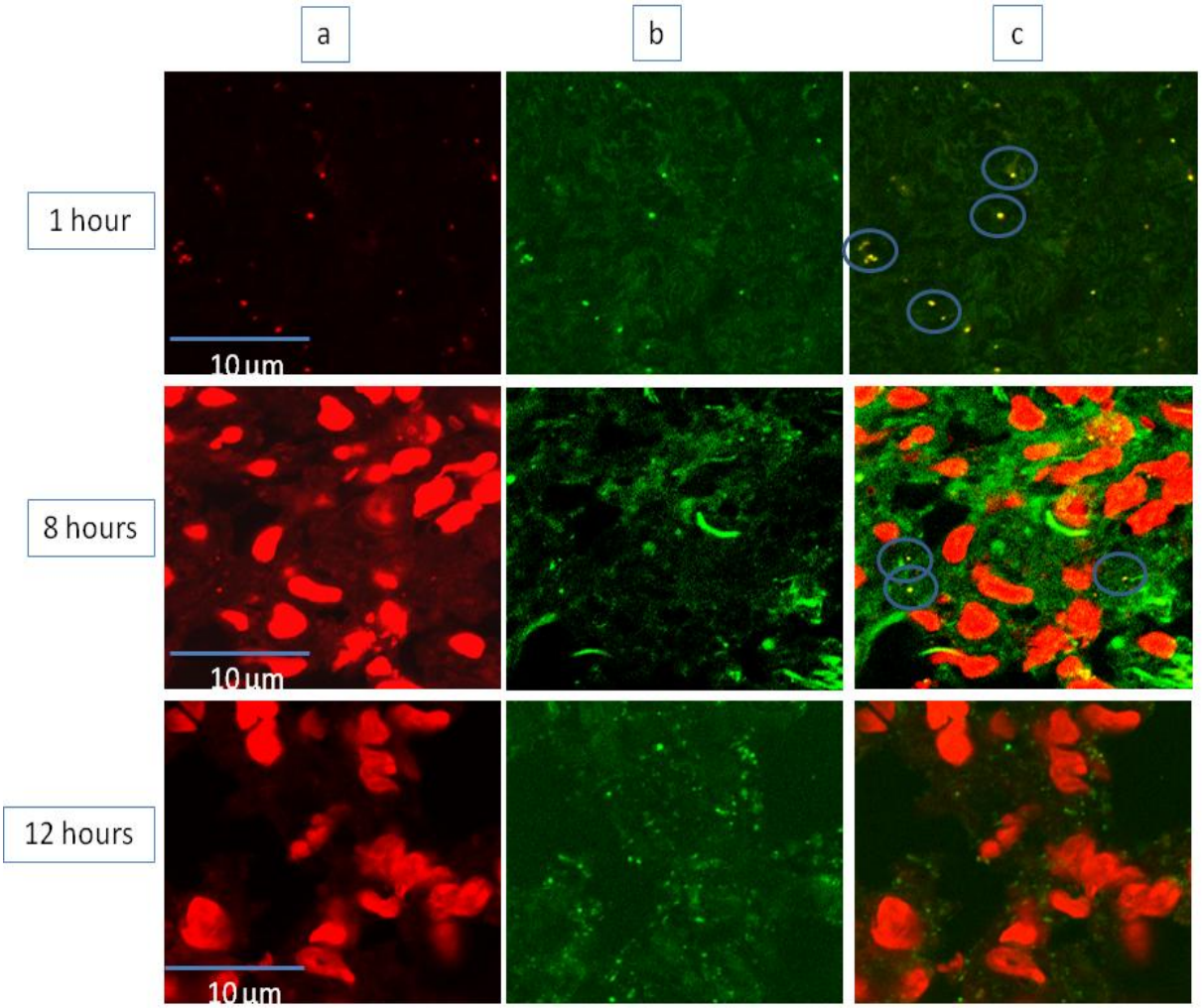

Fig. 26. Confocal laser scanning microscopy images taken for cryosections of isolated lungs from mice received a single dose of effervescent inhalable NPs and euthanized after 1, 8 and 24 hours. Column A represents images collected at 650 nm for DOX detection, column B represents images collected at 530 nm for FITC detection and column C is an overlay image of column A and B. Reprinted with permission of ©Future sciences publisher

CHAPTER 4 – DISCUSSION

4.1 Secondary cytotoxicity of NPs mediated by alveolar macrophages

BALB/C nude mice are a commonly used model for establishing the antitumor efficacy of newly developed anticancer molecules or delivery systems. We previously reported that inhalable NPs are well tolerated in this species [165]. The experiments were designed to mimic, *in vitro*, a lung cancer tumor xenograft animal model in which murine alveolar macrophages are in contact with human lung cancer cells. Moreover, to investigate other pathways that NPs might affect cancer cells other than the direct cytotoxic effect [32]. The aim was to investigate whether other anticancer mechanisms exist besides the primary cytotoxic effect of NPs on cancer cells.

DOX-loaded NPs showed superiority in reducing the viability of both macrophages and cancer cells as a result of primary cytotoxicity. Although MH-S and H460 cell lines reacted in a similar way to DOX-loaded NPs, they showed different sensitivities to blank NPs and DOX solution. Alveolar macrophages were more affected by blank NPs when compared to lung carcinoma cells. This can be explained by the difference in the phagocytotic functionality between the cell lines[205]. Alveolar macrophages are expected to have a higher ability to internalize blank NPs; thus they receive a higher amount of cytotoxic PIBCA polymer [206]. The results also showed that the cytotoxicity of the individual components in a mixture of blank NPs and DOX solution was neither synergistic nor additive. This can be explained by the fact that DOX can decrease the phagocytosis of macrophages by about 10% [207]. Therefore, this mixture was excluded from further investigation. The primary cytotoxicity of different treatments was assessed after a short period of incubation (1 h). Using a short incubation time allowed us to measure the primary cytotoxicity of different treatments before it caused an inhibitory effect; 1 h was sufficient for macrophages to complete the phagocytosis process. Lower concentrations with longer incubation times might show different results [196]. To assess

secondary cytotoxicity, macrophages were incubated with aliquots containing EC50 concentrations of different treatments for 1 h, which is a sufficient time for phagocytosis to be completed [208]. The secondary cytotoxicity detected in this study showed two main characteristics. First, it was exclusive to NPs (blank or DOX-loaded), as DOX solution did not induce secondary cytotoxicity at any time point. Second, unlike primary toxicity, secondary toxicity was not instantaneous, as no significant increase in secondary toxicity was detected after 1 h (Fig. 2). The fact that blank NPs but not DOX solution showed a high ability to trigger secondary cytotoxicity confirms that the act of phagocytosis triggers intracellular changes causing secondary cytotoxicity. A high macrophage to cancer cell ratio was required to achieve a significant increase in secondary cytotoxicity; the best results were observed with a 5:1 call ratio. The need for a high cell ratio can be explained by the lack of direct contact between macrophages and cells due to the volume of the medium used in the co-culture system. The fact that macrophages are in close proximity to cancer cells at the tumor site might augment the effect of secondary toxicity seen *in vitro* and enhance its significance. Future *in vivo* studies are needed to validate this assumption. However, other studies have shown that non-small cell lung cancer tumors are usually infiltrated with a large number of macrophages, up to 1823 cells/mm3 [209]. Furthermore, lung cancer cells eventually spread to the regional lymph node which is considered to be an important factor in lung cancer staging [210]. Videira et al. reported a significant lymphatic NP uptake after inhalation; this was explained by the ability of macrophages to act as NP reservoirs linking the alveolar spaces to lymph nodes [130]. Therefore, lymph nodes can be considered potential locations for secondary cytotoxicity.

In order to investigate the mechanism of secondary cytotoxicity, samples were collected for further analysis from the lower compartment of the co-culture system after 1, 8, and 24 h.

The ability of macrophages to release back the DOX was treatment dependent. Macrophages treated with DOX solution did not release back any DOX; however, macrophages treated with DOX-loaded NPs released back a fraction of the DOX applied to the NPs. This is explained by the macrophage cellular reaction for different treatments. When in contact with macrophages, DOX solution diffuses passively through the cell membrane, whereas DOX-loaded NPS are internalized actively by phagocytosis [211]. Exocytosis, a natural consequence of phagocytosis, could also be used to explain this observation [212]. We differentiated between two types of DOX released from the macrophages treated with NPs: free DOX and NP-attached DOX. PIBCA NPs are water insoluble, yet they are biodegradable. The release of the encapsulated drug depends mainly on NP degradation by surface erosion and/or solubilization [76]. Therefore, in order to measure the total DOX in the collected samples (free and bound), NPs must be totally dissolved. Acetonitrile was used to dissolve NPs in the collected samples [198]. In the samples collected after 1 h, the total DOX was not significantly different from free DOX, suggesting that the amount of DOX released from NPs was insignificant. Conversely, a significant increase in total DOX was detected after 8 and 24 h. This increase is attributed to the DOX attached to NP fragments, but not to the free DOX as no significant increase was detected in the free DOX at different time points. The significant difference between total and free DOX after 8 and 24 h, but not after 1 h, suggests that additional DOX, attached to NP fragments, was released from macrophages. This process was not instantaneous; there was a delay before a significant increase in total DOX concentration was observed. This can be explained by the time required to complete the exocytosis process [213]. Even though surface-associated NPs may contribute to the total DOX detected in the samples, the ratio of surface-associated NPs to phagocytized NPs in the phagocytotic cells did not exceed 1:4 [214]. Moreover, using 1% trypsin–EDTA solution

to de-attach macrophages may have also decreased the number of NPs associated with macrophage surfaces [215]. Even though alveolar macrophages were able to release fragments of NPs, the concentrations of total DOX detected at different time points were not itself enough to explain the secondary toxicity. It is well documented that after phagocytosis, macrophages undergo different intra- and extracellular changes as defensive measures [216]. Changes in the macrophage cytokine secreting pattern are one of these measures [217]. Cytokines compromise numerous numbers of mediators that profoundly affect biological aspects of a tumor such as proliferation, infiltration, and cell–cell interactions [218, 219]. Some cytokines have direct antitumor effects, and others act indirectly by recruiting and activating cytotoxic cells [220]. Moreover, cytokines such as TNF-α, IL-2, and IFN-γ have been tested *in vitro* and *in vivo* as agents for cancer therapy [218].

Our results showed a significant increase in Th1 cytokines after 8 and 24 h, but not after 1 h, in macrophages exposed to NPs compared with naïve macrophages and macrophages treated with DOX solution. Changes in the cytokine secreting profiles were limited to macrophages treated with NPs, either blank or DOX-loaded, and these changes were very similar Fig.4 and Fig.5. This indicates that these changes were not related to DOX but were related to the presence of NPs, and consequently to phagocytosis. Cytokines induced by NPs were MCP-1, MIP-1, TNF-α, and IFN-γ, listed in order of the extent of induction. MCP-1 and MIP-1 belong to the chemokines superfamily. Chemokines possess chemotactic activity for immune and inflammatory cells [221]. MCP-1 activates the tumoricidal activity of monocytes and macrophages *in vitro* and *in vivo* [222]. Besides its ability to activate and recruit immune cells, MCP-1 induces macrophages to release nitric oxide [222]. Nitric oxide mediates DNA damage and demonstrates anticancer activity [223]. MIP-1 is mainly excreted by macrophages after

phagocytosis, and its role in the inflammation process has been investigated in diseases such as asthma, arthritis, and multiple sclerosis [224]. Derivatives of MIP-1 were effective in inhibiting of tumor growth after local radiation [225]. In the same context, TNF-α has a direct cytolysis effect on cancer cells and promotes apoptotic response to some anticancer agents [226]. IFN-γ is an immune modulator and is synergistic with the TNF-α cytolytic effect on cancer cells [227]. Due to the study design, these results may not reflect an instantaneous macrophage secretion of cytokines after NP exposure. However, our aim was to focus on the later consequences of macrophage activation by NPs. As shown in Fig. 4 and Fig. 5, the increase in cytokine secretion was significant over time, but not after 1 h. Due to the time required for macrophage migration and infiltration [228], the therapeutic effect of secondary cytotoxicity might be delayed. Endotoxins are known to stimulate macrophages and induce the excretion of pro-inflammatory factors such as cytokines. However, it has been shown that endotoxin contamination is mainly associated with high levels of IL-1, IL-6, and TNF-α [229]. The NP preparations used in this experiment were endotoxin free. Our study showed that MCP-1 and MIP-1 were the main chemokines induced by NPs followed by TNF-α and IFN-γ; IL-1 and IL-6 were not induced significantly by NPs.

Cancer builds its own microenvironment surrounded by chronic inflammation. Chronic inflammation is generally associated with antibody-mediated humoral immune response, which is mainly mediate by Th2 cytokines [230]. Th1 cytokines promote acute inflammation and cell-mediated immune responses that aid cancer rejection [231]. Therefore, Th1 cytokines are associated with higher survival, whereas Th2 cytokines help build a microenvironment that makes a tumor resistant to anticancer agents [232]. Because immune responses are controlled mainly by pro-inflammatory secondary toxicity, aggressive behavior of alveolar macrophages

induced by NPs might favor cell immunity and help in cancer rejection. Thus, inhalable NPs might be effective in lung cancer treatment. Induction of other cytokines was consistent among all treatment groups, including the naïve macrophages (no treatment received); their concentrations were low and irrelevant to the type of the treatment.

We used H460 and MH-S cell lines to mimic the mouse model that has become an important tool to establish *in vivo* antitumor activity of new anticancer agents and/or delivery systems. In this model, many cell–cell interactions during tumor development and recession are common to both human and murine species [233]. The interspecies activity of cytokines such as TNF-α, MCP-1, and IL-6 has been demonstrated [234] and [235]. An increase in murine cytokine secretion was associated with a significant decrease in H460 cell viability. Apparently, cytokines detected in our study have interspecies activity, as they affected the human non-small cell lung carcinoma *in vitro*. This interspecies activity of cytokines supports the use of cancer-bearing mouse models to investigate the efficacy of new approaches, such as inhalable NPs, in treating lung cancer.

4.2 Pulmonary toxicity of polysorbate-80-coated inhalable NPs

The recorded surface pressure-area isotherm of DPPC over a subphase of purified water was close to previously reported data. The differences in values emerge from the different dimensions of the mini-trough used for this experiment [236]. The addition of free polysorbate 80 to the subphase influenced the phases of the isotherm differently (Fig. 6.b). These changes indicate an interaction of polysorbate 80 and DPPC mono-films upon compression. Molecular interactions were facilitated indicated by the fact that the gas phase was abolished. Although polysorbate 80 influenced the onset and formation of the different monolayer phases, it is important to notice that the collapse pressure of the DPPC mono-film was not significantly

affected. This observation suggests that the film was intact and its integrity was not compromised. Isotherms of DPPC monolayer spread on top of subphase containing 1 mg/ml of non-coated NPs showed also interaction between NPs and film components (Fig. 6.c). These interactions were manifested mainly by the absence of the gas phase. Previous studies have shown that particle size is also a factor which influences the penetration of NP into the DPPC monofilms [167]. The presence of NPs between DPPC molecules in monofilms is expected to change the packing of these molecules under compression. Nevertheless, it is important that the collapse pressure was very close to that observed with DPPC alone. Similar to previously observed non-coated NPs, polysorbate-80-coated NPs abolished the gas phase. The plateau region in the liquid expanded phase was comparable to the DPPC isotherm. However, the collapse pressure was almost one half of those recorded in other experiments. This indicates that polysorbate-80-coated NPs significantly reduce the stability of the DPPC monolayer film and its ability to compensate for high compression forces. The fact that polysorbate 80 alone has no significant effect on the collapse pressure supports the theory that coated NPS enhanced the interaction between NPs and the DPPC monolayer

The *in vivo* results confirmed the *in vitro* observations. As seen in the tissue sections taken from lungs of mice treated with polysorbate-80-coated NPs (Fig. 7.c), their anatomical structure was compromised. This indicates that the surfactant film lining the alveolar sacs was not able to tolerate the compression forces caused by breathing and the alveolar sacs eventually collapsed. In order to keep the lung functions, the surfactant layer must have the ability to spread as well as getting compressed during inhalation and exhalation. The surfactant layer must stay in a balance between fluidity and rigidity to stabilize the alveolar sacs. Decreasing the collapse pressure of the surfactant monolayer caused by polysorbate-80-coated NPs disturbed the

naturally occurring balance of the surfactant and caused the lungs to collapse. Even though non-coated NPs induced some changes in the DPPC monolayer, the collapse pressure was only slightly affected. No histological differences were observed between lung slices taken from a control group and the group treated with non-coated inhalable NPs. This observation supports the *in vitro* results in which the collapse pressure of a DPPC film was not affected by the addition of non-coated NPs to the subphase.

Previous studies showed that inhalable NPs were associated with pulmonary side effects depending mainly on their size [166, 237]. However, the interactions of coating materials with the lung surfactant film were not investigated till now. Monolayer systems as an *in vitro* lung surfactant model have been previously used to investigate the biophysical interaction of nano-materials with lung surfactants especially for inorganic NPs and nano-crystals [166]. In the present study, we investigated the effect of polysorbate 80 as NP coating material on the integrity of the lung surfactant layer using an *in vitro* model. The result showed that polysorbate-80-coated NPs affected the integrity and the ability of a DPPC monofilm to compensate for compression forces, resulting in a significantly reduced collapse pressures. These results were associated with higher pulmonary toxicity *in vivo* as shown by histological examinations.

4.3 Microcalorimetric method to assess phagocytosis: macrophage-NP interactions

NP characteristics found were similar to those reported previously [87, 165, 199]. The positive zeta potential of gelatin NPs can be explained by using a pH lower than the isoelectrical point of gelatin during NP preparation. The positively charged primary amine groups (−NH3 +) result in a positive zeta potential. Mannosylated gelatin NPs were bigger than non-mannosylated NPs and had less positive charge on the surface (Table 3). This can be attributed to the formation

of a Schiff's base (−C = N−) between the primary amine groups on the surface of NPs and the aldehyde groups of the ring-opened mannose moieties [87]. An IR spectrum of mannosylated gelatin NPs (Fig. 8) confirms the success of the synthesis. The stretches between 1,465–1,500 and 1,505–1,550 cm−1 correspond to Schiff's bases (−C = N−) and secondary amine groups, respectively [87].

The thermal activity profile of macrophages alone, Fig. 9.a, is different from what was reported previously [106, 108]. The thermal activity of living cells is comprised of an ascending phase followed by a descending phase. Previous reports describe both phases to be linear with no exponential subphase. The observations can be explained by a difference in experimental settings. In the previous reports, experiments were performed on macrophages suspended in cell culture media with no surface to adhere to; this is not optimal. In the present study, macrophages were seeded on special cell culture slabs that provided optimum conditions for the expression of biological functions. The ascending phase of the thermal activity profile represents a period in which the macrophages are metabolically active, with oxygen and nutrients still abundant in the cell culture medium. The exponential increase in heat exchange can be attributed to growth and multiplication of macrophages. Later, due to the increasing number of macrophages, oxygen and other essential nutrients will be depleted and cellular death will follow. This is represented by a decrease in thermal activity during the descending phase.

Titration with polysorbate-80-coated PIBCA NPs resulted in a significant decrease in the total heat production as shown in Fig. 9.c. The polysorbate-80 coating material decreased the macrophage cellular response to PIBCA NPs. Polysorbate alone or in a physical mixture with NPs had no effect on the thermal activity profiles. This suggests that the inhibition of NP

phagocytosis by polysorbate-80 is limited to the formation of a surfactant layer on the NP surface.

Cyto B is a mycotoxin with high cell permeability properties. It inhibits the formation of contractile actin microfilaments which results in inhibition of cellular movement and phagocytosis functionality [238]. Cyto B has been used as a phagocytosis inhibitor to study this cellular function [200, 239]. Cyto B was included in this experiment design to confirm that the increase in heat exchange observed after NP titration is a direct result of the phagocytosis process. If the increase in heat exchange observed after NP titration is inhibited by Cyto B, this would imply that phagocytosis is responsible for the heat exchange. As shown in Fig. 10.a, in the presence of Cyto B the macrophage thermal activity profile was significantly lower and there was a significant decrease in the total heat exchange in the medium compared with experiments performed without Cyto B, 3.9 ± 1.3 J and 9.8 ± 2.3 J, respectively. In addition to its effect on phagocytosis, Cyto B could affect other aspects of cellular function such as inhibition of glucose transportation and induction of nuclear extrusion [239], and this would impact the thermal activity profile. However, Cyto B totally inhibited an increase in heat production after NP titration, as shown in Fig. 11 (b, c). On the other hand, Cyto B had no effect on the ligand–receptor reaction of mannose and mannose receptor as shown in Fig. 12.c. Therefore, it could be concluded that the observed increase in heat exchange induced by NP titration (Figs. 1.b and 12(b, c)) was directly connected to the phagocytosis process.

Targeting mannose receptors on the macrophage cellular surface using mannose-decorated NPs is an established strategy to enhance phagocytosis [91]. Therefore, mannosylated NPs are expected to be associated with enhanced phagocytosis and, consequently, with higher heat production as detected by ITMC. The initial sharp increase in heat production associated

with mannosylated gelatin NPs (Fig. 11.c) can be explained by ligand–receptor interaction between mannose moieties and mannose receptors on the surface of macrophages. The similarity between the heat activity profiles of mannosylated gelatin NPs and the non-chemically bonded mixture of mannose and gelatin NPs (Figs. 12.c and 13.a) suggests that the presence of mannose in solution is enough to provoke and enhance the phagocytotic functionality of macrophages. This observation is in contrast to what was noticed with polysorbate-80-coated PIBCA NPs. The fact that mannose solution induced an initial sharp increase in heat production implies that the similar sharp increase observed with mannosylated gelatin NPs is a result of interaction between mannose moieties and mannose receptors. Moreover, the initial sharp increase in the heat production observed in the presence of Cyto B after titrating 100 μL (Fig. 12.c) implies that Cyto B affects phagocytosis process, yet has not effect on ligand–receptor interaction.

Flow cytometry analysis was used to validate the data obtain from ITMC. Macrophages were exposed to different NP formulations and the results were expressed in relative to the untreated macrophages. The locations of the macrophages on the dot plot along with the value of MFI were used to assess the uptake of different NP formulations. The percentage of macrophages that relocated from LL to LR quadrant represents the portion of macrophages that has been taken up NPs, however, the MFI value represents the extent of uptake.

Mannosylated gelatin NPs were associated with the highest uptake. 58.69% of the macrophages were detected in LR quadrant Fig. 14.e. These portion of macrophages showed a high MFI values, 46.08. Polysorbate-80-coated PIBCA showed the lowest uptake. Only 1% of macrophages expressed an increase in the fluorescence properties with low MFI value of 5.07. Macrophages treated with uncoated PIBCA and gelatin NPs showed similar MFI values of 16.8

and 18.39, respectively. However, gelatin NPs were associated with higher percentage of macrophages in the LR quadrant and, consequently, a higher uptake.

The results of the flow cytometry highly confirm the data collected via ITMC. The higher uptake of mannosylated gelatin NPs detected by flow cytometry was associated with the highest heat exchange and relative interactive coefficient as discussed earlier. Moreover, titrating polysorbate-coated NPs into the ITMC was associate with insignificant increase in the heat exchange detected via ITMC as shown in Fig. 9.c. This fact was supported by flow cytometry as these NPs showed almost no cellular uptake. Flow cytometry showed that gelatin NPs had a higher uptake compared with uncoated PIBCA NPs and a lower uptake in comparison with mannosylated gelatin NPs. These results are in agreement with what was observed using ITMC. ITMC showed that heat exchange and relative interactive coefficient of gelatin NPs falls in between compared with uncoated PIBCA and mannosylated gelatin NPs as shown in Table 4.

4.4 Inhalable nanoparticles as lung cancer treatment in mouse model

We investigated a new concept for the treatment of lung cancer using DOX-loaded NPs incorporated into micrometer-sized carrier particles for local delivery to the lungs. Aerosol powders with particle diameters ranging from approximately 1 to 5 μm are considered the optimum size for deposition in the lung [240]. In our previous studies we showed that NPs can be incorporated into carrier particles to make inhalable particles for alveolar deposition [196]. Spray–freeze drying rather than conventional spray drying or freeze drying was used to prepare the carrier particles with a desired MMAD. Using spray–freeze drying, the drug is not exposed to high temperatures as it may be with spray drying, and the NPs are naturally prepared with a uniform distribution throughout the carrier particle rather than accumulating at the evaporation front as may occur in spray drying [132]. The active release mechanism used in the effervescent

formulations disperses the NPs and prevents agglomeration when the carrier matrix dissolves and releases the NPs as previously reported [164].

An *in vivo* pilot study showed that Balb/c nude mice tolerate inhalable blank NPs powders [165]. These animals did not show any significant body weight loss or increased morbidity score over eight weeks. To test different formulations *in vivo*, animals were implanted with H460 lung cancer cells through the tail vein. This method was been successfully used in the past to evaluate drug treatments in mice [241].

Tumor bearing mice were treated with two different types of inhalable drug loaded nanoparticle powders, effervescent and non-effervescent. The animals treated with effervescent nanoparticle carrier showed longer survival times than animals treated with non-effervescent nanoparticle carrier. The active release mechanism resulted from the effervescent reaction of the carrier powder proved to prevent nanoparticle agglomeration and enhance the dispersion of NPs over the non-effervescent powder as shown *in vitro* [164].

To compare the effects of the route of administration, an equivalent drug dose of 30 μg DOX was injected intravenously. The animals in this group did not show any improved survival time compared to the no-treatment control group. The same dose of DOX was injected in the form of a nanoparticle suspension, however this group of animals also did not show any better survival time compared to the control group. This result might be due to a high accumulation of the NPs in the liver as shown by other studies after *i.v.* injection [242-244]. The same dose of inhalable free DOX in lactose powder was associated with high cardiac toxicity indicated by the huge increase in the AST, ALT and CPK.

The present study showed that the route of administration along with the delivery system have a crucial impact on the treatment outcome. All animals were treated with the same amount

of DOX but using different formulations and different routes of administration. There were significant differences in the survival times among groups. Local delivery of the drug via inhalation is expected to place the DOX NPs in the vicinity of lung cancer cells with less systemic exposure resulting in less toxic side effects. The loading of DOX into NPs significantly reduced the cardiotoxicity due to the lower concentration of free drug. The enhanced tolerability of DOX-loaded inhalable NPs over the inhalable free DOX made the pulmonary delivery of this anticancer agent a viable option and significantly increased the therapeutic effect of the treatment.

It was expected that the inhalable nanoparticle powder would decrease the tumor mass and tumor number in the lungs due to localized delivery. It was not necessarily expected that the mice would have an increased survival time. Animals that died in the inhalable nanoparticle treatment groups died of huge tumor burdens in other parts of their body but not because of high tumor burden in the lungs.The results showed that inhalable nanoparticle powders significantly increased the survival time of the mice compared to all control groups. After deposition and dispersion in the lungs, DOX NPs may migrate to other organs through the lymphatic system or by translocation from the alveolar space to the blood. NPs could then passively accumulate in tumors located outside the lungs. Further studies are ongoing to establish this mechanism. The lungs, as a part of the MPS, are extensively rich with alveolar macrophages [167]. Therefore, macrophages are expected to have a substantial effect on the fate of inhaled NPs and the efficacy of any treatment using inhalable NPs as a delivery system [201] and [121]. In general, a portion of the inhaled NPs evades macrophages and translocates out of the alveolar spaces to other lung tissues and to the general circulation [176]. Another fraction of the inhaled NPs might be cleared by the alveolar macrophages, similar to other foreign objects brought into the lungs during

breathing [245]. Consequently, the effectiveness of any anticancer therapy using inhalable NPs might be affected by the extent to which inhaled NPs are cleared by macrophages. The presence of alveolar macrophages limits the chance of NPs to reach cancer cells and decreases their efficacy as anticancer agents.

Evading macrophages by using hydrophilic surfactants, such as polysorbate 80 to coat the NPs surface is not a viable option in the pulmonary delivery of NPs as polysorbate-80-coated inhalable NPs were associated the pulmonary toxicity and decrease the tolerance *in vitro* and *in vivo* [188].

Another strategy to evade macrophage might be using smaller NPs as they are associated with less macrophage uptake and enhanced accumulation at tumor sites [62, 246-248]

The fact that effervescent carrier powders have an active release mechanism that prevents NP agglomeration and enhances NP dispersion after inhalation might have contributed to the difference observed between effervescent and non-effervescent carrier powders. NPs released from effervescent carrier powders after pulmonary delivery were smaller in size than the ones released from the non-effervescent carrier powders [164].

The present study showed that inhalable drug loaded NPs were effective in treating lung cancer and may have the potential to be used in cancer treatments of organs other than the lung.

4.5 Distribution of inhalable NPs after pulmonary delivery

Our previous results showed that an effervescent formulation of inhalable NPs was more effective than a non-effervescent formulation. This was attributed to the active mechanism of NP release from the microcarrier powder [125]. Because of the high cost and limited availability of ^{14}C-labelled DOX, an effervescent inhalable NP formulation only was used in this experiment.

Fig. 23.c shows that inhalable NPs achieved deep lung deposition as the radioactivity was detected as a cloud in the central part of the lungs. This is attributed mainly to optimization of the MMAD during the spray-freeze drying process. Use of a DP-4M insufflator as described in the method might help to achieve deep-lung deposition of the inhalable NPs; however, deep lung delivery is not achieved simply by the location of the insufflator tip. Optimization of the MMAD is necessary so that the NPs do not deposit in the trachea and other parts of the pulmonary tracks after they leave the insufflator tip (this usually happens with particles of MMAD > 5 mm) nor are the NPs exhaled immediately after inhalation (this usually happens with particles of MMAD < 1 μm). No radioactivity was detected in other organs or tissues. Eight hours postinhalation, the autoradiogram showed that radioactivity, which corresponds to radio-labelled NPs, had spread to larger areas of the lungs. Importantly, the heart showed no radioactivity. These results agree with the high cardiac safety profile of inhalable DOX-loaded NPs when compared with inhalable or injectable free DOX (not loaded in NPs) [125].

The autoradiogram in Fig. 24.c shows some extrapulmonary hot spots (outlined by red circles). Comparing the autoradiograms of 1 and 8 hours postdosing we observe that NPs disseminates to different parts of the lung and migrate to other tissues over time. Because of the unique sample nature (freeze-dried and attached to a piece of tape), we were unable to perform pathology to confirm the nature of the extrapulmonary tissues associated with radioactivity.

After settling in the alveolar spaces, the fate of inhalable NPs is determined mainly by their physical characteristics such as size and surface [181]. A portion of the inhaled NPs—mainly the ultrafine NPs (about 20 nm)—evades macrophages and migrates out of the alveolar spaces to other lung tissues and to the general circulation [175]. Larger NPs are expected to stay in the

lung or be taken up by alveolar macrophages, similar to impurities brought into the lungs during breathing [201].

Inhalable rifampicin-loaded PLGA NPs showed a prolonged rifampicin presence in the lungs, with detectable drug levels up to 8 hours after pulmonary delivery in guinea pigs [122] [122]. Tomoda et al. studied the body distribution of TAS-103 (an anticancer agent) after pulmonary delivery in the form of nanocomposites; the TAS-103 concentration in the lungs after pulmonary delivery was 13 times higher than the lung concentration after *i.v.* injection of the same dose [177]. Another study showed gold colloid particles in endocytic vesicles in alveolar epithelial cells (types I & II) and in phagocytotic vacuoles in alveolar macrophages postinhalation [178]. These results suggested an important role of transcytosis of NPs across the alveolar epithelium and migration of particle-loaded alveolar macrophages to different parts of the lungs and to extrapulmonary organs. The results of the current study are different from results reported by Videria et al [130] in which the biodistribution of SLNs was evaluated in healthy rats. SLNs were labelled using ^{99m}Tc and administered to the lungs using a nebulizer. Their results showed that after 4 hours postinhalation only 25% of the total radioactivity was retained in the lung; the rest of the radioactivity was spotted mainly in the lymph nodes (para-aortic, axillary, and inguinal) followed by the MPS organs such as the liver. Apart from the differences in the nature of the NPs and the administration methods between this experiment the one performed by Videria et al., the most important factor attributed to the different results was the health status of the animal models: healthy rats were used in the Videria et al. study, whereas our rats had been implanted with cancer cells two weeks before the present study. The nature of the animal model used in this biodistribution study might explain the longer retention time of the inhalable NPs in

the lungs. Unlike normal cells, cancer cells multiply in a microenvironment associated with chronic inflammation that is generally caused by inflammatory cytokines [180].

These cytokines attract alveolar macrophages that infiltrate the tumor tissue and turns them into TAM [181, 182] . This fact suggests that, due to nonfunctional macrophages, inhalable NPs may have less chance to translocate to extrapulmonary benign tissues via transcytosis. However, TAMs might play an important role in NP transcytosis to different parts of cancerous lung tissues. Moreover, a tumor is associated with poor lymph draining due to the lack of a well-defined lymphatic system [52] . This may delay the lymphatic uptake of the inhalable NPs and result in longer retention time in the lungs. Twenty-four hours postinhalation, the autoradiogram (Fig. 25) shows that radioactive NPs have spread over the whole lung and traces of radioactivity are observed in the intestinal loops. This observation supports the theory that the promising result of inhalable NPs may be a result of local activity in the lungs. The biodistribution of polyisobutyl and polyisohexyl cyanoacrylate NPs was studied previously and results showed that NPs were mainly sequestrated in the MPS organs, mainly by the liver and spleen [78, 206]. Therefore, the design of this experiment did not include the biodistribution of PIBCA NPs after *i.v.* administration. The autoradiogram of DOX solution administered by tail vain injection after 8 hours (Fig. 26) showed that DOX was distributed nonspecifically everywhere: the liver, the kidney, fatty brown muscle, fatty tissues, and the heart. Unlike the DOX in inhaled NPs, the DOX radioactivity in tail vein administration was traced to the heart where DOX exerts its most dose-limiting side effect, cardiotoxicity [249]. Most side effects produced by anticancer agents are a result of their wide distribution in normal as well as malignant tissues. The long retention of NPs in the lung due to pulmonary delivery, and the wide distribution in lung tissue due to the

active mechanism of NP release, can contribute to the high efficacy of effervescent inhalable NPs in lung cancer treatment.

Confocal microscope images recorded 1 hour postdosage (Fig. 25.a) show what remained of the effervescent microparticle carrier loaded with DOX-loaded NPs and labelled with FITC, as indicated by the overlay of green and red (orange). After 8 hours, images showed the appearance of red nuclei. DOX exerts its anticancer effect via DNA intercalation, interrupting DNA replication and consequently preventing mitosis [250]. After cellular uptake, PIBCA NPs undergo enzymatic degradation (mainly ester hydrolysis). This degradation is responsible for DOX release [76]. DOX released from NPs intracellularly is mainly taken up by nuclei which make it bright red, and some DOX is detected in the cytosol. FITC is mainly observed in the cytosol but is barely noticed inside the nucleus. These observations support the hypothesis that DOX, but not FITC, was selectively transported to nuclei. Images recorded after 24 hours showed that DOX was mostly confined within the nucleus of shrunken cells. The novelty of this NP cellular uptake study is that it was performed *in vivo*, which makes it more applicable to human treatment than similar cellular uptake studies performed *in vitro* on cell cultures.

4.6 General conclusion

The interaction between delivery systems (i.e., NPs), tumors, and macrophages is considered the holy trinity of cancer therapy. Controlling and modulating the consequences of these interactions (cancerous cell-macrophage, NP-macrophage and NP-cancerous cells) might assist in designing more effective cancer treatments. Each of these interactions is considered a two-way interaction, with both sides affecting each other positively or negatively. The importance of this relationship becomes clearer when a tumor is located in an organ reached by macrophages, such as the lungs. Pulmonary delivery of inhalable NPs might offer several

advantages over the traditional *i.v.* administration; one of the most important being the localized effect of NPs after deep lung deposition with successful release of the NPs. However, different aspects need to be understood before optimal formulations of inhalable NPs are identified for lung cancer treatment. The present investigations included: *(i)* studying the effect of NPs on macrophages and the behaviour of macrophages after they are exposed to NPs; *(ii)* determining the safety and tolerability of different NPs formulations; *(iii)* assessing the affinity of macrophages to different NP formulations; and finally *(iv)* evaluating the efficacy and the distribution of inhalable NPs after pulmonary delivery *in vivo*.

Our results showed that DOX-loaded NPs were taken up by alveolar macrophages, and fragments of NPs were released from macrophages over time. The phagocytosis of NPs caused an inflammatory response in macrophages hours after exposure. Normally, an inflammatory reaction caused by NPs is an undesirable effect. However, Th1 cytokines, which are secreted by alveolar macrophages, caused a significant secondary cytotoxicity effect on H460 cancer cells. Th1 cytokines may add an immune pathway to the chemotherapy approach of DOX-loaded NPs, thus contributing to the overall effectiveness of the treatment *in vivo*.

The role of macrophages in cancer treatment is still debatable. Several strategies have been implemented in the production of NPs to avoid their rapid phagocytosis by macrophages after *i.v.* administration; however, our in vitro results showed that one of these strategies (using polysorbate-80 as coating material) might be associated with pulmonary toxicity. Moreover, these results were confirmed *in vivo* using an animal model. Therefore, the presented *in vitro* model for studying the Surface Pressure-Area Isotherms should be considered as an early screening tool to assess the biophysical compatibility of selected drug carriers with lung surfactant films. The decrease in the collapse pressure of the monolayer film caused by coated

NPs, *in vitro,* was associated with an acute pulmonary toxicity *in vivo*. This *in vivo* toxicity was not observed when uncoated NPs were used. Therefore, the toxicity of colloidal carriers intended for pulmonary delivery is mainly determined by their final composition rather than their individual components. More investigations are required to determine different cut-off points for the collapse pressure to correlate them with different stages of pulmonary toxicity *in vivo*. These outcomes, though, should not be generalized to all surfactants or bi-block polymers; other surfactants with different hydrophilic-lipophilic properties might interact differently with lung surfactant films. This method may be useful to establish upper deposition limits for inhalable dry powders.

After proving the safety of any strategy to modify formulations that aims to change the affinity of NPs to macrophages, it is important assess the efficiency. Our results showed that ITMC is able to differentiate, in real-time, between the cellular responses of macrophages to different NP formulations in terms of heat exchange. The thermal activity was dependent on the type of NP present. Additionally, the flow cytometry confirmed cellular NP uptake and it provided insight to the cellular responses of macrophages to NPs by way of continuous monitoring for the heat production from macrophages. The advantages of using ITMC over other techniques such as flow cytometry are the ability to use NPs without use of tagging fluorophore and the real-time monitoring of the cellular responses.

In terms of efficacy, inhalable DOX NP powders, as compared to *i.v.* administration of the same drug dose, increased the survival time of cancer-bearing mice. The inhalable NP preparation showed less cardiotoxicity than did administration of free DOX. This might be useful clinically to increase the total DOX dose. In addition, the effervescent carrier was more effective when compared to a non-effervescent formulation.

In terms of bodily distribution, the whole body autoradiograms showed that inhalable NPs carried in effervescent microparticles achieved deep lung deposition. Moreover, NPs disseminated to different parts of the lung and to some extrapulmonary tissues. The long retention time (24 hours) of inhalable NPs in the lungs contributes to their efficacy and safety. Confocal microscopy images indicated that DOX was released from the inhalable NPs after deep lung deposition and reached cell nuclei to exert anticancer activity. The ability of inhalable NPs to achieve deep lung deposition, to be actively released from microcarrier particles, to spread to different parts of the lung, and to release DOX *in vivo* all contribute to the efficacy of the delivery and localization of the effervescent inhalable NPs and demonstrate this as a novel approach to cancer treatment. The current results, and previous studies of the safety and efficacy of inhalable effervescent NPs, support the use of this delivery system as a lung cancer treatment in humans.

4.7 Future perspectives

The results of this work highlight the importance of the delivery system and route of administration in cancer treatment. The formulation of NPs and microcarriers showed to affect the tolerability, the interactions with macrophages, and the efficacy and distribution of inhalable NPs. Further experiments should investigate the following:

(i) Active targeting properties (antibodies or other targeting moieties) could be added to effervescent inhalable NPs to recognize cancerous cells in lung or extrapulmonary organs after pulmonary delivery.

(ii) The effect of the effervescent reaction on the stability of the targeting moiety should be evaluated.

(iii) The macrophage-NP relationship should be studied further, and effects of inhalable NPs on targeting or avoiding alveolar macrophages could be investigated.

CHAPTER 5- REFERENCES

1. Soerjomataram, I., et al., *Reducing inequalities in lung cancer incidence through smoking policies.* Lung Cancer, 2011. **73**(3): p. 268-73.
2. O'Connor, S.J., *Review of the incidence, prevalence, mortality and causative factors for lung cancer in Europe.* Eur J Cancer, 2011. **47 Suppl 3**: p. S346-7.
3. Field, R.W., et al., *An overview of the North American residential radon and lung cancer case-control studies.* J Toxicol Environ Health A, 2006. **69**(7): p. 599-631.
4. Dela Cruz, C.S., L.T. Tanoue, and R.A. Matthay, *Lung cancer: epidemiology, etiology, and prevention.* Clin Chest Med, 2011. **32**(4): p. 605-44.
5. McErlean, A. and M.S. Ginsberg, *Epidemiology of lung cancer.* Semin Roentgenol, 2011. **46**(3): p. 173-7.
6. Cohen, M.H., et al., *FDA drug approval summary: pemetrexed for injection (Alimta) for the treatment of non-small cell lung cancer.* Oncologist, 2005. **10**(6): p. 363-8.
7. Cohen, M.H., et al., *FDA drug approval summary: gefitinib (ZD1839) (Iressa) tablets.* Oncologist, 2003. **8**(4): p. 303-6.
8. Cohen, M.H., et al., *FDA drug approval summary: erlotinib (Tarceva) tablets.* Oncologist, 2005. **10**(7): p. 461-6.
9. Eaton, K.D. and R.G. Martins, *Maintenance chemotherapy in non-small cell lung cancer.* J Natl Compr Canc Netw, 2010. **8**(7): p. 815-21.
10. Haura, E.B., et al., *Molecular origins of lung cancer: prospects for personalized prevention and therapy.* J Thorac Oncol, 2010. **5**(6 Suppl 3): p. S207-13.
11. Mountain, C.F., *Revisions in the International System for Staging Lung Cancer.* Chest, 1997. **111**(6): p. 1710-7.
12. Armstrong, P., et al., *Guidelines on the selection of patients with lung cancer for surgery.* Thorax, 2001. **56**(2): p. 89-108.
13. Kobayashi, K., *[Guide line for the treatment of stage I and stage II non small cell lung cancer].* Nihon Geka Gakkai Zasshi, 2004. **105**(7): p. 392-403.
14. Pfister, D.G., et al., *American Society of Clinical Oncology treatment of unresectable non-small-cell lung cancer guideline: update 2003.* J Clin Oncol, 2004. **22**(2): p. 330-53.
15. Kim, Y.H. and M. Mishima, *Maintenance chemotherapy for non-small-cell lung cancer.* Cancer Treat Rev, 2011. **37**(7): p. 505-10.
16. Liu, J. and M.R. Johnston, *Animal models for studying lung cancer and evaluating novel intervention strategies.* Surg Oncol, 2002. **11**(4): p. 217-27.
17. Livingood, L.E., *Tumors in the mouse.* Johns Hopkins Bulletin, 1986. **66/67**: p. 177.
18. Tuveson, D.A. and T. Jacks, *Modeling human lung cancer in mice: similarities and shortcomings.* Oncogene, 1999. **18**(38): p. 5318-24.
19. Corbett, T.H., et al., *Tumor induction relationships in development of transplantable cancers of the colon in mice for chemotherapy assays, with a note on carcinogen structure.* Cancer Res, 1975. **35**(9): p. 2434-9.
20. Corbett, T.H., et al., *Induction and chemotherapeutic response of two transplantable ductal adenocarcinomas of the pancreas in C57BL/6 mice.* Cancer Res, 1984. **44**(2): p. 717-26.
21. Wang, Y., et al., *A chemically induced model for squamous cell carcinoma of the lung in mice: histopathology and strain susceptibility.* Cancer Res, 2004. **64**(5): p. 1647-54.
22. Ambrosini, V., et al., *Assessment of a chemically induced model of lung squamous cell carcinoma in mice by 18F-FDG small-animal PET.* Nucl Med Commun, 2007. **28**(8): p. 647-52.
23. Balmain, A. and C.C. Harris, *Carcinogenesis in mouse and human cellsparallels and paradoxes.* Carcinogenesis, 2000. **21**: p. 371-377.
24. Curt, C.A., *The use of animal models in cancer drug discovery and development.* stem cells, 1994. **12**: p. 23-29.

25. Povlsen, C.O. and J. Rygaard, *Heterotransplantation of human adenocarcinomas of the colon and rectum to the mouse mutant Nude. A study of nine consecutive transplantations.* Acta Pathol Microbiol Scand A, 1971. **79**(2): p. 159-69.
26. Kuo, T.H., et al., *Site-specific chemosensitivity of human small-cell lung carcinoma growing orthotopically compared to subcutaneously in SCID mice: the importance of orthotopic models to obtain relevant drug evaluation data.* Anticancer Res, 1993. **13**(3): p. 627-30.
27. Howard, R.B., et al., *Irradiated nude rat model for orthotopic human lung cancers.* Cancer Res, 1991. **51**(12): p. 3274-80.
28. Howard, R.B., et al., *Characterization of a highly metastatic, orthotopic lung cancer model in the nude rat.* Clin Exp Metastasis, 1999. **17**(2): p. 157-62.
29. Wang, X., et al., *A new patient-like metastatic model of human small-cell lung cancer constructed orthotopically with intact tissue via thoracotomy in nude mice.* Anticancer Res, 1992. **12**(5): p. 1403-6.
30. McLemore, T.L., et al., *Novel intrapulmonary model for orthotopic propagation of human lung cancers in athymic nude mice.* Cancer Res, 1987. **47**(19): p. 5132-40.
31. Kuo, T.H., et al., *Orthotopic reconstitution of human small-cell lung carcinoma after intravenous transplantation in SCID mice.* Anticancer Res, 1992. **12**(5): p. 1407-10.
32. Yu, D., et al., *c-erbB-2/neu overexpression enhances metastatic potential of human lung cancer cells by induction of metastasis-associated properties.* Cancer Res, 1994. **54**(12): p. 3260-6.
33. Yang, L., et al., *Predominant suppression of apoptosome by inhibitor of apoptosis protein in non-small cell lung cancer H460 cells: therapeutic effect of a novel polyarginine-conjugated Smac peptide.* Cancer Res, 2003. **63**(4): p. 831-7.
34. Dallavalle, S., et al., *Novel 7-oxyiminomethyl derivatives of camptothecin with potent in vitro and in vivo antitumor activity.* J Med Chem, 2001. **44**(20): p. 3264-74.
35. Liu, Y., H. Miyoshi, and M. Nakamura, *Nanomedicine for drug delivery and imaging: a promising avenue for cancer therapy and diagnosis using targeted functional nanoparticles.* Int J Cancer, 2007. **120**(12): p. 2527-37.
36. Banerjee, D. and S. Sengupta, *Nanoparticles in cancer chemotherapy.* Prog Mol Biol Transl Sci, 2011. **104**: p. 489-507.
37. Gelperina, S., et al., *The potential advantages of nanoparticle drug delivery systems in chemotherapy of tuberculosis.* Am J Respir Crit Care Med, 2005. **172**(12): p. 1487-90.
38. Davis, M.E., Z.G. Chen, and D.M. Shin, *Nanoparticle therapeutics: an emerging treatment modality for cancer.* Nat Rev Drug Discov, 2008. **7**(9): p. 771-82.
39. Fukami, T., et al., *Nanoparticle processing in the solid state dramatically increases the cell membrane permeation of a cholesterol-lowering drug, probucol.* Mol Pharm, 2009. **6**(3): p. 1029-35.
40. Khan, J.A., et al., *Water soluble nanoparticles from PEG-based cationic hyperbranched polymer and RNA that protect RNA from enzymatic degradation.* Biomacromolecules, 2006. **7**(5): p. 1386-8.
41. Wong, H.L., et al., *A mechanistic study of enhanced doxorubicin uptake and retention in multidrug resistant breast cancer cells using a polymer-lipid hybrid nanoparticle system.* J Pharmacol Exp Ther, 2006. **317**(3): p. 1372-81.
42. Gipps, E.M., et al., *Distribution of polyhexylcyanoacrylate nanoparticles in nude mice over extended times and after repeated injection.* J Pharm Sci, 1988. **77**(3): p. 208-9.
43. Brannon-Peppas, L. and J.O. Blanchette, *Nanoparticle and targeted systems for cancer therapy.* Adv Drug Deliv Rev, 2004. **56**(11): p. 1649-59.
44. Moghimi, S.M., A.C. Hunter, and J.C. Murray, *Long-circulating and target-specific nanoparticles: theory to practice.* Pharmacol Rev, 2001. **53**(2): p. 283-318.

45. Brigger, I., C. Dubernet, and P. Couvreur, *Nanoparticles in cancer therapy and diagnosis.* Adv Drug Deliv Rev, 2002. **54**(5): p. 631-51.
46. Byrne, J.D., T. Betancourt, and L. Brannon-Peppas, *Active targeting schemes for nanoparticle systems in cancer therapeutics.* Adv Drug Deliv Rev, 2008. **60**(15): p. 1615-26.
47. Folkman, J., *Angiogenesis in cancer, vascular, rheumatoid and other disease.* Nat Med, 1995. **1**(1): p. 27-31.
48. Jain, R.K., *Delivery of molecular medicine to solid tumors: lessons from in vivo imaging of gene expression and function.* J Control Release, 2001. **74**(1-3): p. 7-25.
49. Maeda, H., et al., *Enhanced vascular permeability in solid tumor is mediated by nitric oxide and inhibited by both new nitric oxide scavenger and nitric oxide synthase inhibitor.* Jpn J Cancer Res, 1994. **85**(4): p. 331-4.
50. Jain, R.K., *Determinants of tumor blood flow: a review.* Cancer Res, 1988. **48**(10): p. 2641-58.
51. Hobbs, S.K., et al., *Regulation of transport pathways in tumor vessels: role of tumor type and microenvironment.* Proc Natl Acad Sci U S A, 1998. **95**(8): p. 4607-12.
52. Haley, B. and E. Frenkel, *Nanoparticles for drug delivery in cancer treatment.* Urol Oncol, 2008. **26**(1): p. 57-64.
53. Gordon, S., *The macrophage.* Bioessays, 1995. **17**(11): p. 977-86.
54. Illum, L., et al., *Evaluation of carrier capacity and release characteristics for poly(butyl 2-cyanoacrylate) nanoparticles* Int. J. Pharm, 1985. **30**(1): p. 17-28.
55. Chonn, A., S.C. Semple, and P.R. Cullis, *Association of blood proteins with large unilamellar liposomes in vivo. Relation to circulation lifetimes.* J Biol Chem, 1992. **267**(26): p. 18759-65.
56. Moghimi, S.M. and S.S. Davis, *Innovations in avoiding particle clearance from blood by Kupffer cells: cause for reflection.* Crit Rev Ther Drug Carrier Syst, 1994. **11**(1): p. 31-59.
57. Absolom, D.R., *Opsonins and dysopsonins: an overview.* Methods Enzymol, 1986. **132**: p. 281-318.
58. Patel, H.M., *Serum opsonins and liposomes: their interaction and opsonophagocytosis.* Crit Rev Ther Drug Carrier Syst, 1992. **9**(1): p. 39-90.
59. Senior, J. and G. Gregoriadis, *Is half-life of circulating liposomes determined by changes in their permeability?* FEBS Lett, 1982. **145**(1): p. 109-14.
60. Narkates, A.J. and J.E. Volanakis, *C-reactive protein binding specificities: artificial and natural phospholipid bilayers.* Ann N Y Acad Sci, 1982. **389**: p. 172-82.
61. Volanakis, J.E. and A.J. Narkates, *Interaction of C-reactive protein with artificial phosphatidylcholine bilayers and complement.* J Immunol, 1981. **126**(5): p. 1820-5.
62. Gref, R., et al., *Biodegradable long-circulating polymeric nanospheres.* Science, 1994. **263**(5153): p. 1600-3.
63. Alyaudtin, R.N., et al., *Interaction of poly(butylcyanoacrylate) nanoparticles with the blood-brain barrier in vivo and in vitro.* J Drug Target, 2001. **9**(3): p. 209-21.
64. Nguyen, M., F.R. Eilber, and S. Defrees, *Novel synthetic analogs of sialyl Lewis X can inhibit angiogenesis in vitro and in vivo.* Biochem Biophys Res Commun, 1996. **228**(3): p. 716-23.
65. Ramphal, J.Y., et al., *Ligand interactions with E-selectin. Identification of a new binding site for recognition of N-acyl aromatic glucosamine substituents of sialyl Lewis X.* J Med Chem, 1996. **39**(7): p. 1357-60.
66. Lee, R.J. and L. Huang, *Folate-targeted, anionic liposome-entrapped polylysine-condensed DNA for tumor cell-specific gene transfer.* J Biol Chem, 1996. **271**(14): p. 8481-7.
67. Lee, R.J. and P.S. Low, *Folate-mediated tumor cell targeting of liposome-entrapped doxorubicin in vitro.* Biochim Biophys Acta, 1995. **1233**(2): p. 134-44.
68. Phillips, N.C., et al., *mmunoliposome targeting to murine CD4+ leucocytes is dependent on immune status.* J Immunol, 1194. **152**(3168–3174).

69. Soppimath, K.S., et al., *Biodegradable polymeric nanoparticles as drug delivery devices.* J Control Release, 2001. **70**(1-2): p. 1-20.
70. Scholes, P.D., et al., *The preparation of sub-500 nm poly(lactide-co-glycolide) microspheres for site-specific drug delivery.* J Control Release, 1993. **25**: p. 145-153.
71. Niwa, T., et al., *Preparations of biodegradable nanospheres of water-soluble and insoluble drugs with d,l-lactide/glycolide copolymer by a novel spontaneous emulsification solvent diffusion method and the drug release behavior.* J Control Release, 1993. **25**(89-98).
72. Hu, Y., et al., *Preparation and drug release behaviors of nimodipine-loaded poly(caprolactone)-poly(ethylene oxide)-polylactide amphiphilic copolymer nanoparticles.* Biomaterials, 2003. **24**(13): p. 2395-404.
73. Pani, K.C., et al., *The degradation of n-butyl alpha-cyanoacrylate tissue adhesive. II.* Surgery, 1968. **63**(3): p. 481-9.
74. Couvreur, P., *Polyalkylcyanoacrylates as colloidal drug carriers.* Crit Rev Ther Drug Carrier Syst, 1988. **5**(1): p. 1-20.
75. Rollot, J.M., et al., *Physicochemical and morphological characterization of polyisobutyl cyanoacrylate nanocapsules.* J Pharm Sci, 1986. **75**(4): p. 361-4.
76. Lenaerts, V., et al., *Degradation of poly (isobutyl cyanoacrylate) nanoparticles.* Biomaterials, 1984. **5**(2): p. 65-8.
77. Muller, R.H., et al., *In vitro model for the degradation of alkylcyanoacrylate nanoparticles.* Biomaterials, 1990. **11**(8): p. 590-5.
78. Verdun, C., et al., *Tissue distribution of doxorubicin associated with polyisohexylcyanoacrylate nanoparticles.* Cancer Chemother Pharmacol, 1990. **26**(1): p. 13-8.
79. Gibaud, S., et al., *Increased bone marrow toxicity of doxorubicin bound to nanoparticles.* Eur J Cancer, 1994. **30A**(6): p. 820-6.
80. Soma, C.E., et al., *Investigation of the role of macrophages on the cytotoxicity of doxorubicin and doxorubicin-loaded nanoparticles on M5076 cells in vitro.* J Control Release, 2000. **68**(2): p. 283-9.
81. Chiannilkulchai, N., et al., *Hepatic tissue distribution of doxorubicin-loaded nanoparticles after i.v. administration in reticulosarcoma M 5076 metastasis-bearing mice.* Cancer Chemother Pharmacol, 1990. **26**(2): p. 122-126.
82. Lobenberg, R. and J. Kreuter, *Macrophage targeting of azidothymidine: a promising strategy for AIDS therapy.* AIDS Res Hum Retroviruses, 1996. **12**(18): p. 1709-15.
83. Bender, A., et al., *Inhibition of HIV in vitro by antiviral drug-targeting using nanoparticles.* Res Virol, 1994. **145**(3-4): p. 215-220.
84. Gaspar, R., et al., *Macrophage activation by polymeric nanoparticles of polyalkylcyanoacrylates: activity against intracellular Leishmania donovani associated with hydrogen peroxide production.* Pharm Res, 1992. **9**(6): p. 782-7.
85. Bazile, D., et al., *Stealth Me.PEG-PLA nanoparticles avoid uptake by the mononuclear phagocytes system.* J Pharm Sci, 1995. **84**(4): p. 493-8.
86. Peracchia, M.T., et al., *Stealth PEGylated polycyanoacrylate nanoparticles for intravenous administration and splenic targeting.* J Control Release, 1999. **60**(1): p. 121-8.
87. Jain, S.K., et al., *Mannosylated gelatin nanoparticles bearing an anti-HIV drug didanosine for site-specific delivery.* Nanomedicine, 2008. **4**(1): p. 41-8.
88. Gulyaev, A.E., et al., *Significant transport of doxorubicin into the brain with polysorbate 80-coated nanoparticles.* Pharm Res, 1999. **16**(10): p. 1564–1569.
89. Araujo, L., R. Lobenberg, and J. Kreuter, *Influence of the surfactant concentration on the body distribution of nanoparticles.* J Drug Target, 1999. **6**(5): p. 373-85.

90. Cheng, J., et al., *Formulation of functionalized PLGA-PEG nanoparticles for in vivo targeted drug delivery.* Biomaterials, 2007. **28**(5): p. 869-76.
91. Irache, J.M., et al., *Mannosetargeted systems for the delivery of therapeutics.* Expert Opin Drug Deliv, 2009. **5**(6): p. 703-724.
92. Cui, Z., C.H. Hsu, and R.J. Mumper, *Physical characterization and macrophage cell uptake of mannan-coated nanoparticles.* Drug Dev Ind Pharm, 2003. **29**(6): p. 689-700.
93. Moghimi, S.M. and A.C. Hunter, *Capture of stealth nanoparticles by the body's defences.* Crit Rev Ther Drug Carrier Syst, 2001. **18**(6): p. 527-50.
94. Verma, R.K., et al., *Inhaled therapies for tuberculosis and the relevance of activation of lung macrophages by particulate drug-delivery systems.* Therapeutic Delivery, 2011. **2**(6): p. 753-768.
95. Cifarelli, A., et al., *The influence of some metabolic inhibitors on phagocytic activity of mouse macrophages in vitro.* Res Exp Med, 1979. **174**(2): p. 383–93.
96. Sang, X., et al., *The chronic spleen injury of mice following long-term exposure to titanium dioxide nanoparticles.* J Biomed Mater Res A, 2012. **100**(4): p. 894-902.
97. Shvedova, A.A., et al., *Unusual inflammatory and fibrogenic pulmonary responses to single-walled carbon nanotubes in mice.* Am J Physiol Lung Cell Mol Physiol, 2005. **289**(5): p. L698-708.
98. Kagan, V.E., H. Bayir, and A.A. Shvedova, *Nanomedicine and nanotoxicology: two sides of the same coin.* Nanomedicine, 2005. **1**(4): p. 313-6.
99. Liu, Y., et al., *Immunostimulatory properties and enhanced TNF- alpha mediated cellular immunity for tumor therapy by C60(OH)20 nanoparticles.* Nanotechnology, 2009. **20**(41): p. 415102.
100. Panyam, J., et al., *Fluorescence and electron microscopy probes for cellular and tissue uptake of poly(D,L-lactide-co-glycolide) nanoparticles.* Int J Pharm, 2003. **262**(1-2): p. 1-11.
101. Cunningham, R.E., *Overview of flow cytometry and fluorescent probes for flow cytometry.* Methods Mol Biol, 2010. **588**: p. 319-26.
102. Chiellini, F., et al., *Intracellular fate investigation of bio-eliminable polymeric nanoparticles by confocal laser scanning microscopy*

J Bioact Compat Polym, 2007. **22**(6): p. 667-685.
103. Al-Hallak, K.M., et al., *The effect of compression forces on the stability of dibasic calcium phosphate dihydrate tablets in the presence of glutamic acid hydrochloride*

monitored by isothermal calorimetry. Thermochim Acta 2007. **467**(1-2): p. 86-90.
104. Velazquez-Campoy, A., et al., *Isothermal titration calorimetry.* Curr Protoc Cell Biol, 2004. **Chapter 17**: p. Unit 17 8.
105. Wadso, I., *Isothermal microcalorimetry in applied biology.* Thermochim Acta, 2002. **11**: p. 394:305.
106. Backman, P., *Effects of experimental factors on the metabolic rate of T-lymphoma cells as measured by microcalorimetry.* Thermochim Acta, 1990. **172**: p. 123-130.
107. Sbarra, A.J. and M.L. Karnovsky, *The biochemical basis of phagocytosis. I. Metabolic changes during the ingestion of particles by polymorphonuclear leukocytes.* J Biol Chem, 1959. **234**(6): p. 1355-62.
108. Gebreselassie, D., et al., *A microcalorimetric method to study the activation of murine peritoneal macrophages.* Thermochim Acta, 1996. **275**(1): p. 109-115.
109. Calvo, P., V.-J.J. l., and M.J. Alonso, *Comparative in vitro evaluation of several colloidal systems, nanoparticles, nanocapsules, and nanoemulsions, as ocular drug carriers.* J Pharm Sci, 1996. **85**(5): p. 530-536.

110. Cosco, D., et al., *Colloidal carriers for the enhanced delivery through the skin.* Expert Opin Drug Deliv, 2008. **5**(7): p. 737-55.
111. Azarmi, S., W.H. Roa, and R. Lobenberg, *Targeted delivery of nanoparticles for the treatment of lung diseases.* Adv Drug Deliv Rev, 2008. **60**(8): p. 863-75.
112. Kaialy, W., et al., *Effect of carrier particle shape on dry powder inhaler performance.* Int J Pharm, 2011. **421**(1): p. 12-23.
113. Chow, A.H., et al., *Particle engineering for pulmonary drug delivery.* Pharm Res, 2007. **24**(3): p. 411-37.
114. Dailey, L.A., et al., *Nebulization of biodegradable nanoparticles: impact of nebulizer technology and nanoparticle characteristics on aerosol features.* J Control Release, 2003. **86**(1): p. 131-44.
115. Shrewsbury, S.B., A.P. Bosco, and P.S. Uster, *Pharmacokinetics of a novel submicron budesonide dispersion for nebulized delivery in asthma.* Int J Pharm, 2009. **365**(1-2): p. 12-7.
116. Pandey, R., et al., *Poly (DL-lactide-co-glycolide) nanoparticle-based inhalable sustained drug delivery system for experimental tuberculosis.* J Antimicrob Chemother, 2003. **52**(6): p. 981-6.
117. Finlay, W.H., *The mechanics of inhaled pharmaceutical aerosols : an introduction*. 1 ed. Vol. 1. 2001, London: Academic Press.
118. Crompton, G.K., *Dry powder inhalers: advantages and limitations.* J Aerosol Med, 1991. **4**(3): p. 151-6.
119. Atkins, P.J., *Dry powder inhalers: an overview.* Respir Care, 2005. **50**(10): p. 1304-12; discussion 1312.
120. Vidgren, M., et al., *In vitro and in vivo deposition of drug particles inhaled from pressurized aerosol and dry powder inhaler.* Drug Dev Ind Pharm, 1988. **14**(15-17): p. 2649-2665
121. Edwards, D.A., et al., *Large porous particles for pulmonary drug delivery.* Science, 1997. **276**(5320): p. 1868-71.
122. Sung, J.C., et al., *Formulation and pharmacokinetics of self-assembled rifampicin nanoparticle systems for pulmonary delivery.* Pharm Res, 2009. **26**(8): p. 1847-55.
123. Cheow, W.S., M.W. Chang, and K. Hadinoto, *Antibacterial efficacy of inhalable levofloxacin-loaded polymeric nanoparticles against E. coli biofilm cells: the effect of antibiotic release profile.* Pharm Res, 2010. **27**(8): p. 1597-609.
124. Suk, J.S., et al., *Rapid transport of muco-inert nanoparticles in cystic fibrosis sputum treated with N-acetyl cysteine.* Nanomedicine (Lond), 2011. **6**(2): p. 365-75.
125. Roa, W.H., et al., *Inhalable nanoparticles, a non-invasive approach to treat lung cancer in a mouse model.* J Control Release, 2011. **150**(1): p. 49-55.
126. Sharma, A., S. Sharma, and G.K. Khuller, *Lectin-functionalized poly (lactide-co-glycolide) nanoparticles as oral/aerosolized antitubercular drug carriers for treatment of tuberculosis.* J Antimicrob Chemother, 2004. **54**(4): p. 761-6.
127. Davda, J. and V. Labhasetwar, *Characterization of nanoparticle uptake by endothelial cells.* Int J Pharm, 2002. **233**(1-2): p. 51-9.
128. Muttil, P., et al., *Immunization of guinea pigs with novel hepatitis B antigen as nanoparticle aggregate powders administered by the pulmonary route.* AAPS J, 2010. **12**(3): p. 330-7.
129. Muttil, P., et al., *Pulmonary immunization of guinea pigs with diphtheria CRM-197 antigen as nanoparticle aggregate dry powders enhance local and systemic immune responses.* AAPS J, 2010. **12**(4): p. 699-707.
130. Videira, M.A., et al., *Lymphatic uptake of pulmonary delivered radiolabelled solid lipid nanoparticles.* J Drug Target, 2002. **10**(8): p. 607-13.
131. Carvalho, T.C., J.I. Peters, and R.O. Williams, 3rd, *Influence of particle size on regional lung deposition--what evidence is there?* Int J Pharm, 2011. **406**(1-2): p. 1-10.

132. Tsapis, N., et al., *Trojan particles: large porous carriers of nanoparticles for drug delivery.* Proc Natl Acad Sci U S A, 2002. **99**(19): p. 12001-5.
133. Kabbaj, M. and N.C. Phillips, *Anticancer activity of mycobacterial DNA: effect of formulation as chitosan nanoparticles.* J Drug Target 2001. **9**(5): p. 317-328
134. Pilcer, G. and K. Amighi, *Formulation strategy and use of excipients in pulmonary drug delivery.* Int J Pharm, 2010. **392**(1-2): p. 1-19.
135. Hinds, W.C., *Aerosol technology: Properties, behavior and measurement of airborne particles*. 1 ed. 1999, New York: Wiley-interscience.
136. Misra, A., et al., *Inhaled drug therapy for treatment of tuberculosis.* Tuberculosis (Edinb), 2011. **91**(1): p. 71-81.
137. Kawakami, K., et al., *Investigation of the dynamic process during spray-drying to improve aerodynamic performance of inhalation particles.* Int J Pharm, 2010. **390**(2): p. 250-9.
138. Tomoda, K., et al., *Preparation and properties of inhalable nanocomposite particles: effects of the temperature at a spray-dryer inlet upon the properties of particles.* Colloids Surf B Biointerfaces, 2008. **61**(2): p. 138-44.
139. Tomoda, K., et al., *Preparation and properties of inhalable nanocomposite particles: effects of the size, weight ratio of the primary nanoparticles in nanocomposite particles and temperature at a spray-dryer inlet upon properties of nanocomposite particles.* Colloids Surf B Biointerfaces, 2008. **64**(1): p. 70-6.
140. Kho, K. and K. Hadinoto, *Aqueous re-dispersibility characterization of spray-dried hollow spherical silica nano-aggregates.* Powder technology 2010. **198**(3): p. 354-363.
141. Hadinoto, K. and W.S. Cheow, *Hollow spherical nanoparticulate aggregates as potential ultrasound contrast agent: shell thickness characterization.* Drug Dev Ind Pharm, 2009. **35**(10): p. 1167-1179.
142. Hadinoto, K., et al., *Novel formulation of large hollow nanoparticles aggregates as potential carriers in inhaled delivery of nanoparticulate drugs.* Ind Eng Chem Res, 2006. **45**(10): p. 3697-3706.
143. Cheow, W.S., S. Li, and K. Hadinoto, *Spray drying formulation of hollow spherical aggregates of silica nanoparticles by experimental design.* Chemical Engineering Research and Design, 2010. **88**(5-6): p. 673-685.
144. Hadinoto, K., et al., *Dry powder aerosol delivery of large hollow nanoparticulate aggregates as prospective carriers of nanoparticulate drugs: effects of phospholipids.* Int J Pharm, 2007. **333**(1-2): p. 187-198.
145. Kho, K. and K. Hadinoto, *Effects of excipient formulation on the morphology and aqueous re-dispersibility of dry-powder silica nano-aggregates.* Colloids and Surfaces A: Physicochem. Eng. Aspects, 2010. **359**: p. 71-81.
146. Yamamoto, H., et al., *Engineering of poly(DL-lactic-co-glycolic acid) nanocomposite particles for dry powder inhalation dosage forms of insulin with the spray-fluidized bed granulating system.* Advanced Powder Technology, 2007. **18**(2): p. 215-228.
147. Jensen, D.M., et al., *Spray drying of siRNA-containing PLGA nanoparticles intended for inhalation.* J Control Release, 2010. **142**(1): p. 138-45.
148. Lebhardt, T., et al., *Surfactant-free redispersible nanoparticles in fast-dissolving composite microcarriers for dry-powder inhalation.* Eur J Pharm Biopharm, 2011. **78**(1): p. 90-6.
149. Wang, Z.l., et al., *Powder formation by atmospheric spray-freeze-drying.* Powder Technology, 2006. **170**(1): p. 45-52.
150. Cheow, W.S., et al., *Spray-freeze-drying production of thermally sensitive polymeric nanoparticle aggregates for inhaled drug delivery: effect of freeze-drying adjuvants.* Int J Pharm, 2011. **404**(1-2): p. 289-300.

151. El-Gendy, N., et al., *Budesonide nanoparticle agglomerates as dry powder aerosols with rapid dissolution.* J Pharm Sci, 2009. **98**(8): p. 2731-2746.
152. El-Gendy, N., V. Desai, and C. Berkland, *Agglomerates of ciprofloxacin nanoparticles yield fine dry powder aerosols.* J Pharm Innov, 2009. **5**(3): p. 79-86.
153. El-Gendy, N. and C. Berkland, *Combination chemotherapeutic dry powder aerosols via controlled nanoparticle agglomeration.* Pharm Res, 2009. **26**(7): p. 1752-63.
154. El-Gendy, N., K.L. Aillon, and C. Berkland, *Dry powdered aerosols of diatrizoic acid nanoparticle agglomerates as a lung contrast agent.* Int J Pharm, 2010. **391**(1-2): p. 305-12.
155. Plumley, C., et al., *Nifedipine nanoparticle agglomeration as a dry powder aerosol formulation strategy.* Int J Pharm, 2009. **369**(1-2): p. 136-43.
156. Aillon, K.l., et al., *Iodinated NanoClusters as an inhaled computed tomography contrast agent for lung visualization.* Mol Pharm, 2010. **7**(4): p. 1274-1282.
157. Al-Hallak, M.K., et al., *Pulmonary delivery of inhalable nanoparticles: Dry powder inhalers.* Therapeutic Delivery, 2011. **2**(10): p. 1313-1324
158. Sham, J.O., et al., *Formulation and characterization of spray-dried powders containing nanoparticles for aerosol delivery to the lung.* Int J Pharm, 2004. **269**(2): p. 457-67.
159. Iskandar, F., L. Gradon, and K. Okuyama, *Control of the morphology of nanostructured particles prepared by the spray drying of a nanoparticle sol.* J Colloid Interface Sci, 2003. **265**(2): p. 296-303.
160. Pilcer, G. and K. Amighi.
161. Schiffter, H., J. Condliffe, and S. Vonhoff, *Spray-freeze-drying of nanosuspensions: the manufacture of insulin particles for needle-free ballistic powder delivery.* J R Soc Interface, 2010. **7 Suppl 4**: p. S483-500.
162. Abdelwahed, W., G. Degobert, and H. Fessi, *A pilot study of freeze drying of poly(epsilon-caprolactone) nanocapsules stabilized by poly(vinyl alcohol): formulation and process optimization.* Int J Pharm, 2006. **309**(1-2): p. 178-88.
163. Abdelwahed, W., et al., *Freeze-drying of nanoparticles: formulation, process and storage considerations.* Adv Drug Deliv Rev, 2006. **58**(15): p. 1688-713.
164. Ely, L., et al., *Effervescent dry powder for respiratory drug delivery.* Eur J Pharm Biopharm, 2007. **65**(3): p. 346-53.
165. Azarmi, S., et al., *Formulation and in vivo evaluation of effervescent inhalable carrier particles for pulmonary delivery of nanoparticles.* Drug Dev Ind Pharm, 2008. **34**(9): p. 943-7.
166. Ku, T., et al., *Size dependent interactions of nanoparticles with lung surfactant model systems and the significant impact on surface potential.* J Nanosci Nanotechnol, 2008. **8**(6): p. 2971-8.
167. Gill, S., et al., *Nanoparticles: characteristics, mechanisms of action, and toxicity in pulmonary drug delivery—a review.* J Biomedl Nanotech, 2007. **3**((2)): p. 107-19.
168. Smith, F.B., *Role of the pulmonary surfactant system in lung diseases of adults.* N Y State J Med, 1983. **83**((6)): p. 851-6.
169. Schief, W.R., et al., *Liquid crystalline collapse of pulmonary surfactant monolayers.* Biophys J, 2003. **6**: p. 3792–806.
170. Nel, A.E., et al., *Understanding biophysicochemical interactions at the nano-bio interface.* Nat Mater, 2009. **8**: p. 543.
171. Stuart, D., et al., *Biophysical investigation of nanoparticle interactions with lung surfactant model systems.* J Biomed Nanotech, 2006. **2**(2-3): p. 245-52.
172. Torchilin, V.P., *Polymer-coated long-circulating microparticulate pharmaceuticals.* J Microencapsul, 1998. **15**(1): p. 1-19.

173. Vandorpe, J., et al., *Long circulating biodegradable poly(phosphazene) nanoparticles surface modified with poly(phosphazene)-poly(ethylene oxide) copolymer.* Biomaterials, 1997. **18**(17): p. 1147-52.
174. Gref, R., et al., *'Stealth' corona-core nanoparticles surface modified by polyethylene glycol (PEG): influences of the corona (PEG chain length and surface density) and of the core composition on phagocytic uptake and plasma protein adsorption.* Colloids Surf B Biointerfaces, 2000. **18**(3-4): p. 301-313.
175. Elder, A., et al., *Translocation of inhaled ultrafine manganese oxide particles to the central nervous system.* Environ Health Perspect, 2006. **114**(8): p. 1172-8.
176. Oberdorster, G., E. Oberdorster, and J. Oberdorster, *Nanotoxicology: an emerging discipline evolving from studies of ultrafine particles.* Environ Health Perspect, 2005. **113**(7): p. 823-39.
177. Tomoda, K., et al., *Preparation and properties of inhalable nanocomposite particles for treatment of lung cancer.* Colloids Surf B Biointerfaces, 2009. **71**(2): p. 177-82.
178. Furuyama, A., et al., *Extrapulmonary translocation of intratracheally instilled fine and ultrafine particles via direct and alveolar macrophage-associated routes.* Arch Toxicol, 2009. **83**(5): p. 429-37.
179. Al-Hallak, M.K., et al., *Distribution of effervescent inhalable nanoparticles after pulmonary delivery: an in vivo study.* Therapeutic Delivery, 2012. **3**(6): p. 725-734.
180. O'Byrne, K., *The link between inflammation and cancer: wounds that do not heal*. 2006: Springer.
181. Montuenga, L.M. and R. Pio, *Tumour-associated macrophages in nonsmall cell lung cancer: the role of interleukin-10.* Eur Respir J, 2007. **30**(4): p. 608-10.
182. Condeelis, J. and J.W. Pollard, *Macrophages: obligate partners for tumor cell migration, invasion, and metastasis.* Cell, 2006. **124**(2): p. 263-6.
183. Parkin, D.M., et al., *Global cancer statistics, 2002.* CA Cancer J Clin, 2005. **55**(2): p. 74-108.
184. Mantovani, A., et al., *Macrophage polarization: tumor-associated macrophages as a paradigm for polarized M2 mononuclear phagocytes.* Trends Immunol, 2002. **23**(11): p. 549-55.
185. Aderem, A. and D.M. Underhill, *Mechanisms of phagocytosis in macrophages.* Annu Rev Immunol, 1999. **17**: p. 593-623.
186. Takenaka, S., et al., *Distribution pattern of inhaled ultrafine gold particles in the rat lung.* Inhal Toxicol, 2006. **18**(10): p. 733-40.
187. Scarpelli, E.M., *Physiology of the alveolar surface network.* Comp Biochem Physiol A Mol Integr Physiol, 2003. **135**(1): p. 39-104.
188. Al-Hallak, M.H., et al., *Pulmonary toxicity of polysorbate-80-coated inhalable nanoparticles; in vitro and in vivo evaluation.* AAPS J, 2010. **12**(3): p. 294-9.
189. Warheit, D.B., et al., *Testing strategies to establish the safety of nanomaterials: conclusions of an ECETOC workshop.* Inhal Toxicol, 2007. **19**(8): p. 631-43.
190. Möhwald, H., *Phospholipid and phospholipid-protein monolayers at the air/water interface* Annual Review of Physical Chemistry, 1990. **41**(1): p. 441-476.
191. Gopal, A. and K.Y.C. Lee, *Morphology and collapse transitions in binary phospholipid monolayers.* Journal of Physical Chemistry B, 2001. **105**(42): p. 10348-10354.
192. Al-Hallak, M.H., et al., *Microcalorimetric method to assess phagocytosis: macrophage-nanoparticle interactions.* AAPS J, 2011. **13**(1): p. 20-9.
193. Grenha, A., B. Seijo, and C. Remunan-Lopez, *Microencapsulated chitosan nanoparticles for lung protein delivery.* Eur J Pharm Sci, 2005. **25**(4-5): p. 427-37.
194. Shi, L., C.J. Plumley, and C. Berkland, *Biodegradable nanoparticle flocculates for dry powder aerosol formulation.* Langmuir, 2007. **23**(22): p. 10897-901.

195. Wang, W.N., I.W. Lenggoro, and K. Okuyama, *Dispersion and aggregation of nanoparticles derived from colloidal droplets under low-pressure conditions.* J Colloid Interface Sci, 2005. **288**(2): p. 423-31.
196. Azarmi, S., et al., *Formulation and cytotoxicity of doxorubicin nanoparticles carried by dry powder aerosol particles.* Int J Pharm, 2006. **319**(1-2): p. 155-61.
197. Couvreur, P., et al., *Toxicity of polyalkylcyanoacrylate nanoparticles II: Doxorubicin-loaded nanoparticles.* J Pharm Sci, 1982. **71**(7): p. 790-2.
198. Monza da Silveira, A., et al., *Combined poly(isobutylcyanoacrylate) and cyclodextrins nanoparticles for enhancing the encapsulation of lipophilic drugs.* Pharm Res, 1998. **15**(7): p. 1051-5.
199. Azarmi, S., et al., *Optimization of a two-step desolvation method for preparing gelatin nanoparticles and cell uptake studies in 143B osteosarcoma cancer.* J Pharm Sci, 2006. **9**(1): p. 124-32.
200. Axline, S.G. and E.P. Reaven, *Inhibition of phagocytosis and plasma membrane mobility of the cultivated macrophage by cytochalasin B. Role of subplasmalemmal microfilaments.* J Cell Biol, 1974. **62**(3): p. 647-59.
201. Al-Hallak, K.M., et al., *Secondary cytotoxicity mediated by alveolar macrophages: a contribution to the total efficacy of nanoparticles in lung cancer therapy?* Eur J Pharm Biopharm, 2010. **76**(1): p. 112-9.
202. Sweeney, L.G., et al., *Spray-freeze-dried liposomal ciprofloxacin powder for inhaled aerosol drug delivery.* Int J Pharm, 2005. **305**(1-2): p. 180-5.
203. Rouleau, C. and J. Kohli, *Distribution of ^{14}C-labelled Atrazine, Methoxychlor, Glyphosate, and Bisphenol-A in Goldfish Studied by Whole-Body Autoradiography (WBARG).* Water Qual. Res. J. Can, 2008. **43**(4): p. 265-274.
204. Rouleau, C., et al., *Uptake of waterborne tributyltin in the brain of fish: axonal transport as a proposed mechanism.* Environ Sci Technol, 2003. **37**(15): p. 3298-302.
205. Hillaireau, H. and P. Couvreur, *Nanocarriers' entry into the cell: relevance to drug delivery.* Cell. Mol. Life Sci., 2009. **66**: p. 2873–2896.
206. Kante, B., et al., *Toxicity of polyalkylcyanoacrylate nanoparticles I: Free nanoparticles.* J Pharm Sci, 1982. **71**(7): p. 786-90.
207. Athlin, L., L. Domellof, and B. Norberg, *Effect of therapeutic concentrations of anthracyclines on monocyte phagocytosis of yeast cells.* Eur J Clin Pharmacol, 1989. **36**(2): p. 155-9.
208. Evora, C., et al., *Relating the phagocytosis of microparticles by alveolar macrophages to surface chemistry: the effect of 1,2-dipalmitoylphosphatidylcholine.* J Control Release, 1998. **51**(2-3): p. 143-52.
209. Kim, D.W., et al., *High tumour islet macrophage infiltration correlates with improved patient survival but not with EGFR mutations, gene copy number or protein expression in resected non-small cell lung cancer.* Br. J. Cancer, 2008. **98**: p. 1118–1124.
210. Yasuda, I., et al., *Mediastinal Lymph Node Staging in Potentially Resectable Non-Small Cell Lung Cancer: A Prospective Comparison of CT and EUS/EUS-FNA.* Respiration, 2009. **78**(4): p. 423-431.
211. de Verdiere, A.C., et al., *Reversion of multidrug resistance with polyalkylcyanoacrylate nanoparticles: towards a mechanism of action.* Br J Cancer, 1997. **76**(2): p. 198-205.
212. Panyam, J. and V. Labhasetwar, *Dynamics of endocytosis and exocytosis of poly(D,L-lactide-co-glycolide) nanoparticles in vascular smooth muscle cells.* Pharm Res, 2003. **20**(2): p. 212-20.
213. Tomoda, H., Y. Kishimoto, and Y.C. Lee, *Temperature effect on endocytosis and exocytosis by rabbit alveolar macrophages.* J Biol Chem, 1989. **264**(26): p. 15445-50.
214. Bjerknes, R., *Exocytosis of zymosan particles by human phagocytes.* Scand J Haematol, 1984. **33**(2): p. 197-206.

215. Hasegawa, T., et al., *Exact determination of phagocytic activity of alveolar macrophages toward polymer microspheres by elimination of those attached to the macrophage membrane.* Colloids Surf. B Biointerfaces, 2008. **63**: p. 209–216.
216. Majai, G., G. Petrovski, and L. Fesus, *Inflammation and the apopto-phagocytic system.* Immunol Lett, 2006. **104**(1-2): p. 94-101.
217. Chung, E.Y., S.J. Kim, and X.J. Ma, *Regulation of cytokine production during phagocytosis of apoptotic cells.* Cell Res, 2006. **16**(2): p. 154-61.
218. Burke, F., *Cytokines (IFNs, TNF-alpha, IL-2 and IL-12) and animal models of cancer.* Cytokines Cell Mol Ther, 1999. **5**(1): p. 51-61.
219. Burke, F. and F.R. Balkwill, *Cytokines in animal models of cancer.* Biotherapy, 1996. **8**(3-4): p. 229-41.
220. Bosco, M.C., et al., *The tryptophan catabolite picolinic acid selectively induces the chemokines macrophage inflammatory protein-1 alpha and -1 beta in macrophages.* J Immunol, 2000. **164**(6): p. 3283-91.
221. Driscoll, K.E., *Macrophage inflammatory proteins: biology and role in pulmonary inflammation.* Exp Lung Res, 1994. **20**(6): p. 473-90.
222. Biswas, S.K. and A. Sodhi, *Tyrosine phosphorylation-mediated signal transduction in MCP-1-induced macrophage activation: role for receptor dimerization, focal adhesion protein complex and JAK/STAT pathway.* Int Immunopharmacol, 2002. **2**(8): p. 1095-107.
223. Wink, D.A., et al., *The multifaceted roles of nitric oxide in cancer.* Carcinogenesis, 1998. **19**(5): p. 711-21.
224. Maurer, M. and E. von Stebut, *Macrophage inflammatory protein-1.* Int J Biochem Cell Biol, 2004. **36**(10): p. 1882-6.
225. Shiraishi, K., et al., *Enhancement of antitumor radiation efficacy and consistent induction of the abscopal effect in mice by ECI301, an active variant of macrophage inflammatory protein-1alpha.* Clin Cancer Res, 2008. **14**(4): p. 1159-66.
226. Thongphasuk, P., W. Stremmel, and W. Chamulitrat, *Potent direct or TNF-alpha-promoted anticancer effects of 2,3-dehydrosilybin: comparison study with silybin.* Chemotherapy, 2008. **54**(1): p. 23-30.
227. Itano, S., S. Fuchimoto, and K. Orita, *Synergistic antitumor effects of natural human tumor necrosis factor and mouse interferon beta and gamma.* Hiroshima J Med Sci, 1987. **36**(2): p. 219-25.
228. Yumura, M., *Macrophage migration inhibition-activity after implantation of methylcholanthrene-induced sarcoma, Ehrlich ascites cancer or mouse ascites hepatoma-134 cancer cells in mice.* Acta Med Okayama, 1976. **30**(1): p. 37-48.
229. Gao, B. and M.F. Tsan, *Induction of cytokines by heat shock proteins and endotoxin in murine macrophages.* Biochem Biophys Res Commun, 2004. **317**(4): p. 1149-54.
230. Lee, P.P., et al., *T helper 2-dominant antilymphoma immune response is associated with fatal outcome.* Blood 1997. **90**: p. 1611–1617.
231. Dinarello, C.A., *Historical insights into cytokines.* Eur. J. Immunol, 2007. **37**(SUPPL. 1): p. S34-S45.
232. Romagnani, S., *The Th1/Th2 paradigm.* Immunol Today, 1997. **18**(6): p. 263-6.
233. Manzotti, C., R.A. Audisio, and G. Pratesi, *Importance of orthotopic implantation for human tumors as model systems: relevance to metastasis and invasion.* Clin. Exp. Metastasis, 1993. **11**: p. 5-14.
234. Shalaby, M.R., D. Pennica, and M.A. Palladino, Jr., *An overview of the history and biologic properties of tumor necrosis factors.* Springer Semin Immunopathol, 1986. **9**(1): p. 33-7.
235. Salcedo, R., et al., *Human endothelial cells express CCR2 and respond to MCP-1: direct role of MCP-1 in angiogenesis and tumor progression.* Blood, 2000. **96**(1): p. 34-40.

236. Kodama, M., et al., *A monolayer study on three binary mixed systems of dipalmitoyl phosphatidyl choline with cholesterol, cholestanol and stigmasterol.* Colloids Surf B Biointerfaces, 2004. **33**(3-4): p. 211–26.
237. Brown, D.M., et al., *Size-dependent proinflammatory effects of ultrafine polystyrene particles: a role for surface area and oxidative stress in the enhanced activity of ultrafines.* Toxicol Appl Pharmacol, 2001. **175**(3): p. 191-9.
238. Zigmond, S.H. and J.G. Hirsch, *Effects of cytochalasin B on polymorphonuclear leucocyte locomotion, phagocytosis and glycolysis.* Exp Cell Res, 1972. **73**(2): p. 383-93.
239. Malawista, S.E., J.B. Gee, and K.G. Bensch, *Cytochalasin B reversibly inhibits phagocytosis: functional, metabolic, and ultrastructural effects in human blood leukocytes and rabbit alveolar macrophages.* Yale J Biol Med, 1971. **44**(3): p. 286-300.
240. Finlay, W.H., *The Mechanics of Inhaled Pharmaceutical Aerosols: an Introduction*. 2001, San Diego: Academic Press.
241. Naomoto, Y., et al., *Novel experimental models of human cancer metastasis in nude mice: lung metastasis, intraabdominal carcinomatosis with ascites, and liver metastasis.* J Cancer Res Clin Oncol, 1987. **113**(6): p. 544-9.
242. Choi, S.W. and J.H. Kim, *Design of surface-modified poly(D,L-lactide-co-glycolide) nanoparticles for targeted drug delivery to bone.* J Control Release, 2007. **122**(1): p. 24-30.
243. Sakamoto, J., et al., *Antibiological barrier nanovector technology for cancer applications.* Expert Opin Drug Deliv, 2007. **4**(4): p. 359-69.
244. Matsumura, Y. and K. Kataoka, *Preclinical and clinical studies of anticancer agent-incorporating polymer micelles.* Cancer Sci, 2009. **100**(4): p. 572-9.
245. Muhlfeld, C., et al., *Interactions of nanoparticles with pulmonary structures and cellular responses.* Am J Physiol Lung Cell Mol Physiol, 2008. **294**(5): p. L817-29.
246. Goncalves, C., et al., *Dextrin nanoparticles: studies on the interaction with murine macrophages and blood clearance.* Colloids Surf B Biointerfaces, 2010. **75**(2): p. 483-9.
247. He, C., et al., *Effects of particle size and surface charge on cellular uptake and biodistribution of polymeric nanoparticles.* Biomaterials, 2010. **31**(13): p. 3657-66.
248. Clift, M.J., et al., *The impact of different nanoparticle surface chemistry and size on uptake and toxicity in a murine macrophage cell line.* Toxicol Appl Pharmacol, 2008. **232**(3): p. 418-27.
249. Johansen, P.B., *Doxorubicin pharmacokinetics after intravenous and intraperitoneal administration in the nude mouse.* Cancer Chemother Pharmacol, 1981. **5**(4): p. 267-70.
250. Wartenberg, M. and H. Acker, *Induction of cell death by Doxorubicin in multicellular spheroids as studied by confocal laser scanning microscopy.* Anticancer Res, 1996. **16**(2): p. 573-9.